

Aus der Medizinischen Poliklinik – Innenstadt
der Ludwig-Maximilians-Universität München
Direktor: Prof. Dr. med. Martin Reincke

Role of TNF- α on progressive glomerulosclerosis in Alport nephropathy

Dissertation

**zum Erwerb des Doktorgrades der Humanbiologie
an der Medizinischen Fakultät der
Ludwig-Maximilians-Universität zu München**

vorgelegt von

Mi Ryu

Changwon, South Korea
2012

Mit Genehmigung der Medizinischen Fakultät
der Universität München

Berichterstatter: Prof. Dr. med. Hans-Joachim Anders
Mitberichterstatter: Priv. Doz. Dr. Philippe Khalil
Mitberichterstatter: Prof. Dr. André Werner Brändli
Mitberichterstatter: Priv. Doz. Dr. Wolfgang Neuhofer
Dekan: Prof. Dr. med. Dr. h.c. M. Reiser, FACR, FRCR

Tag der mündlichen Prüfung: 19.09.2012

Mi Ryu, Dipl.-Biotechnol.

Med. Poliklinik, Klinische Biochemie,
Ludwig-Maximilians University (LMU),
Schillerstraße 42, Munich- 80336,
Germany
mi.ryu@hotmail.com

DECLARATION

I here by declare that the present work embodied in this thesis was carried out by me under the supervision of OA Prof. Dr. Hans-Joachim Anders, Internist-Nephrologe-Rheumatologe, Medizinische Poliklinik-Innenstadt Klinikum der Universität München. This work has not been submitted in part or full to any other university or institute for any degree or diploma.

Mi Ryu

Date: 19.09.2012

ACKNOWLEDGEMENTS

I would like to express my deepest sense of gratitude to my supervisor Prof. Dr. Hans-Joachim Anders for his correct and scrupulous guidance and supervision during my graduate study. I appreciate his excellent advice, discussion, constant support and encouragement, which all contributed to my scientific and personal development.

I would like to acknowledge Dr. Oliver Gross (Department of Nephrology and Rheumatology University of Göttingen, Germany) for providing me animal models and constructive suggestions and Prof. Dr. Nicolai Miosge (Department of Prosthodontics, University of Göttingen, Germany) for providing me excellent experimental support for electron microscopy during my research work.

I wish to express my profound gratitude to Ewa Radomska, Dan Draganovici, and Jana Mandelbaum for providing skillful technical assistance to carry out the research work successfully.

I wish to thank all the staff members, colleagues of the groups of Dr. Bruno Luckow and Dr. Peter Nelson of the Department of Clinical Biochemistry, Medizinische Poliklinik, LMU for their suggestion and support of my research work.

I am very grateful to all my colleagues of the institute for the cooperative spirit, the warm and friendly working atmosphere, and sharing scientific discussion. My special thanks to Onkar and Supriya for providing the excellent Indian food every lunch. Many thanks to Adrinana, Anela, Anji, Dana, Heni, Julia, Khader, Kirstin, Maciej, Murthy, Nuru, Santosh, Shrikant, Stephie, Sufyan, and all other medical students who are too many to enumerate but are still deeply in my heart.

I also owe special gratitude to all my friends who give me warm encouragement from Korea, Germany, and elsewhere. To name a few Yoon-Hee, Jeong-Eun, Mi-Jeong, Mi-Hyun & Hyun-Il, Yu-Jin, Da-Young, Eon-Jeong, Il-Bum, Linn, Stefan, and Sascha.

Words fail me to express my deepest appreciation to my parents, my sisters Hee-Jung and Hye-Jin, my first nephew Luca and second nephew Josua, and my brother-in-law Christoph. They always give me profound love and moral support through my entire life. They are all my treasures who can not be taken the place of anyone.

Finally, I would like to thank my love Yoon-Seuk who gives me unconditional true love, constant encouragement, and patience.

Dedicated to

My loving parents and sisters

사랑하는 나의 가족에게 바칩니다.

Contents

1. Introduction	3
1.1 Chronic Kidney disease	3
1.1.1 Development of glomerulosclerosis	4
1.1.2 Glomerulosclerosis-associated chronic kidney diseases	8
1.2 Contributing factors of disease progression in CKD.....	9
1.2.1 Leukocyte infiltration in CKD.....	10
1.2.2 Role of tumor necrosis factor- α in CKD	14
1.2.3 Pattern recognition receptors and innate immunity	17
1.3 Alport Syndrome	23
1.3.1 Structure and distribution of type IV collagen	23
1.3.2 Genetics of Alport Syndrome	25
1.3.3 Clinical and pathologic features of Alport Nephropathy.....	26
1.3.4 Animal models of Alport Syndrome	27
1.3.5 Mouse autosomal recessive Alport model.....	27
1.3.6 Treatment of Alport syndrome	29
2. Hypothesis/Objectives	30
3. Materials and Methods	31
3.1 Materials	31
3.1.1 Equipment.....	31
3.1.2 Chemicals and materials	32
3.1.4 Solutions	36
3.2 Methods	39
3.2.1 Animal studies	39
3.2.1.1 Homing conditions and animal procedures	39
3.2.1.2 Study design and experimental procedures	39
3.2.1.3 Plasma and urine sample analysis	40
3.2.1.4 Immunohistochemical methods and histopathological evaluation.....	43
3.2.1.4 Electron microscopy	44
3.2.1.5 TUNEL assay	44
3.2.2 Cytokines	45
3.2.3 RNA analysis.....	45
3.2.4 cDNA synthesis and real-time RT-PCR (SYBR Green)	46

3.2.5 Flow cytometry	48
3.2.6 Isolation of renal macrophages	48
3.2.7 Protein isolation and Western blotting	49
3.2.8 <i>In vitro</i> studies	49
3.2.6 Statistical analysis.....	50
4. Results	51
4.1 Endogenous factors contributing to Alport nephropathy	51
4.1.1 Leukocyte infiltration of Alport nephropathy in <i>Col4a3</i> ^{-/-} mice	51
4.1.2 TNF- α expression in <i>Col4a3</i> ^{-/-} mice with Alport nephropathy	53
4.1.3 TNF- α expression in intrarenal leukocytes of <i>Col4a3</i> ^{-/-} mice	54
4.1.4 TNF- α blockade prolongs life span of <i>Col4a3</i> ^{-/-} mice	56
4.1.5 TNF- α blockade improves renal function in <i>Col4a3</i> ^{-/-} mice	57
4.1.6 TNF- α blockade protects <i>Col4a3</i> ^{-/-} mice from glomerulosclerosis.....	58
4.1.7 TNF- α blockade prevents podocyte loss in <i>Col4a3</i> ^{-/-} mice	61
4.2 Exogenous factors that accelerate the progression of Alport nephropathy	65
4.2.1 Effect of innate immunity on renal parenchymal cells.....	65
4.2.2 Macrophage activation via TLRs in Alport nephropathy	67
4.2.2.1 Effect of LPS or CpG-DNA on life span of <i>Col4a3</i> ^{-/-} mice	67
4.2.2.2 CpG-DNA, but not LPS, aggravates Alport nephropathy	68
4.2.2.3 CpG-DNA increases activated renal macrophages in <i>Col4a3</i> ^{-/-} mice ...	74
4.2.2.4 CpG-DNA and LPS modulate the expression of macrophage markers .	77
4.2.2.5 Effect of CpG-DNA on Alport nephropathy is mediated by TNF- α	77
5. Discussion.....	82
6. Summary and conclusion.....	90
7. Zusammenfassung	91
8. References	92
9. Abbreviations.....	106
Curriculum Vitae	110

1. Introduction

1.1 Chronic Kidney disease

Chronic kidney disease (CKD) is a gradual progressive loss of kidney function leading to end-stage renal failure which requires kidney replacement for survival. The prevalence of this disease is increasing worldwide. For example, CKD affects about 11.6% of the adult population in the United States (US) and its rising prevalence also appears in Europe and in other countries (Coresh et al., 2003). The guidelines published in the Kidney Disease Outcomes Quality Initiative (K/DOQI) of the National Kidney Foundation describe the definition of CKD and classify stages of kidney disease progression (MacGregor et al., 2006; National Kidney Foundation, 2002). CKD is defined as a decline in glomerular filtration rate (GFR) and kidney damage with the increase of proteinuria or urinary albumin or protein to creatinine ratio or albuminuria to creatinine ratio. K/DOQI defines CKD as $GFR < 60 \text{ ml/min/1.73 m}^2$ for ≥ 3 months, with or without the presence of kidney damage. Kidney Disease Improving Global Outcomes (KDIGO) provides the guideline for the definition and classification of CKD and its management (Levey et al., 2005). It is to improve the care and outcomes of kidney disease patients worldwide through promoting coordination, collaboration and intergration of initiatives to develop and implement clinical practice guidelines. CKD in KDIGO guideline has been classified into 5 stages based for K/DOQI definition and classification (Table 1 and 2). The causes of CKD are mainly diabetic nephropathy (type 1 or 2 diabetes mellitus) and hypertension. Other conditions including glomerulonephritis, nephrosclerosis, and hereditary renal disease can also affect kidneys.

Table 1. Definition of chronic kidney disease. Taken from (Levey et al., 2005)

Kidney damage for ≥ 3 months, as defined by structural or functional abnormalities of the kidney, with or without decreased GFR, that can lead to decreased GFR, manifest by either:
- Pathologic abnormalities; or
- Markers of kidney damage, including abnormalities in the composition of the blood or urine, or abnormalities in imaging tests
$GFR < 60 \text{ mL/min/1.73 m}^2$ for ≥ 3 months, with or without kidney damage
GFR, glomerular filtration rate

Table 2. Definition and classification of chronic kidney disease. Kidney Disease Improving Global Outcomes (KDIGO). Taken from (Levey et al., 2005)

Stage	Description	GFR ml/min/1.73m ²	Related terms	Classification by treatment
1	Kidney damage with normal or ↑ GFR	≥ 90	Albuminuria, proteinuria, hematuria	T if kidney transplant, recipient
2	Kidney damage with mild ↓ GFR	60 – 89	Albuminuria, proteinuria, hematuria	
3	Moderate ↓ GFR	30 – 59	Chronic renal insufficiency, early renal insufficiency	
4	Severe ↓ GFR	15 – 29	Chronic renal insufficiency, late renal insufficiency, pre-ESRD	
5	Kidney failure	< 15 (or dialysis)	Renal failure, ureamia, end-stage, renal disease	
				D if dialysis (hemodialysis, peritoneal dialysis)

“T” for all kidney transplant recipients, at any level (CKD stages 1 to 5) and “D” for dialysis, for CDK stage 5 patients treated by dialysis. GFR, glomerular filtration rate; ESRD, end-stage renal disease.

1.1.1 Development of glomerulosclerosis

Progressive renal disease is generally characterized by glomerulosclerosis, interstitial leukocyte infiltration, tubular atrophy, and interstitial fibrosis (Remuzzi and Bertani, 1998). Both the glomerulus and the tubulointerstitium are involved in the pathophysiologic changes contributing to progression of the disease. Glomerulosclerosis is a major cause of chronic and end-stage renal disease (ESRD). A normal structure of glomerulus consists of endocapillary compartment containing mesangial cells and capillary and extracapillary compartment containing podocytes and Bowman’s capsule (Abrahamson, 1987; Kriz et al., 1995). The glomerular tuft is composed of three types of cells: endothelial cells at the inside of the capillary, podocytes on the outside of the capillary, and mesangial cells filling the space between the capillary loops (Leeuwis et al., 2010). Podocyte loss is a common feature in many kidney diseases including diabetic (Pagtalunan et al., 1997; Steffes et al., 2001; Stieger et al., 2011) and non-diabetic renal diseases, e.g. focal segmental glomerulosclerosis (FSGS) or membranous glomerulopathy or amyloid nephropathy (Kriz, 1996; Shankland, 2006). Podocytes are terminally differentiated glomerular visceral epithelial cells that are specialized to their location, architecture, and cellular character. During nephrogenesis, podocytes derive

from mesenchymal cells and develop as a distinct cell layer at the stage of the so-called S-shaped bodies. At the stage of capillary loop, podocytes establish their characteristic complex cell architecture, including the formation of foot processes and a slit membrane (Figure 1). The cell body of podocytes lies in the urinary space. From these cell bodies arise long primary processes that extend further to secondary foot processes by attaching to the underlying glomerular basement membrane (GBM) via integrins and dystroglycans. The foot processes interdigitate with foot processes of neighboring podocytes, leaving in between the filtration slit which is bridged by the slit diaphragm. Finally, the large structure of the cells hangs in the urinary space of capillary wall (Mundel and Kriz, 1995; Smoyer and Mundel, 1998). Ultimately, differentiated adult podocytes may undergo mitosis (nuclear division), but are unable to undergo cytokinesis (cell division) resulting in bi-(multi)-nucleated podocytes. As a consequence, injured podocytes are incapable to proliferate or cannot be easily replaced, whereas other renal parenchymal cells, e.g. mesangial cells are able to regenerate. Therefore, podocyte damage involves the problem of insufficient podocyte repair resulting in secondary scarring processes leading to progressive glomerulosclerosis (Kriz, 1996; Pavenstadt et al., 2003; Wiggins, 2007).

The development and progression of glomerulosclerosis is described in a model shown in Figure 2 (Kriz, 1996; Kriz et al., 1998). When an area of denuded capillary comes into contact with parietal cells of Bowman's capsule, the latter are apparently triggered to attach to the capillary basement membrane. A "beach head" of parietal epithelium is thereby established on the tuft which represents the beginning of a synechia or tuft adhesion for the further development of segmental sclerosis. At the site of the attachment of parietal cells to the capillary, a gap in the parietal epithelium comes into existence, permitting filtration/exudation towards the cortical interstitium (Figure 2b). The parietal epithelium spreads to neighboring capillary loops. Capillaries inside the adhesion either collapse or are occluded by hyalinosis (shown in a dark grey pattern). Podocytes which are located at the flanks of the adhesion will degenerate by several mechanisms. The parietal epithelium may either appose those podocytes (arrowhead) or attach directly to the GBM at the flanks of the adhesion. Fluid leakage from perfused capillaries inside the adhesion has created a paraglomerular space (shown in yellow) that contains the sclerotic tuft remnants (that is, collapsed or hyalinized GBM formations). Towards the cortical interstitium, the paraglomerular space has become separated by a layer of sheet-like fibroblast processes (shown in green) (Figure 2c).

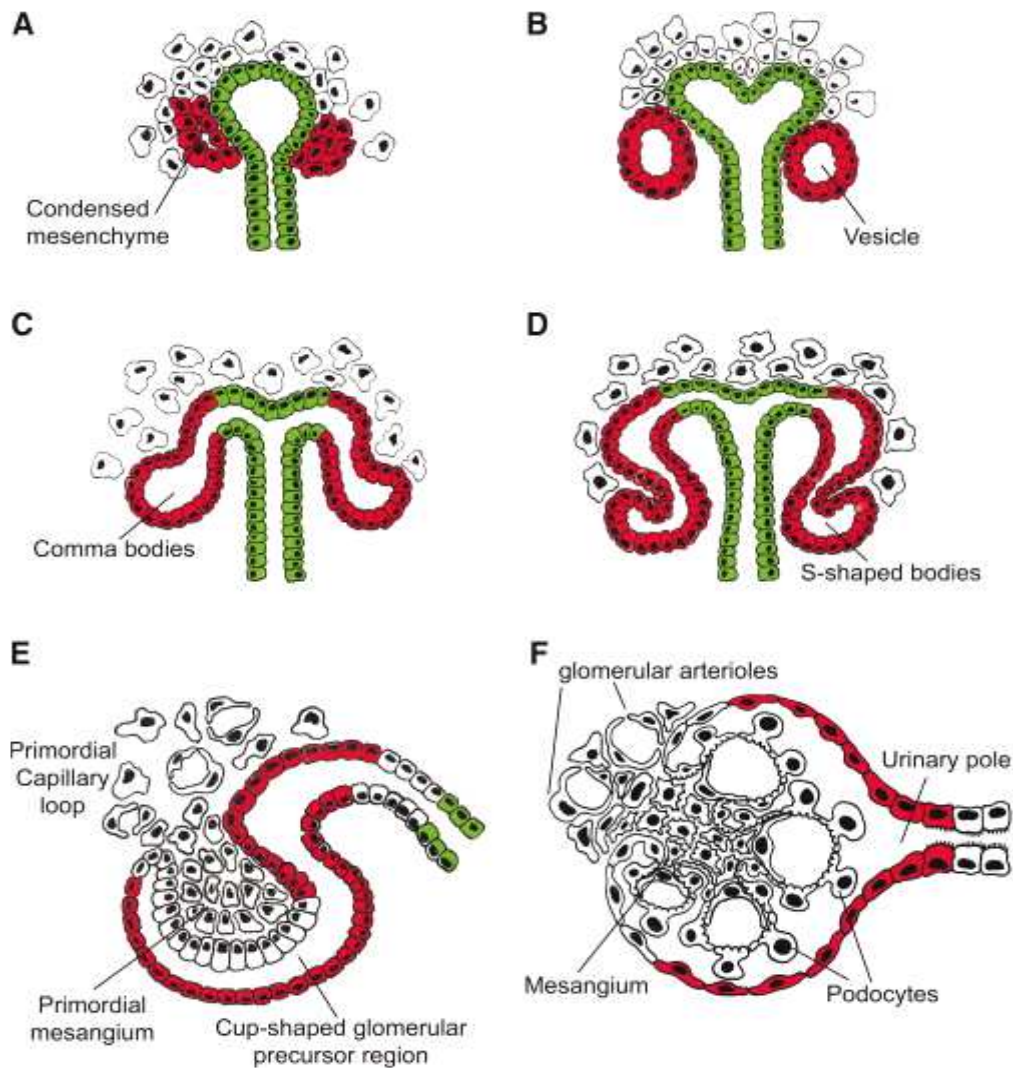


Figure 1. Development of nephron. During the induction of the metanephric mesenchyme, cells condense around the tips of the branching ureteric bud, and convert to an epithelial cell type (MET, mesenchymal-to-epithelial transition). These early epithelial cells form a spherical cyst called the renal vesicle (B), the renal vesicle aggregates to the comma-shaped (C), and then the S-shaped bodies (D). At this stage, the proximal end of the S-shaped body becomes invaded by blood vessel, differentiates into podocytes and parietal epithelial cells, and then generates the glomerular tuft (E, F). Simultaneously, the middle and the distal segments of the S-shaped body that had remained in contact with the ureteric bud epithelium fuse to form a single, continuous epithelial tube and begin to express proteins that are characteristic of tubular epithelia (Romagnani, 2009).

The sclerotic process has reached a further lobule via the vascular pole. A small "intact" tuft remnant protrudes into the urinary space still covered by the parietal epithelium. The sclerotic tuft remnants are located outside the parietal epithelium in the paraglomerular space that is separated from the cortical interstitium by a complete layer of cortical fibroblasts. Even in late stages of injury, perfused capillaries are regularly found within the sclerotic regions, probably accounting for the further expansion of the paraglomerular space that may extend to the proximal tubule. In later stages, fibroblasts will invade the sclerotic area, resulting in fibrous organization (Figure 2d) (Kriz et al., 1998).

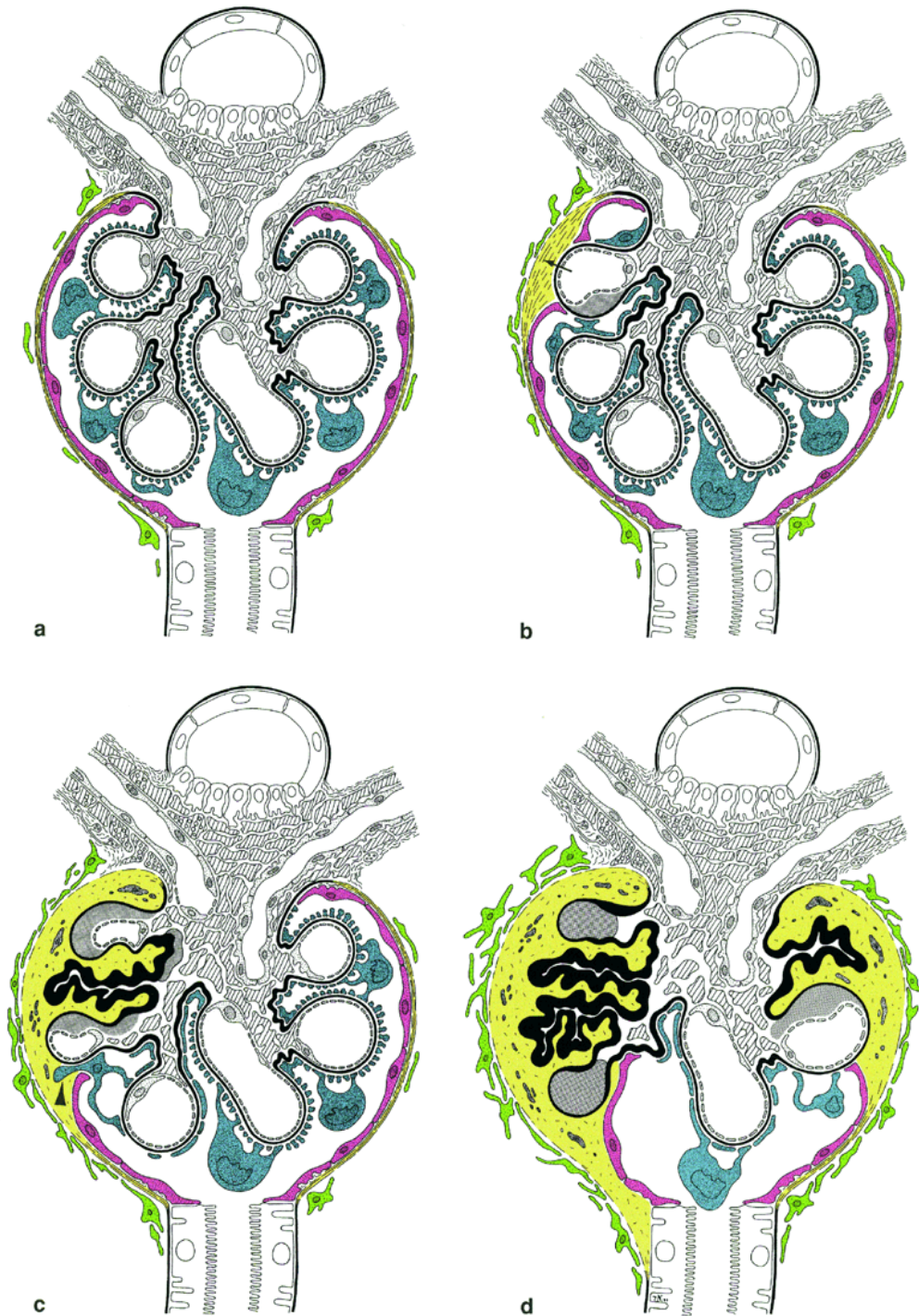


Figure 2. Schematic to show the progression of segmental to global glomerulosclerosis. (a) Normal glomerulus with vascular and urinary poles. Smooth muscle cells, extra glomerular mesangial cells, and mesangial cells are hatched; podocytes are shown in blue-green, parietal epithelial cells in red. The GBM is shown in black, the parietal basement membrane in yellow, tubular epithelia are shown in white (b) A denuded capillary is attached to Bowman's capsule. Parietal cells attach to the naked GBM. (c) The adhesion has spread to neighboring capillaries resulting in either the collapse or in hyalinosis (shown in a dark grey pattern). The parietal epithelium may either appose the degenerated podocytes (arrowhead) or attach directly to the GBM at the flanks of the adhesion. Fluid leakage from perfused capillaries inside the adhesion has created a paraglomerular space (shown in yellow) that contains the sclerotic tuft remnants (that is, collapsed or hyalinized GBM formations). Towards the cortical interstitium this paraglomerular space has become separated by a layer of sheet-like fibroblast processes (shown in green). (d) The sclerotic process jumps, via the vascular pole, to a neighbouring lobule. Even in late stages of injury perfused capillaries are regularly found within the sclerotic regions. In later stages, In the sclerotic area invaded by cortical fibroblasts, fibrosis will appear. Taken from (Kriz et al., 1998).

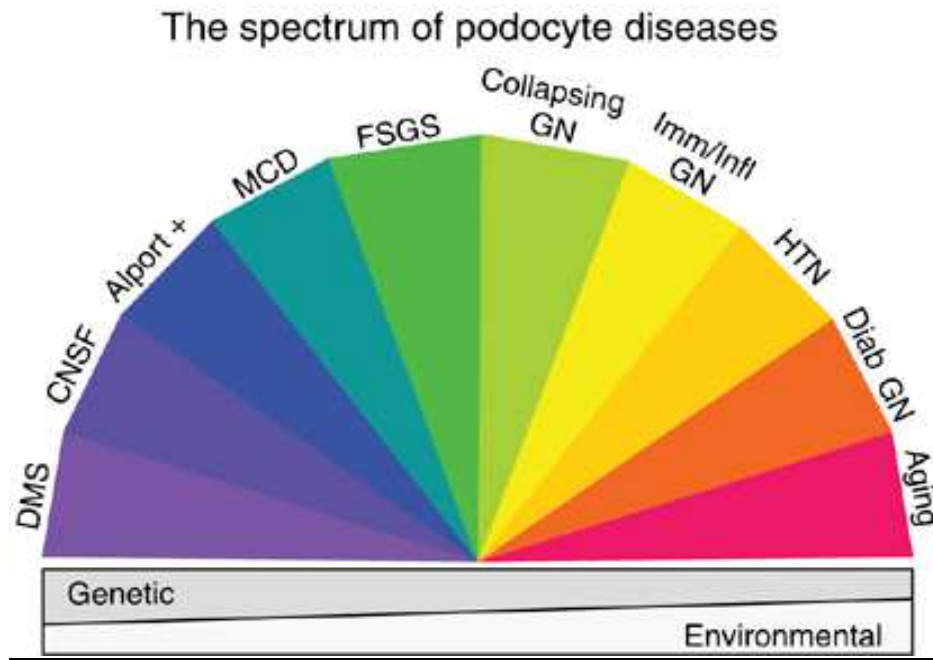


Figure 3. The spectrum of podocyte diseases. Glomerular diseases with podocyte dysfunction are developed by genetic and/or environmental factors. Depending on the stage of glomerular development and associated environmental factors, podocyte dysfunction, injury, or loss can result in a broad spectrum of clinical syndromes. All these conditions account for 90% of end-stage kidney disease. DMS, Diffuse mesangial sclerosis; CNSF, congenital nephrotic syndrome of the Finnish type; Alport +, Alport syndrome and variants; MCD, minimal change disease; FSGS, focal segmental glomerulosclerosis; Collapsing GN, collapsing glomerulonephropathy; Imm/Infl GN, immune and inflammatory glomerulopathies; HTN, hypertensive nephropathy; Diab GN, diabetic glomerulonephropathy; Aging, age-associated glomerulonephropathy. Taken from (Wiggins, 2007).

1.1.2 Glomerulosclerosis-associated chronic kidney diseases

Understanding the pathomechanisms of glomerular diseases requires profound knowledge of podocyte biology. Glomerular injury results in a sequence of events including podocyte injury, dysfunction, and loss. These pathologic events are consistent with an increase of proteinuria and a global glomerulosclerosis. Genetic as well as environmental factors also control the development and maintenance of normal glomerular structure and function by targeting podocytes. The most common forms of glomerular diseases occur in patients with diabetes and focal segmental glomerulosclerosis. Another form is chronic glomerulonephritis caused by systemic disorders (Systemic lupus erythematosus [SLE], Goodpasture's syndrome, and IgA nephropathy) or post-infection by bacteria or viruses. There are also hereditary diseases, e.g. Alport nephropathy, minimal change disease (MCD), and membranous nephropathy (MN) (Figure 3) (Leeuwis et al., 2010; Shankland, 2006; Wiggins, 2007).

1.2 Contributing factors of disease progression in CKD

Progressive renal disease involves glomerulosclerosis and fibrosis in response to renal injury which is caused by various factors of age, immunological reactions, hypoxia/ischemia, endo- and exogenous products, metabolic syndrome, and genetic defects (Kronenberg, 2009). In the processes of inflammation and fibrosis, both glomerular and tubulointerstitial compartments including renal parenchymal cells, infiltrating and resident immune cells, and fibroblasts contribute to disease progression. These cells are major sources of many soluble mediators such as cytokines/chemokines, growth factors, and lipid mediators, which mediate proinflammatory and profibrotic responses (Schlondorff, 2008).

Renal inflammation is not only present in kidney diseases such as glomerulonephritis, and renal vasculitis but also in other types of kidney diseases such as diabetic glomerulosclerosis, renal atherosclerosis, Alport nephropathy, and polycystic kidney disease. Several factors including infectious, toxic, metabolic, ischemic, traumatic, and genetic factors may directly or indirectly trigger tissue injury resulting in renal inflammation (Figure 4) (Anders, 2010).

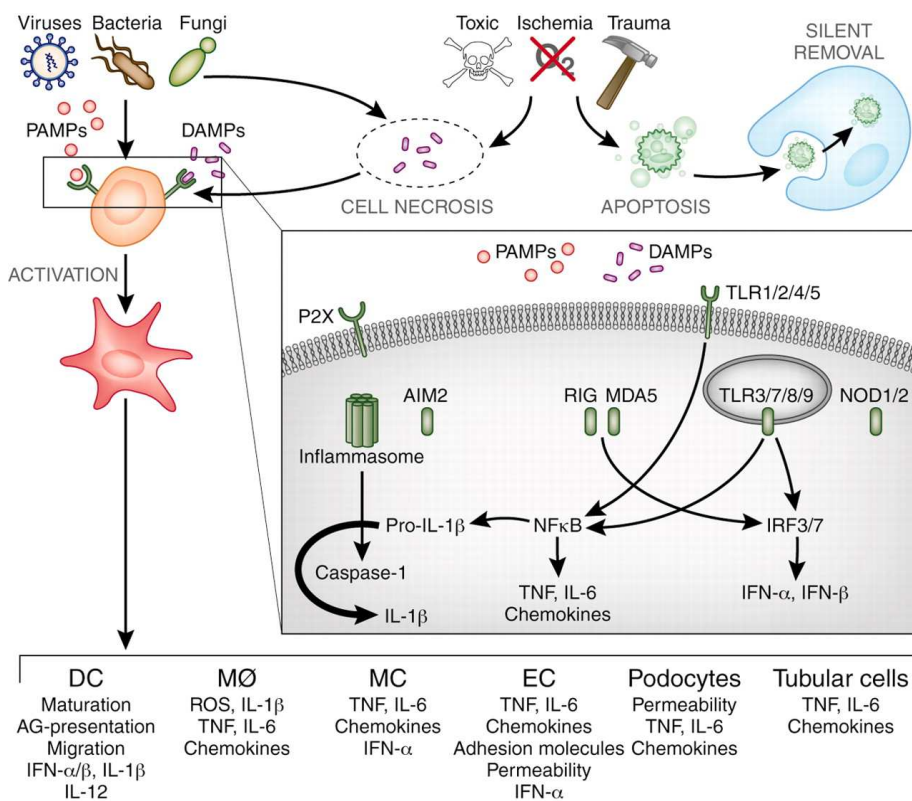


Figure 4. Scheme of factors triggering the disease progression. The pathogen- or non-pathogen factors activate sensors expressed by immune and renal cells to produce a variety of proinflammatory and profibrotic mediators aggravating the disease. Taken from (Anders, 2010).

1.2.1 Leukocyte infiltration in CKD

Monocyte/Macrophage-driven renal inflammation and parenchymal cell loss

Studies have shown that infiltrating immune cells such as lymphocytes, neutrophils, dendritic cells, and macrophages are associated with the progression of kidney disease (Kluth et al., 2004; Ricardo et al., 2008). Circulating monocytes or tissue macrophages are well-known to have a pivotal role in pathogenesis of many kidney diseases. For example, increased number of macrophages has been found in several renal disease models including nephrotoxic or anti-GBM glomerulonephritis (Duffield et al., 2005; Ikezumi et al., 2003), IgG or lupus nephritis (Tesch et al., 1999), renal allograft injury (Jose et al., 2003), ischemia reperfusion injury (IRI) (Bonventre and Zuk, 2004), unilateral ureteric obstruction (UUO) (Kipari et al., 2006), adriamycin nephrosis (Wang et al., 2008), and diabetic nephropathy (DN) (Chow et al., 2004a; Chow et al., 2004b; Ninichuk et al., 2007). These cells contribute to aggravation of renal injury and renal failure by releasing a variety of proinflammatory cytokines, chemokines, nitric oxide (NO), and reactive oxygen species (ROS) that cause inflammation in kidney.

Several interventional studies demonstrated that inhibition of monocyte/macrophage recruitment and their activation reduced renal inflammation and fibrosis. Other evidences using rodent models also provided that depletion (ablation) of monocyte/macrophage attenuated kidney diseases. For example, the effects of liposomal clodronate on renal inflammation and fibrosis have been investigated using several kidney disease models such as IRI and UUO (Jo et al., 2006; Kitamoto et al., 2009). Using CD11b-DTR (Diphtheria toxin receptor) transgenic mice, circulating monocytes and renal macrophages but not Kupffer cells or alveolar macrophages can be depleted and their effect on renal protection has been studied (Duffield et al., 2005; Qi et al., 2008). Inhibition of colony stimulating factor-1 (CSF-1) can modulate monocyte/macrophage accumulation and proliferation. Furthermore, it also decreases tubular cell apoptosis (Lenda et al., 2003; Ma et al., 2009). Chemokine or chemokine receptor antagonists can also be used to block the recruitment of activated monocytes/macrophages. The role of proinflammatory chemokine C-C motif ligand 2/monocyte chemoattractant protein-1 (CCL2/MCP-1) as well as the chemokine C-C motif receptor 2 (CCR2) has been studied in various renal disease models. CCL2/MCP-1 inhibition reduces intra-renal macrophage infiltration and improves lupus nephritis in

MRL/lpr mice (Kulkarni et al., 2009; Kulkarni et al., 2007) and diabetic nephropathy in db/db mice (Ninichuk et al., 2008). CCR2 deficiency or blockade also reduces monocyte infiltrate and renal injury in IRI (Li et al., 2008) or DN (Kang et al., 2010; Sayyed et al., 2011). CCR5 deficiency also improves renal allograft injury by increasing a number of alternatively activated macrophages (Dehmel et al., 2010).

Several evidences indicate multiple mediators produced by macrophages induce apoptosis of renal parenchymal cells including mesangial cells, podocytes, and tubular cells. Duffield *et al.* demonstrated that activated macrophages regulate mesangial cell number via apoptosis. M1 macrophages primed with interferon- γ (IFN- γ), lipopolysaccharides (LPS) or tumor necrosis factor- α (TNF- α) induced apoptosis and suppressed mitosis of mesangial cells (Duffield et al., 2000). Podocyte loss is a sign for kidney disease progression. Leukocyte-mediated inflammation may be a major factor of the podocyte apoptosis. *In vitro* studies show that TNF- α released from M1 macrophages causes down-regulation of nephrin and podocin expression in podocytes (Ikezumi et al., 2008). In addition, macrophages are associated with apoptosis of other types of parenchymal cells such as tubular cells using IRI and UO models. Macrophage accumulation can be blocked using CD11b-DTR transgenic mice or the macrophage colony-stimulating factor receptor (c-fms) inhibitors. The approaches can also inhibit the recruitment of other immune cells, e.g. CD4 Th1 cells, which have a potential to activate macrophages, and lead to the reduction of proinflammatory cytokine such as TNF- α and matrix metalloproteinase-12 (MMP-12), and tubular cell apoptosis in the obstructed kidney (Duffield et al., 2005; Ma et al., 2009; Qi et al., 2008). Another study reported that direct inhibition of the macrophage products, e.g. inducible isoform nitric oxide synthase (iNOS) also reduced tubular cell apoptosis (Kipari et al., 2006). Finally, *ex vivo* programmed M1 macrophage induced more renal injury, whereas M2 macrophage ameliorated chronic inflammatory renal disease in mouse model (Wang et al., 2007).

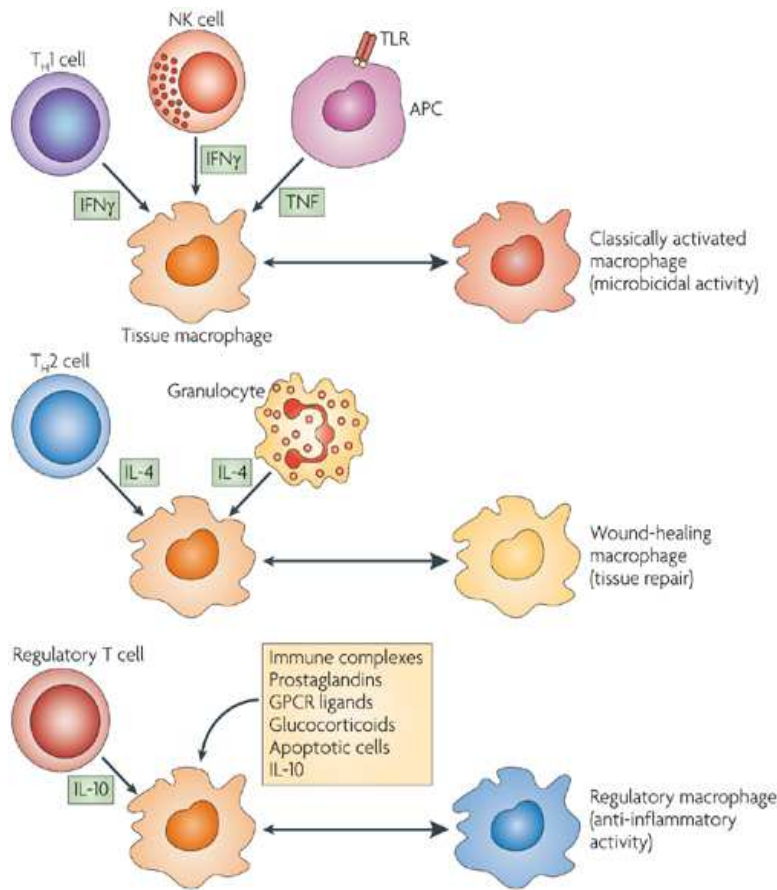


Figure 5. The phenotype switch of macrophages by immune cell-produced cytokines. Classically activated macrophages (M1) arise in response to interferon- γ (IFN- γ), which are produced by T helper 1 (Th1) cells or CD8+ T cells or by natural killer (NK) cells, and tumor necrosis factor- α (TNF- α), which is produced by antigen-presenting cells (APCs). Wound-healing (alternatively activated) macrophages (M2a) arise in response to interleukin-4 (IL-4), which is produced by Th2 cells or by granulocytes. Anti-inflammatory macrophages (M2c) are generated in response to various stimuli including apoptotic cells, glucocorticoids, or IL-10. Taken from (Mosser and Edwards, 2008).

Macrophage phenotypes

Circulating monocytes that originate from bone-marrow myeloid progenitor cells can differentiate into renal macrophages and dendritic cells (DCs). Macrophages are characteristically and functionally classified into two distinct subsets that are described as classically activated (M1) and alternatively activated (M2) macrophages (Figure 5) (Mantovani et al., 2004; Mosser and Edwards, 2008). IFN- γ which is produced by CD4+ T helper 1 (Th1) cells, CD8+ cytotoxic T cells, and natural killer (NK) cells, can activate macrophages either alone or the combination with LPS, TNF- α , and other microbial products. The activated macrophages (M1) can be characterized by enhanced microbicidal capacity and high level of proinflammatory cytokines (e.g. interleukin-12 [IL-12] and IL-23) (Trinchieri, 2003), major histocompatibility complex class II

(MHCII), toxic nitric oxide and reactive oxygen intermediates (ROI) (Mantovani et al., 2004). In contrast to the M1 polarized cells, which have a proinflammatory function, the alternative M2 macrophages are known as antiinflammatory cells. They generally deactivate macrophages via Th2 cell response resulting in tissue remodeling and repair, resistance to parasites, immunoregulation and tumour induction (Gordon, 2003; Gordon and Martinez, 2010). M2 cells are divided into three groups. M2a cells arise in response to IL-4 or IL-13, M2b macrophages are exposed to immunocomplexes and activated with LPS, and M2c macrophages are activated by antiinflammatory molecules such as IL-10, transforming growth factor- β (TGF- β), and glucocorticoids. IL-4 or IL-13 produced by Th2 cells or granulocytes induces the M2a phenotype, which expresses low levels of proinflammatory cytokines and high levels of antiinflammatory cytokines. The synthesis of IL-1 receptor antagonist and the decoy IL-1 receptor (IL-1RII) is increased and mannose and scavenger receptors are also highly expressed. M2a macrophages activated by IL-4 strongly produce chitinase and chitinase-like molecules including Ym-1 (CHI3L3) and Fizz-1 (RELM α). These alternatively activated macrophages inhibit NO synthesis (NOS activity) and enhance to produce polyamines by increasing arginase-1 (Arg-1). M2b macrophages primed with IgG immune complexes are activated by LPS produce high levels of IL-10 and low levels of IL-12. These cells have a more antiinflammatory phenotype, although they also produce MHCII and some proinflammatory cytokines such as IL-1, IL-6, and TNF- α . M2c macrophages termed as deactivated macrophages are induced by IL-10, TGF- β , and glucocorticoids. They produce high levels of IL-10 and adopt an immunosuppressive role contributing to the resolution of inflammation, tissue repair, and matrix remodeling (Gordon and Martinez, 2010; Mantovani et al., 2004; Varin and Gordon, 2009a).

An additional macrophage type, tumor-associated macrophages (TAMs) originate from blood monocytes and mostly occur at tumor sites. Monocytes recruited by tumor-derived factors promote differentiation of monocytes to mature macrophages (M2-like macrophage) and simultaneously block the differentiation of DCs. TAMs can release a vast diversity of growth factors, proteolytic enzymes, cytokines, and inflammatory mediators. Main functions of TAMs are tumor progression and metastasis and show mostly similar characteristics of M2 polarized macrophage by expressing abundant immunosuppressive cytokines such as IL-10 and TGF- β . Moreover, TAMs are poor producers of NO, ROI, and proinflammatory cytokines contrast to M1 macrophages (Coffelt et al., 2009; Sica et al., 2008; Solinas et al., 2009). These cells can sometimes be

termed as myeloid-derived suppressor cells (MDSCs) that expand during cancer, inflammation and infection. Under these pathological conditions, some myeloid precursor cells, which fail to develop functionally competent antigen-presenting cells, differentiate into MDSCs and produce either Arg-1 or iNOS. The phenotypes of MDSCs have been identified as CD11b+Gr1+ in mice, and as LIN-HLA-DR-CD33+ or CD11b+CD14-CD33+ in human. Although most of phenotypes are shared with TAMs, MDSCs can be distinguished from TAMs due to several criteria, for example, high expression of Gr-1, low expression of F4/80, and the expression of both Arg-1 and iNOS (Almand et al., 2001; Gabrilovich and Nagaraj, 2009; Ribechini et al., 2010).

Fibrocytes are another type of monocyte lineage, which share the phenotypic characteristics of leukocytes as well as mesenchymal cells. Generally, these cells are characterized by a distinct cell surface phenotype, for example, the hematopoietic stem cell/progenitor marker CD34, the pan-leukocyte marker CD45, monocyte lineage markers (CD11b, CD13), and fibroblast products (collagen I, fibronectin, and vimentin) (Bellini and Mattoli, 2007; Bucala et al., 1994). Many recent studies indicate that fibrocytes contribute to the renal fibrosis in progressive kidney diseases (Niedermeier et al., 2009; Wada et al., 2007).

1.2.2 Role of tumor necrosis factor- α in CKD

CKD is accompanied by progressive loss of parenchymal cells such as podocytes and tubular epithelia. In Alport nephropathy, the digestion of GBM leads to GBM damage and podocyte loss. The factors which accelerate loss of renal cells may have a role in cellular apoptosis. TNF- α is a pleiotropic cytokine that regulates several cellular responses including proinflammatory cytokine production, cell survival, cell proliferation, and paradoxically, cell death (Varfolomeev and Ashkenazi, 2004). A variety of cell types such as macrophages, lymphocytes, natural killer cells, and epithelial cells secrete TNF- α . It is primarily expressed as a type II transmembrane protein arranged in stable homotrimers. From its transmembrane precursor form, the soluble homotrimeric cytokine (sTNF) is released via proteolytic cleavage by the metalloprotease TNF-alpha converting enzyme (TACE). Three classes of TNFs have been identified: TNF- α , LT- α (lymphotoxin- α also known as TNF- β), and LT- β (Ware, 2005). Soluble TNF- α is a homotrimer of 17 kDa cleaved monomers and transmembrane TNF- α is 26 kDa uncleaved monomers (Tang et al., 1996; Wajant et al., 2003).

Biological functions of TNF- α are initiated by interacting with their membranous receptors: TNF receptor 1 (TNF-R1) and TNF-R2. TNF-R superfamily members are composed of cysteine-rich extracellular domains that bind their respective ligands, and intracellular interaction motifs such as the death domain (DD) and the TNF-receptor associated factor (TRAF)-binding domain. DD containing receptors such as TNF-R1, FAS, and DR3 activate caspase cascade and apoptosis induction by recruiting intracellular adaptor molecules such as FAS-associated death domain (FADD), TNFR-associated death domain (TRADD), and receptor interacting protein (RIP). TNF- α can also activate cell survival and death via nuclear factor-kappa B (NF- κ B) pathway by binding to either TNF-R1 or TNF-R2. These receptors recruit TRAF family molecules to activate both NF- κ B inducing kinase (NIK) and mitogen-activated protein (MAP) kinase (MAPK) kinase-1 (MEKK1), which converge on the I κ B kinase (IKK) signalosome complex. This signaling cascade ultimately leads to NF- κ B nuclear translocation (Figure 6) (Hehlhans and Pfeffer, 2005; Rahman and McFadden, 2006; Wajant et al., 2003).

Pharmacologically, TNF- α signaling can be blocked by biologic agents targeting soluble or transmembranous TNF- α . Anti-TNF agents have been successfully applied to the treatment of patients with a number of immune-mediated inflammatory disorders such as rheumatoid arthritis (RA), ankylosing spondylitis (AS), inflammatory bowel disease (IBD), and psoriasis with or without complicating arthritis (Feldmann and Maini, 2003). Commercially available blockers of TNF- α activity for patient use are, for example, the TNF-specific monoclonal antibodies, infliximab (Remicade®), adalimumab (Humira®), and golimumab (Simponi®). In addition, the PEGylated Fab'antibody fragment certolizumab pegol (Cimzia®) has also been approved for clinical use. Etanercept (Enbrel®) is another biological drug. It is a fusion protein of TNFR2 with the Fc portion of human IgG and it is specific for a soluble TNF (Figure 7). Etanercept is composed of the extracellular region of the two human TNFR2 (p75 TNF receptor) linked to the Fc region (CH2 and CH3 domains) of human IgG1. It consists of 934 amino acids with an approximate molecular weight of 150 kDa. Etanercept inhibits binding both TNF- α and LT α to TNF receptors on the cell surface (Horiuchi et al., 2010; Taylor, 2010).

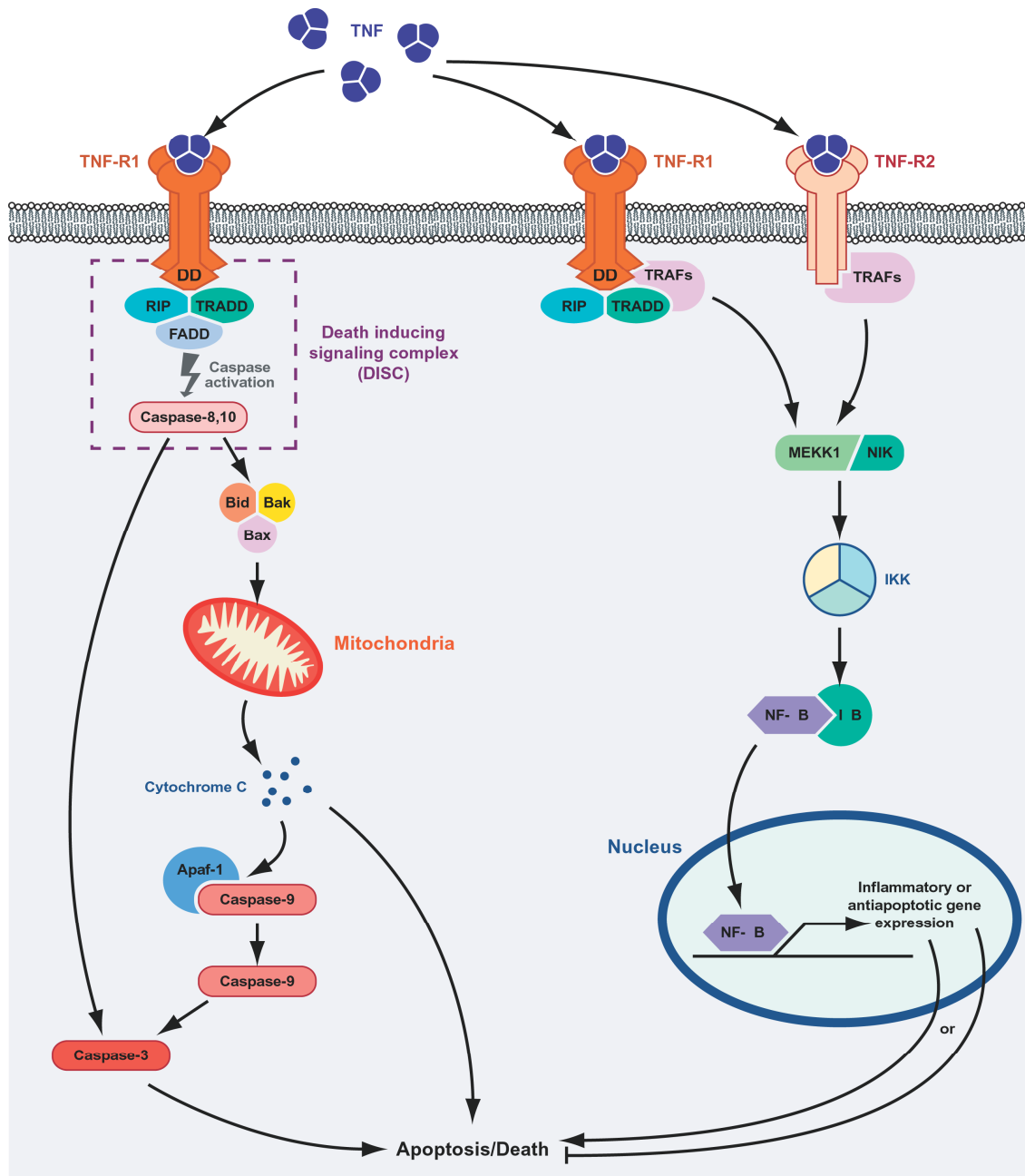


Figure 6. TNF- α -mediated death and survival pathways. TNF- α -mediated death and survival pathways are activated following interaction with the TNFRs. The apoptotic pathway is activated through TNFR1 by forming the DISC, which activates caspases. Activated caspase-8 or -10 then activate proapoptotic Bcl-2 family members, which leads to cell death by releasing cytochrome c from mitochondria and loss of mitochondrial membrane potential (MMP). The NF- κ B-mediated survival pathway is activated by both TNFR1 and TNFR2. Association of TRAFs with these receptors activate signaling proteins like NIK (NF- κ B inhibitor kinase) and MEKK1 (MAPK kinase 1), which activate the inhibitor of NF- κ B (I κ B) kinase (IKK) signalosome complex. IKK phosphorylates I κ B, resulting in the degradation of the inhibitor. The free NF- κ B then translocates to nucleus to induce the expression of inflammatory or antiapoptotic genes. Taken from (Rahman and McFadden, 2006)

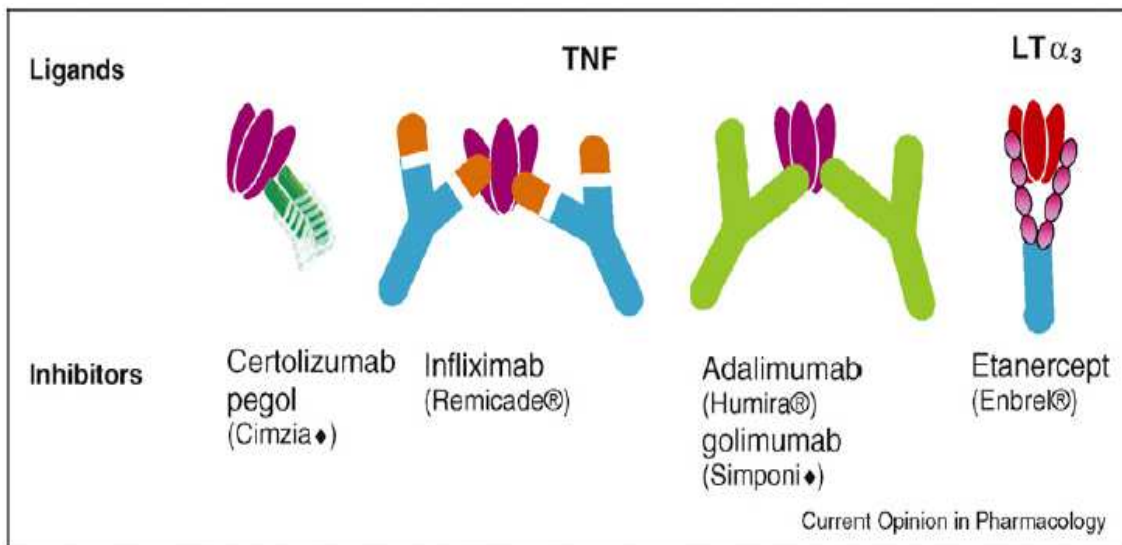


Figure 7. TNF- α -specific antibodies. Certolizumab pegol is a PEGylated Fab antibody fragment. Infliximab is a mouse-human chimeric monoclonal anti-TNF- α antibody of IgG1 isotype. Adalimumab and golimumab are fully human IgG1 monoclonal antibodies. Etanercept is a fusion protein of the extracellular domain of TNFR2 and the Fc region of human IgG1 and binds TNF- α , LT α 3 and LT α 2B1. Taken from (Hoshino et al., 1999; Taylor, 2010).

1.2.3 Pattern recognition receptors and innate immunity

Immune response is a crucial process to defend against invading pathogens and it affects disease pathology. The mammalian immune system consists of two distinct arms, innate and adaptive immunity. Effective cooperation of these two connected systems is essential. The innate immune system is an evolutionarily conserved system to recognize a unique molecular structure on the surface of different pathogens, such as bacteria, viruses, and parasites, using receptors of host cells to eliminate invaders. Innate immune cells express a number of pattern-recognition receptors (PRRs) that recognize microbial molecules known as pathogen-associated molecular patterns (PAMPs) (Janeway and Medzhitov, 2002; Medzhitov and Janeway, 2000). The different classes of PRR families include transmembrane proteins such as toll-like receptors (TLRs), C-type lectin receptors (CLRs), as well as cytoplasmic proteins such as retinoic acid-inducible gene (RIG)-I-like receptors (RLRs) and nucleotide-binding oligomerization domain containing (NOD)-like receptors (NLRs) (Table 3) (Akira et al., 2006; Hoffmann, 2003; Kumar et al., 2009; Medzhitov, 2007).

TLRs are evolutionarily conserved from insects to mammals. 10 and 12 members of the TLR family have so far been identified in humans and in mice, respectively (Akira and

Takeda, 2004; Beutler, 2004; Hoffmann, 2003; Janeway and Medzhitov, 2002). TLR1-9 are conserved in both species. TLR1, TLR2, TLR4, TLR5, TLR6, and TLR11 are expressed on the cell surface and recognize mainly microbial components such as lipids, lipoproteins and proteins. TLR3, TLR7, TLR8, and TLR9 are present exclusively in intracellular compartments such as endoplasmic reticulum (ER), endosomes, lysosomes and endolysosomes and they recognize microbial nucleic acids (Kawai and Akira, 2009). TLRs are type I integral membrane glycoproteins and possess three major domains. The extracellular N-terminal domain, which consists of approximately 16-28 leucine-rich repeat (LRR) motifs. Each LRR consists of 20-30 amino acids with conserved motif "LxxLxLxxN". Furthermore, there is a transmembrane domain and a cytoplasmic signaling domain termed the Toll/IL-1R homology (TIR) domain (Akira and Takeda, 2004).

TLR 4

TLR4 is activated by LPS, the outer membrane glycolipid of Gram-negative bacteria, which promotes innate immune responses (Hoshino et al., 1999; Poltorak et al., 1998). TLR4 is located with MD-2 on the cell surface and the TLR4-MD2 heterodimer is recognized by LPS and initiates signal transduction by intracellular adaptor molecules (Park et al., 2009; Shimazu et al., 1999). LPS also binds additional proteins such as LPS binding protein (LBP) and CD14, a glycosylphosphatidylinositol (GPI)-anchored molecule expressed in monocytes/macrophages. LPS-LBP complex is recognized by CD14 and transferred to the TLR4-MD-2 complex. TLR4 activates two cytoplasmic signal pathways: a MyD88-dependent and a TRIF-dependent pathway (Jiang et al., 2005; Wright et al., 1990).

TLR4 is also involved in the recognition of viral envelope proteins and endogenous ligands, such as heat shock proteins (Hsp60 and Hsp70), the extra domain A of fibronectins, oligosaccharides of hyaluronic acid, heparin sulfate and fibrinogen, although these endogenous ligands require high concentrations to activate TLR4 (Gao and Tsan, 2003; Ohashi et al., 2000).

Table 3. PRRs and their ligands. Taken from (Takeuchi and Akira, 2010)

PRRs	Localization	Ligand	Origin of the ligand
TLR			
TLR1	Plasma membrane	Triacyl lipoprotein	Bacteria
TLR2	Plasma membrane	Lipoprotein	Bacteria, viruses, parasites, self
TLR3	Endolysosome	dsRNA	Virus
TLR4	Plasma membrane	LPS	Bacteria, viruses, self
TLR5	Plasma membrane	Flagellin	Bacteria
TLR6	Plasma membrane	Diacyl lipoprotein	Bacteria, viruses
TLR7			
(humanTLR8)	Endolysosome	ssRNA	Virus, bacteria, self
TLR9	Endolysosome	CpG-DNA	Virus, bacteria, protozoa, self
TLR10	Endolysosome	Unknown	Unknown
TLR11	Plasma membrane	Profilin-like molecule	Protozoa
RLR			
RIG-I	Cytoplasm	Short dsRNA, 5' triphosphate dsRNA	RNA viruses, DNA virus
MDA5	Cytoplasm	Long dsRNA	RNA viruses (Picornaviridae)
LGP2	Cytoplasm	Unknown	RNA viruses
NLR			
NOD1	Cytoplasm	IE-DAP	Bacteria
NOD2	Cytoplasm	MDP	Bacteria
CLR			
Dectin-1	Plasma membrane	β -glucan	Fungi
Dectin-2	Plasma membrane	β -glucan	Fungi
MINCLE	Plasma membrane	SAP130	Self, fungi

TLR, toll-like receptor; LPS, lipopolysaccharides; RIG-I, retinoic acid-inducible gene-I; RLR, RIG- I like receptor; MDA-5, melanoma differentiation-associated gene 5; NOD, Nucleotide-binding oligomerization domain; NLR, NOD-like receptors; MDP, muramyl dipeptide; CLR, C-type lectin receptor; MINCLE, macrophage-inducible C-type lectin.

TLR9

TLR9, an intracellular receptor found in endosomes and lysosomes, recognizes unmethylated 2'-deoxyribo cytidine-phosphate-guanosine (CpG) DNA motifs that frequently exist in bacteria and viruses but are rare in mammalian cells (Hemmi et al., 2000).

Synthetic CpG oligodeoxynucleotides (ODNs) containing CpG DNA motif can directly activate immune cells such as DCs, macrophages, B cells, and NK cells via TLR9 to

release Th1-like cytokines such as IL-12 and IL-18 (Akira et al., 2001). Particularly, high expression of TLR9 by plasmacytoid DCs (pDCs) is a sensor of viral DNA to induce type I interferon response against viral infection, e.g. murine cytomegalovirus, HSV-1 and HSV-2 (Bowie and Unterholzner, 2008; Kawai and Akira, 2006a). TLR9 also recognizes hemozoin, an insoluble crystalline substance formed in the food vacuole of malaria parasite (Coban et al., 2010; Coban et al., 2005).

Other TLRs

Additional TLRs localizing to the cell surface are TLR1, TLR2, TLR5, TLR6, and TLR11.

TLR2 recognizes a variety of microbial components including peptidoglycans, lipoproteins and lipopeptides from Gram-negative bacteria and mycoplasma lipopeptide. TLR2 forms heterodimers with TLR1 or TLR6. TLR2-TLR1 recognizes triacyl-lipopeptides from Gram-negative bacteria and mycoplasma, whereas the TLR2-TLR6 dimer recognizes diacyl-lipopeptides from Gram-positive bacteria and mycoplasma (Akira et al., 2006).

TLR5 is expressed by DCs in the small intestine. The receptor recognizes the flagellin protein from flagellated bacteria (Hayashi et al., 2001). TLR5 in response to flagellin induces the differentiation of naïve T cells into Th17 cells and Th1 cells as well as the differentiation of naïve B cells into immunoglobulin A-producing plasma cells (Uematsu et al., 2008).

Other TLRs, such as TLR3, TLR7, and TLR8 are localized to endolysosomal compartments and recognize nucleic acids from viruses and bacteria (Kawai and Akira, 2009; Takeuchi and Akira, 2010). TLR3 is involved in the recognition of synthetic analogue of double-stranded (ds) RNA, polyinosinic-polycytidylic acid (poly(I:C)) derived from viruses and dsRNA produced during the replication of single-stranded (ss) RNA viruses (Alexopoulou et al., 2001). TLR3 induces anti-viral immune responses by producing type I IFN and inflammatory cytokines. Mouse TLR7 and human TLR7/8 are structurally conserved proteins and they generally recognize ssRNA from RNA viruses and synthetic compounds, imidazoquinolines. TLR7 also recognizes RNA species from bacteria such as Group B *Streptococcus* in conventional DCs and induces type I IFN (Mancuso et al., 2009).

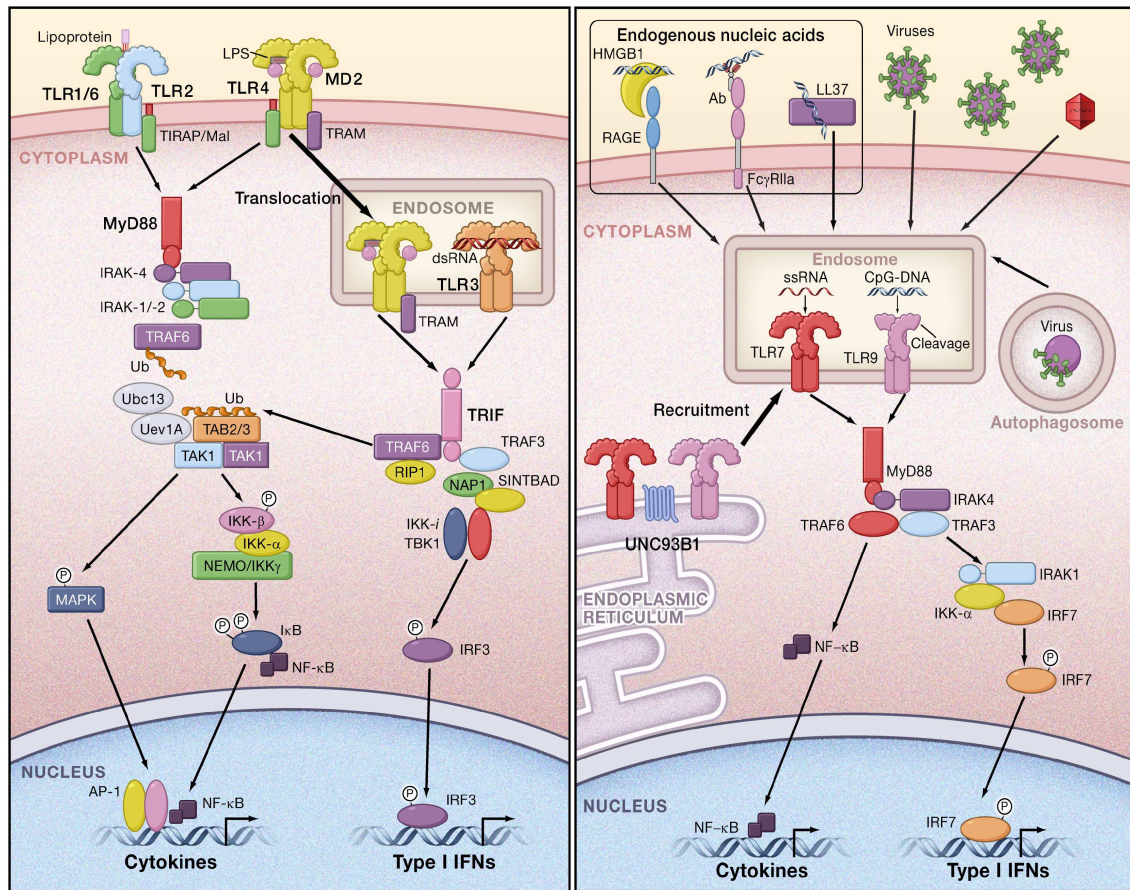


Figure 8. Toll-like receptor signaling pathway. A heterodimer TLR2 and TLR1/TLR6, TLR5/TLR11 (not shown), and 2 sets of TLR4/MD2 complexes are located on the cell surface for ligand recognition. TLR3, TLR7, and TLR9 are located in the endosome. Each receptor specific-ligand stimulation recruits MyD88 and TIRAP to all TLRs except TLR3 and a complex of IRAKs and TRAF6 are subsequently recruited. TLR3 and TLR4 recruit TRIF and TRAF3 subsequently. TRAF6 activates the TAK1, and the activated TAK1 activates IKK complex or the MAPK pathway. The activated TRIF and TRAF3 activate TBK1/IKKi, which activate IRF3 and IRF7. MyD88-dependent or independent signaling pathway ultimately activates the transcription factors such as AP-1, NF- κ B, IRFs inducing proinflammatory cytokine genes and the expression of type I IFN genes. Taken from (Takeuchi and Akira, 2010)

TLR signaling pathway

PAMPs-bound TLRs initiate signaling cascades, which are cell specific and dependent on different TLRs (Figure 8). TLRs form homo- or heterodimers and facilitate the recruitment of TIR domain-containing cytosolic adaptor molecules, such as MyD88, toll-interleukin 1 receptor (TIR) domain containing adaptor protein (TIRAP) (also known as MyD88 adaptor like [MAL]), TIR-domain-containing adapter-inducing interferon- β (TRIF) (also known as TIR domain-containing adaptor molecule [TICAM-1]), TRIF-related adaptor molecule (TRAM, also known as TICAM-2) and sterile-alpha and Armadillo motif-containing protein (SARM). These adaptor molecules are selectively recruited to each TLR. TLR signaling pathway has two distinct pathways depending on the adaptor molecules, MyD88 and TRIF (Akira et al., 2006; Kawai and

Akira, 2006b; Takeda and Akira, 2004; Takeuchi and Akira, 2010). All TLRs with the exception of TLR3 are dependent on MyD88. Certain TLR recruit MyD88 with additional adaptor molecules such as TIRAP or TRAM. For example, TLR1, TLR2, TLR4, and TLR6 recruit TIRAP, which serves as a linker adaptor between the TIR domain of TLR and MyD88. TLR4 binds also TRAM, which further recruits TRIF. Upon stimulation, TLR-MyD88 is recruited to IL-1R-associated kinase (IRAK) family members, a serine/threonine kinase with an N-terminal death domain. IRAK-4 activates IRAK-1 by phosphorylation (Kawagoe et al., 2008) and dissociates from MyD88-TLR complex and associate temporarily with TNFR (TRAF-6) leading to its activation by forming a complex with ubiquitin-conjugating enzymes. TRAF6 activates the kinase complex associating with TGF- β -activated kinase 1 (TAK1), TAK1-binding protein 1 (TAB1), TAP2, and TAP3, which phosphorylates IKK- β complex leading to nuclear translocation of transcription factor NF- κ B. Alternatively, the activated TAK1 complex enhances the activity of the MAPK pathway, which then activates the transcription factor activator protein-1 (AP-1) (Bhoj and Chen, 2009; Kobayashi et al., 2004). MyD88-dependent NF- κ B activation results in the upregulation of proinflammatory cytokine genes including IL-1 β , IL-6, and TNF- α (Yamamoto et al., 2004).

TLR7 and TLR9, expressed by pDCs, also activate the MyD88-dependent pathway to stimulate NF- κ B and AP-1. Additionally, both receptors induce the production of type I IFNs (mainly IFN- α) through the activation of transcription factor IRF7. Direct interaction of MyD88 and IRF7 results in a multiprotein signaling complex with IRAK4, TRAF6, TRAF3, IRAK1 and IKK α . IRF7 is phosphorylated by IRAK1 and/or IKK α and translocated into the nucleus to initiate transcription of the IFN- α gene (Kawai et al., 2004; Kumagai et al., 2009).

Alternatively, MyD88-independent components exist for the TLR4 signaling pathway. The TRAM-co-interacted adaptor molecule, TRIF controls NF- κ B as well as type I IFN in MyD88-independent manner. Upon stimulation with dsRNA, TLR3 directly recruits TRIF and activates additional molecules leading to IFN secretion. TRIF interacts with TRAF6 and RIP1 to activate NF- κ B and MAPKs via TAK1. TRIF also recruits TRAF3 to activate two IKK-related kinases, TBK1 and IKKi, which phosphorylate IRF3 and IRF7. These dimers subsequently translocate to the nucleus resulting in the induction of type I IFN (Hacker and Karin, 2006; Hacker et al., 2006; Yamamoto et al., 2003).

1.3 Alport Syndrome

Alport Syndrome (AS) is a progressive hereditary nephropathy caused by mutations in the genes encoding the $\alpha 3$, $\alpha 4$ or $\alpha 5$ -chains of type IV collagen (COL4), which disturb the normal assembly of GBM (Hudson et al., 1993). AS is characterized by hematuria and proteinuria, progressive renal failure, sensorineural deafness, and ocular lesions (Hudson et al., 1993; Kashtan, 1998). Cecil A. Alport in 1927 reported that progressive hereditary nephritis and deafness were observed in 3 generations of a family and that all males and many females were affected (Alport, 1927). The abnormal GBM structure activates adjacent glomerular cells. Hence, Alport nephropathy is characterized by an increase in glomerular matrix, podocyte detachment, and subsequent glomerular scarring (Heidet and Gubler, 2009; Hudson et al., 2003). Like most other types of chronic kidney disease, later stages of Alport nephropathy are associated with major tubulointerstitial pathology, including mixed interstitial leukocyte infiltrates and interstitial fibrosis (Heidet and Gubler, 2009; Jedlicka et al., 2009).

1.3.1 Structure and distribution of type IV collagen

Upon the discovery of type IV collagen by N Kefalides in 1966 (Kefalides, 1966), six distinct α -chains have been identified as COL4A1-COL4A6. Each of the six chains of collagen IV consists of three domains: a short collagenous domain at the N-terminal (known as 7S domain), a long collagenous domain of Gly-X-Y repeats, and a noncollagenous domain at the C-terminal (known as NC1). Each chain of collagen IV forms three sets of triple helical molecules called protomers, which consist of $\alpha 1\alpha 1\alpha 2(\text{IV})$, $\alpha 3\alpha 4\alpha 5(\text{IV})$ and $\alpha 5\alpha 5\alpha 6(\text{IV})$. These protomers associate at the N-terminus to form tetramers and at C-terminus to form dimers (NC1-to-NC1) (Figure 9) (Hudson et al., 2003). The assembled protomer is flexible and can bend at many triple-helical interruption points in the molecule. The collagen protomers create dimer formation via their NC1 trimers to form hexamers and four 7S domains form tetramers with association of other protomers (Figure 10). Three types of type IV collagen heterotrimers are known to exist in mammalian basement membranes following as $\alpha 1\alpha 1\alpha 2(\text{IV})$ - $\alpha 1\alpha 1\alpha 2(\text{IV})$, $\alpha 3\alpha 4\alpha 5(\text{IV})$ - $\alpha 3\alpha 4\alpha 5(\text{IV})$, and $\alpha 1\alpha 1\alpha 2(\text{IV})$ - $\alpha 5\alpha 5\alpha 6(\text{IV})$.

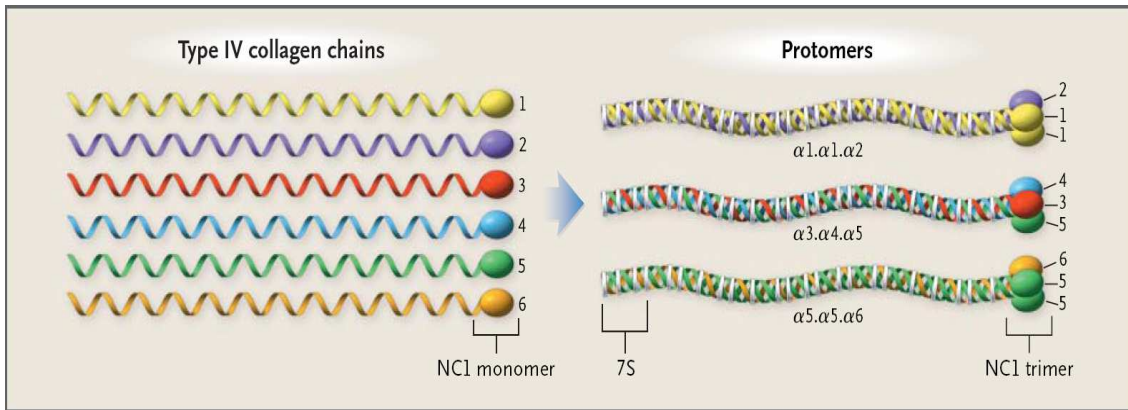


Figure 9. Type IV collagen network formation

Six genetically distinct α chains ($\alpha 1$ - $\alpha 6$) are composed of three domains: a minor amino-terminal 7S domain (about 140 residues), a major triple helical collagenous domain in the middle within Gly-X-Y amino acid sequence (about 1,400 residues), and a carboxyl-terminal noncollagenous domain (about 230 residues). Type IV collagen α chains can be assembled into trimeric protomers called as protomers when the three NC1 domains initiate triple helix interactions. Taken from (Hudson et al., 2003).

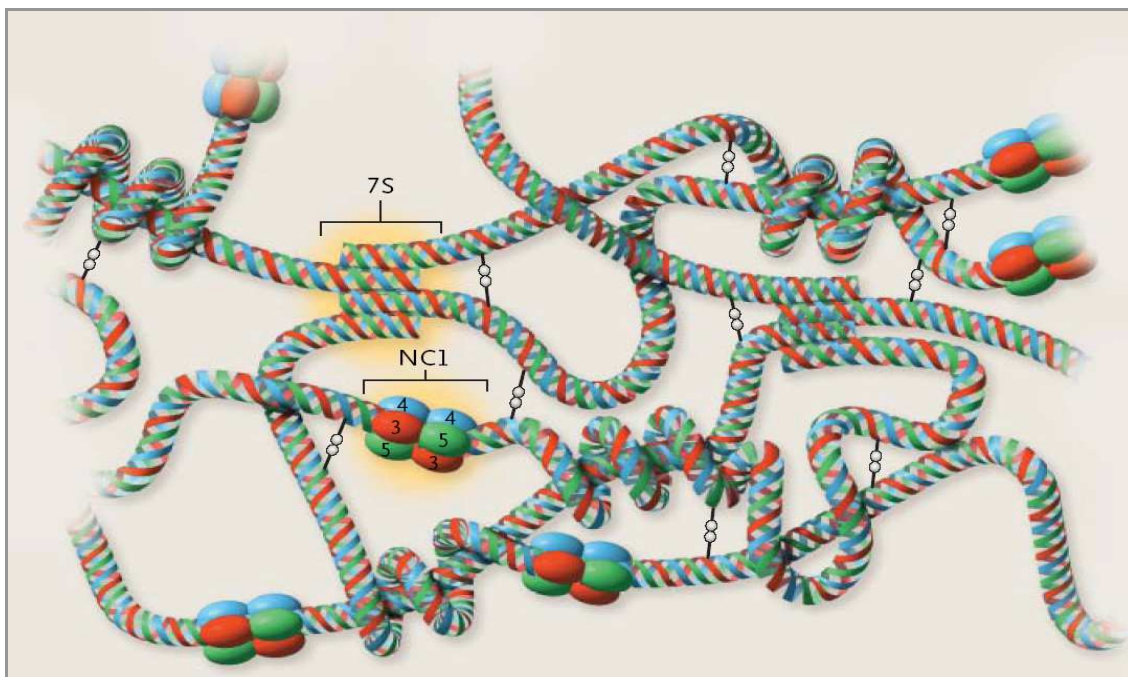


Figure 10. Assembly and network organization of collagen IV protomers

Protomers create basement-membrane networks with other protomers by uniting two NC1 trimers to form an interface hexamer at the C-terminal and by uniting four triple helical 7S domains at the N-terminal. A network composed of $\alpha 3.\alpha 4.\alpha 5$ (IV) protomers is illustrated, showing end-to-end connections of individual protomer units, supercoiling and looping of the triple helices, and disulfide cross-links between triple helical domains. The structure of the NC1 hexamer is determined by the particular α chains that form a triple helical protomer and by the particular canonical protomers that can connect to adjoining protomers (NC1 box). Molecular recognition sequences encoded within NC1 domains govern the selection of partner chains for both protomer and network assembly. The 7S domains also play a key part in determining the specificity, affinity, and geometry of the tetramer formed through the connection of four protomers (7S box). Two other networks are composed of pairs of $\alpha 1.\alpha 1.\alpha 2$ (IV) hexamers or $\alpha 1.\alpha 1.\alpha 2$ (IV)- $\alpha 5.\alpha 5.\alpha 6$ (IV) NC1 hexamers. The $\alpha 3.\alpha 4.\alpha 5$ (IV)- $\alpha 3.\alpha 4.\alpha 5$ (IV) network differs from the others in that it has a greater number of disulfide cross-links between triple helical domains, which increases its resistance to proteolysis. Taken from (Hudson et al., 2003).

Table 4. . Genetic forms of Alport syndrome

Genetic forms	Mutation	Clinical description
X-linked (XLAS)	The most common form (80-85%)	
Adult	COL4A5 gene	Delay onset of renal failure (>30yr of age)
Juvenile	COL4A5 gene	Mild deafness in men; less severe in female carriers Early onset of renal failure (<30 yr of age) Frank deafness and often lenticonus in men
Autosomal recessive (ARAS)	10-15% COL4A3 or COL4A4	Early onset of renal failure (<30 yr of age) in both sexes
Autosomal dominant (ADAS)	Rare form, 5% COL4A3 or COL4A4	Renal failure of varying severity

COL, collagen

The $\alpha1\alpha1\alpha2(\text{IV})$ - $\alpha1\alpha1\alpha2(\text{IV})$ network is found in all basement membranes, whereas other types of the network have a restricted distribution in mammalian tissues. The $\alpha3\alpha4\alpha5(\text{IV})$ network is the predominant component of GBM as well as the Bowman's capsule and the basement membranes of distal and collecting tubules. It is also found in non-kidney parts, e.g. eye and inner ear (Kalluri et al., 1998; Kalluri et al., 1997). The $\alpha1\alpha1\alpha2(\text{IV})$ - $\alpha5\alpha5\alpha6(\text{IV})$ network is present in Bowman's capsule and in basement membranes surrounding smooth muscle cells of vessels and viscera (Borza et al., 2001; Harvey et al., 1998; Yoshioka et al., 1994).

1.3.2 Genetics of Alport Syndrome

Mutations in the $\alpha3$, $\alpha4$, and $\alpha5$ chains of type IV collagen of the basement membranes can cause Alport syndrome. There are three genetic types of Alport syndrome: XLAS (X-linked Alport syndrome), ARAS (autosomal recessive Alport syndrome) and ADAS (autosomal dominant Alport syndrome) (Table 4). XLAS is the most common type that accounts for 80%–85% of the cases and caused by mutations in the COL4A5 gene (Barker et al., 1990; Kashtan, 1998). This gene is located on X-chromosome, therefore, inherited males are severely affected, whereas females are carriers or usually have milder symptoms. The autosomal recessive variant comprises about 15% of the cases, and results from homozygous or compound heterozygous mutations in the COL4A3 or COL4A4 gene (Lemmink et al., 1994; Longo et al., 2002; Mochizuki et al., 1994). A rarely reported form of Alport syndrome is the autosomal dominant Alport syndrome, which is caused by mutations in either the COL4A3 or COL4A4 gene (Pescucci et al., 2004).

1.3.3 Clinical and pathologic features of Alport Nephropathy

Mutations in the COL4A3, COL4A4 or COL4A5 genes result in loss or abnormal assembly of the $\alpha3(\text{IV})$, $\alpha4(\text{IV})$ or $\alpha5(\text{IV})$ chain, respectively. These mutations, therefore, arrest the normal developmental switch from the $\alpha1\alpha1\alpha2$ network to the $\alpha3\alpha4\alpha5$ network causing a failure of formation of the $\alpha3\alpha4\alpha5$ protomer, and lead to an absence of the $\alpha3\alpha4\alpha5$ network which is necessary to create a mature basement membrane. In the glomerulus, these chains are synthesized by podocytes (Heidet et al., 2000). Animal studies for AS have shown that the $\alpha1\alpha1\alpha2$ network is essential for normal glomerular development, whereas the $\alpha3\alpha4\alpha5$ network is not, but is crucial for long-term maintenance of glomerular structure and function (Harvey et al., 1998). The embryonic $\alpha1\alpha1\alpha2$ network is more susceptible to proteolysis by e.g. the matrix metalloproteinase (MMP) family of endopeptidases than the $\alpha3\alpha4\alpha5$ network which is more resistant to proteolysis. Thus, it may explain that Alport GBM is more susceptible to preteolysis because of the absence of the $\alpha3\alpha4\alpha5$ network (Hudson, 2004). Studies of animal and human AS have also documented that the MMP-12 expression was increased in podocytes (Rao et al., 2006a). The progressive proteolysis of GBM leads to irregular thickening of the glomerular membrane and the outer slit diaphragm formed between adjacent podocytes. Ultimately, the GBM deteriorates producing proteinuria. Thus, renal failure in many Alport patients involves the progressive proteinuria leading to glomerulosclerosis including podocyte loss, and tubulointerstitial damage with tubular atrophy and interstitial fibrosis.

Kidneys from patients with Alport syndrome are always affected. The primary observation in all affected males and most of females with XLAS in early childhood is the presence of blood in the urine (hematuria), which is usually persistent microscopic and sometimes shows episodic gross hematuria (Kashtan, 1998). As children with Alport syndrome get older, they develop additional symptoms of kidney disease, e.g. the presence of protein in the urine (proteinuria) and hypertension. Proteinuria occurs in all males with XLAS and in both males and females with ARAS. All teen-aged boys have these symptoms. By contrast, only occasionally they appear in girls with Alport syndrome (Jais et al., 2003; Jais et al., 2000). Progressive increase of proteinuria causes damage to the kidneys and it eventually leads to ESRD in all affected males with XLAS (Jais et al., 2000). Diagnostic renal biopsy studied by electron microscopy indicate diffused irregular thickness of the GBM, consisting of variable thinning and thickening,

as well as splitting or fraying of the lamina densa. Immunohistological analysis by staining for type IV collagen α chains is also available to display the expression of collagen IV α chains.

1.3.4 Animal models of Alport Syndrome

Several animal models of Alport syndrome have been established to understand the disease mechanisms and to provide opportunities for testing potential therapies (Gross and Kashtan, 2009; Kashtan, 2002). Two dog models for the most common type of Alport syndrome (XLAS) have been identified and characterized. A mutation in COL5A5 gene in Samoyed breed has been discovered (Zheng et al., 1994) and a second model has been described in a mixed breed of dogs from Navasota, Texas (Lees et al., 1999). Other canine models for autosomal-recessive and dominant AS have also been found but the mutation has not yet been identified.

Several murine Alport models have also been generated. Autosomal recessive models which have mutations in COL4A3 and/or COL4A4 gene have been developed (Cosgrove et al., 1996; Miner and Sanes, 1996). Recently, another mouse model targeting the COL4A5 gene for XLAS has been produced in the C57BL/6 background (Rheault et al., 2004).

1.3.5 Mouse autosomal recessive Alport model

An autosomal recessive Alport mouse model was generated by gene targeting at the *Col4a3* locus. Two different strains of mouse models are described in both the 129/SvJ and the C57BL/6J background (Cosgrove et al., 2007; Gross et al., 2009).

The onset of glomerular disease and the rates of progression to ESRD are different depending on the genetic background. The rate of progression to ESRD in the 129/SvJ background is much more rapid as compared to the C57BL/6J background (around 3 fold difference on life span, Figure 11A). Identification of GBM composition by e.g. immunostaining of different type IV collagen α chains in Alport mouse kidneys suggests the influence of strain-dependent differences. During development of the murine embryonic GBM, the $\alpha 1\alpha 2(\text{IV})$ collagen network switches to alternative isoform of the robust $\alpha 5\alpha 6(\text{IV})$ network in *Col4a3*-deficient mice in the C57BL/6J background, whereas this is very weak in mice with the 129/SvJ background (Figures 11B and C). (Cosgrove et al., 2007; Gross et al., 2009; Kang et al., 2006).

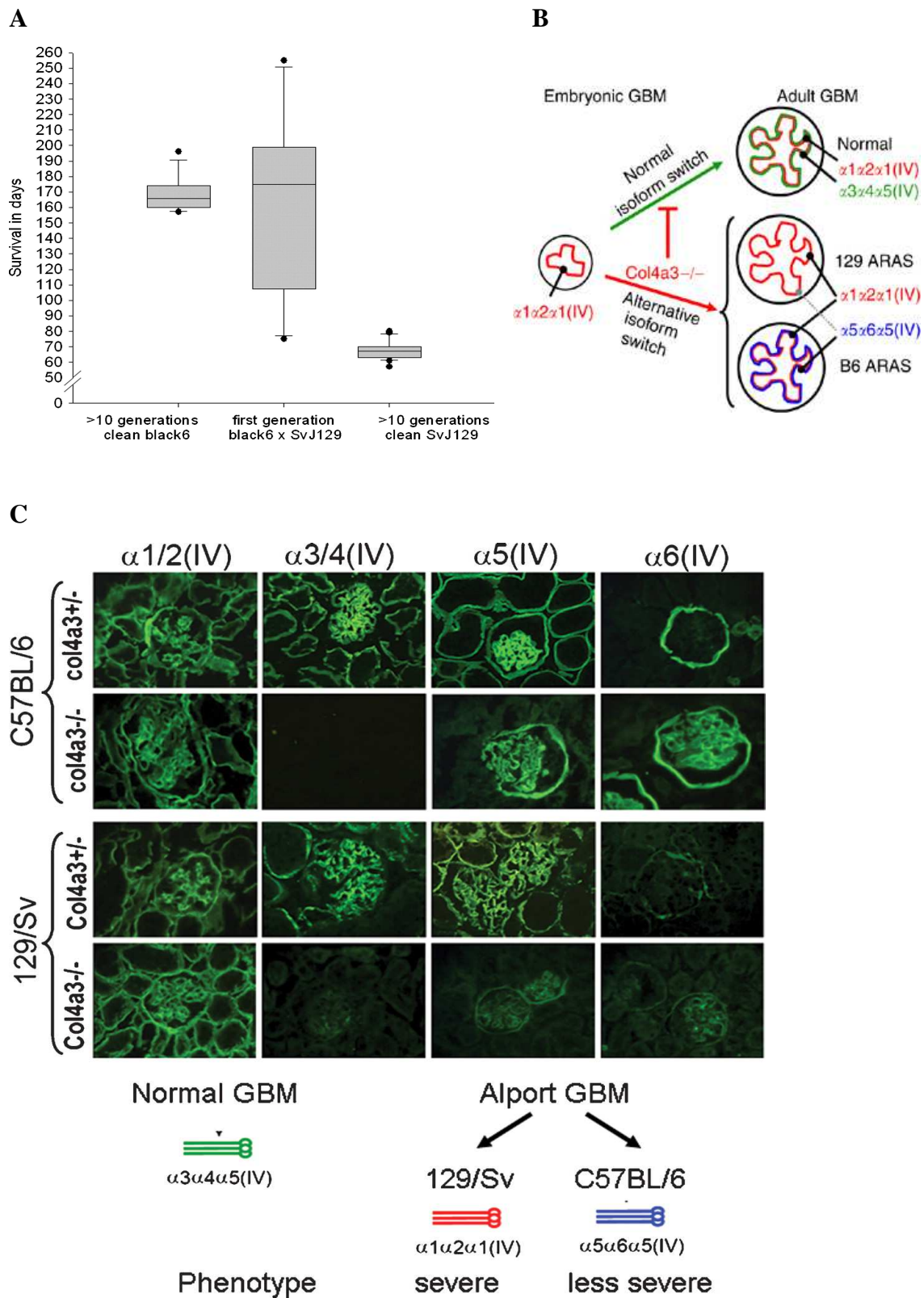


Figure 11. Pathologic and molecular differences depending on the genetic background in *Col4a3*-deficient mice. (A) Life span depends on the different strains. (B) Isoform switches of type IV collagen network (C) Immunostaining of different type IV collagen chains in *Col4a3*-deficient mice kidneys. A and C were taken from (Gross et al., 2009), and B was taken from (Cosgrove et al., 2007).

1.3.6 Treatment of Alport syndrome

Present and future therapeutic targets for CKD might be against inflammation, fibrosis, and glomerular injury (Perico et al., 2008). Particularly, most of glomerular diseases associated with nephrotic syndrome in CKD are characterized by heavy proteinuria leading to glomerulosclerosis (Remuzzi et al., 2006b). Antiproteinuric treatments based on angiotensin (AT) II antagonism are mostly available for regression of glomerular lesions in animals and patients with CKD (Macconi et al., 2009; Perico et al., 2008; Remuzzi et al., 2006a). In Alport syndrome, several animal studies have also suggested potential effect of angiotensin-converting enzyme (ACE) inhibition (Gross et al., 2003; Gross et al., 2004) and AT1-receptor blockade (ARB) (Gross et al., 2003; Gross et al., 2004) because massive proteinuria is main cause of progression of Alport disease. However, till date there are no substantial therapies for human AS. Only ACE inhibition has been shown to be effective in human AS. Recent studies have shown that ACE inhibition delayed the renal failure and improved life expectancy in patients with AS (Gross et al., 2012; Kashtan et al., 2012).

Many other animal studies have also shown that a variety of effective therapies including anti-TGF- β 1 antibody (Cosgrove et al., 2000), inhibition of matrix metalloproteinases (Zeisberg et al., 2006), vasopeptidase inhibition (Gross et al., 2005), HMG-CoA reductase inhibition (Koepke et al., 2007), chemokine receptor 1 blockade (Ninichuk et al., 2005), BMP-7 (Zeisberg et al., 2003), and stem cells (Ninichuk et al., 2006; Sugimoto et al., 2006) to improve Alport kidney disease. However, these approaches have yet to be clinically tested in people with AS. There is a need to understand the pathomechanisms of the progression of AS and to clinically evaluate the novel therapeutic targets for AS. We have tried to understand the role of various factors contributing to podocyte loss in Alport nephropathy. Elevated proteinuria and podocyte loss are main clinically important aspects of AS. It would be worth understanding the contributing factors like infiltrating leukocytes, various proinflammatory cytokines and TLR activation (innate immune response) to podocyte loss. This approach will help us to improve the clinical aspects of patients with chronic kidney disease such as AS. At the same time it helps us to find novel therapeutic targets.

2. Hypothesis/Objectives

Several factors contribute to final remodeling in chronic kidney disease. Here, I used *Col4a3*-deficient mice with Alport nephropathy as a CKD animal model to understand the pathologic mechanisms of disease progression. Alport nephropathy is a non-inflammatory renal disease which involves severe glomerulosclerosis accompanied by progressive loss of parenchymal cells. Podocytes are terminally differentiated glomerular epithelial cells which are rarely replaced after injury. The aim of this study was to determine endogenous and extrinsic factors that might induce podocyte loss during Alport kidney disease in *Col4a3*-deficient mice. Finally, these findings can contribute to identification of novel therapeutic targets for Alport nephropathy.

1. Leukocyte infiltrates are found in Alport mice. It is known that infiltrating leukocytes are the main source of proinflammatory and proapoptotic cytokines/chemokines. Here, I speculated that the proapoptotic cytokine, TNF- α is primarily produced by infiltrating leukocytes and probably by intrinsic renal cells as well. Furthermore, TNF- α contributes to podocyte loss and glomerular injury in the progression of Alport nephropathy.

2. Extrinsic factors, e.g. infections resulting in TLR activation, accelerate the progression of chronic kidney disease by inducing expression of a variety of cytokines, chemokines and proapoptotic factors. Leukocytes and renal cells are known to express a variety of TLRs. First, I hypothesized activation of TLR on renal fibroblasts contributes the aggravation of Alport nephropathy by inducing the expression of proinflammatory and profibrotic molecules.

3. Macrophages may be involved in disease aggravation of Alport nephropathy. I speculated that TLR agonists alter the macrophage phenotypes towards M1 macrophages and worsen the glomerular damage in Alport nephropathy. To address this issue, I determined TLR activation and macrophage phenotype by injecting LPS as a TLR4 agonist and CpG-DNA as a TLR9 agonist into *Col4a3*-deficient mice. I also determined the question whether these factors can regulate TNF- α signaling, which may induce podocyte loss.

3. Materials and Methods

3.1 Materials

3.1.1 Equipment

Balances

Analytic Balance, BP 110 S

Sartorius, Göttingen, Germany

Mettler PJ 3000

Mettler-Toledo, Greifensee, Switzerland

Cell Incubators

Type B5060 EC-CO₂

Heraeus Sepatech, München, Germany

Centrifuges

Heraeus, Minifuge T

VWR Internationl, Darmstadt, Germany

Heraeus, Biofuge primoKendro

Laboratory Products GmbH, Hanau, Germany

Heraeus, Sepatech Biofuge A

Heraeus Sepatech, München, Germany

ELISA-Reader

Tecan, GENios Plus

Tecan, Crailsheim, Germany

Fluorescence Microscopes

Leica DC 300F

Leica Microsystems, Cambridge, UK

Olympus BX50

Olympus Microscopy, Hamburg, Germany

Spectrophotometer

Beckman DU[®] 530

Beckman Coulter, Fullerton, CA, USA

NanoDrop 1000

Thermo Fisher Scientific, Wilmington, DE,
USA

Real-Time PCR System

Light Cycler 480

Roche, Mannheim, Germany

Other Equipments

Homogenizer

IKA GmbH, Staufen, Germany

ULTRA-TURRAX T25

Microtome HM 340E

Microm, Heidelberg, Germany

pH meter WTW

WTW GmbH, Weilheim, Germany

Thermomixer 5436

Eppendorf, Hamburg, Germany

Vortex Genie 2TM

Bender&Hobein AG, Zurich, Switzerland

Water bath HI 1210

Leica Microsystems, Bensheim, Germany

3.1.2 Chemicals and materials

Chemicals

Aceton	Merck, Darmstadt, Germany
Bovines Serum Albumin	Roche Diagnostics, Mannheim, Germany
Calcium chloride	Merck, Darmstadt, Germany
Calcium dihydrogen phosphate	Merck, Darmstadt, Germany
DAPI	Vector Laboratories Inc, Burlingame, USA
D-Glucose	Merck, Darmstadt, Germany
DEPC	Fluka, Buchs, Switzerland
DMSO	Merck, Darmstadt, Germany
EDTA	Calbiochem, SanDiego, USA
Ethanol	Merck, Darmstadt, Germany
Formalin	Merck, Darmstadt, Germany
HCl (5N)	Merck, Darmstadt, Germany
Isopropanol	Merck, Darmstadt, Germany
Magnesium chloride·6H ₂ O	Merck, Darmstadt, Germany
Magnesium sulfate·7H ₂ O	Merck, Darmstadt, Germany
Mercaptoethanol	Roth, Karlsruhe, Germany
Potassium chloride	Merck, Darmstadt, Germany
Potassium phosphate monobasic	Merck, Darmstadt, Germany
Potassium hydroxide	Merck, Darmstadt, Germany
Sodium acetate	Merck, Darmstadt, Germany
Sodium azide	Roth, Karlsruhe, Germany
Sodium chloride	Merck, Darmstadt, Germany
Sodium citrate	Merck, Darmstadt, Germany
Sodium dihydrogen phosphate	Merck, Darmstadt, Germany
Sodium hydrogen carbonate	Merck, Darmstadt, Germany
Sodium phosphate dibasic dihydrate	Merck, Darmstadt, Germany
Tris	Roth, Karlsruhe, Germany
Trypan Blue	Sigma-Aldrich, Steinheim, Germany
Tween 20	Sigma-Aldrich, Steinheim, Germany
Oxygenated water	DAKO, Hamburg, Germany
Xylol	Merck, Darmstadt, Germany

- All other reagents were of analytical grade and are commercially available from Invitrogen, SIGMA or ROTH.

Chemicals for the molecular biology techniques

RNeasy Mini Kit Qiagen GmbH, Hilden, Germany
Invitrogen, Karlsruhe, Germany

ELISA kits

Mouse IL6 BD OptEiA, San Diego, CA, USA
Mouse MCP-1 BD OptEiA, San Diego, CA, USA
Mouse Albumin Bethyl Laboratories, TX, USA
Mouse TGF-beta R &D Systems, Minneapolis, MN, USA

***In Situ* Cell Death Detection Kit, Fluorescein (TUNEL assay)** Roche, Mannheim, Germany

Creatinine FS Diagnostic Systems, Holzheim, Germany
Urea FS Diagnostic Systems, Holzheim, Germany

Cell culture

DMEM-medium GIBCO/Invitrogen, Paisley, Scotland, UK
RPMI-1640 medium GIBCO/Invitrogen, Paisley, Scotland, UK
FCS Biochrom KG, Berlin, Germany
Dulbecco's PBS (1×) PAA Laboratories GmbH, Cölbe, Germany
Trypsine/EDTA (1×) PAA Laboratories GmbH, Cölbe, Germany
Penicillin/Streptomycin (100×) PAA Laboratories GmbH, Cölbe, Germany

Antibodies

anti-CD3ε-FITC (Clone 145-2C11) BD Pharmingen, Heidelberg, Germany
anti-CD4-APC (Clone RM4-5) BD Pharmingen, Heidelberg, Germany
anti-CD8a-PerCp (Clone 53-6.7) BD Pharmingen, Heidelberg, Germany
anti-CD11b-APC or PE (Clone M1/70) BD Pharmingen, Heidelberg, Germany
anti-CD11c-FITC or PE (Clone HL3) BD Pharmingen, Heidelberg, Germany
anti-CD45-PE (Clone 30-F11) BD Pharmingen, Heidelberg, Germany
anti-F4/80-APC (Clone Cl:A3-1) Serotec, Oxford, UK

anti-Ly6C-FITC (Clone AL-21)	BD Pharmingen, Heidelberg, Germany
anti-Ly6G-FITC (Clone 1A8)	BD Pharmingen, Heidelberg, Germany
anti-Ly6G/C (Gr-1)-APC (Clone RB6-8C5)	BD Pharmingen, Heidelberg, Germany
Anti-TNF- α -APC (clone MP6-XT22)	BD Pharmingen, Heidelberg, Germany
anti-CD90-PE (Clone 30-H12)	Acris Antibodies, Hiddenhausen, Germany

Antibodies for immunohistochemistry

Rat anti-CD45	Dianova, Hamburg, Germany
Rat anti-F4/80	Serotec, Oxford, UK
Rat anti-Mac2	Cederlane, Ontario, Canada
guinea pig anti-nephrin	Acris Antibodies, Herford, Germany
Goat anti-TNF- α	R&D Systems, Minneapolis, MN, USA
Rat anti-Wilms Tumor (WT)-1	Santa Cruz, Santa Cruz, CA, USA

Secondary Antibodies for immunohistochemistry

Cy3® goat anti-rat IgG (H+L)	Invitrogen, Karlsruhe, Germany
Alexa Fluor® 488 goat anti-guinea pig IgG (H+L)	Invitrogen, Karlsruhe, Germany
Alexa Fluor® 555 goat anti-guinea pig IgG (H+L)	Invitrogen, Karlsruhe, Germany

Magnetic Activated Cell Sorting (MACS)

Anti-PE MicroBeads	Miltenyi Biotec, Bergish Gladbach, Germany
Mouse CD11b MicroBeads	
MACS LS column	
QuadroMACS™ Separator	

Miscellaneous

Needles	BD Drogheda, Ireland
Nunc Maxisorp ELISA plate	Nunc, Wiesbaden, Germany
Pipette's tip 1-1000 μ L	Eppendorf, Hamburg, Germany
Plastic histosettes	NeoLab, Heidelberg, Germany

Preseparation filters	Miltenyi Biotec, Bergish Gladbach, Germany
Silver Impregnation Kit	Bio-Optica, Milano, Italy
Syringes	Becton Dickinson GmbH, Heidelberg, Germany
Tissue culture dishes Ø 100x20mm	TPP, Trasadingen, Switzerland
Tissue culture dishes Ø 35x10mm	TPP, Trasadingen, Switzerland
Tissue culture flasks 150 cm ²	Becton Dickinson, Franklin Lakes, NJ, USA
Tubes 15 and 50 mL	TPP, Trasadingen, Switzerland
Tubes 1.5 and 2 mL	TPP, Trasadingen, Switzerland

RT-PCR primers Metabion, Martinstried, Germany

Gene	Accession	Sequence	
18s	NR_003278	Forward:	GCAATTATTCCCATGAACG
		Reverse:	AGGGCCTCACTAAACCATCC
Acta2 (α -sma)	NM_007392	Forward:	ACTGGGACGACATGGAAAAG
		Reverse:	G TTCAGTGGTGCCTCTGTCA
Arg1	NM_007482	Forward:	AGAGATTATCGGAGCGCCTT
		Reverse:	TTTTTCCAGCAGACCAGCTT
Ccl2	NM_011333	Forward:	CCTGCTGTTACAGTTGCC
		Reverse:	ATTGGGATCATCTTGCTGGT
Ccl5	NM_013653	Forward:	CCACTTCTTCTCTGGGTTGG
		Reverse:	GTGCCACGTCAAGGAGTAT
Ccl22	NM_009137	Forward:	TCTGGACCTCAAATCCTGC
		Reverse:	TGGAGTAGCTTCTTCACCCA
Colla1	NM_007742	Forward:	ACATG TTCAGCTTTGTGGACC
		Reverse:	TAGGCCATTGTGTATGCAGC
Cxcl10	NM_021274	Forward:	GGCTGGTCACCTTTCAGAAG
		Reverse:	ATGGATGGACAGCAGAGAGC
Fizz-1 (Retnla)	NM_020509	Forward:	CCTTTCATCTGCATCTCC
		Reverse:	CTGGATTGGCAAGAAGTTCC
IL6	NM_031168	Forward:	TGATGCACTTGCAGAAAACA
		Reverse:	ACCAGAGGAAATTTCAATAGGC
IL10	NM_010548	Forward:	ATCGATTTCTCCCCTGTGAA
		Reverse:	TGTCAAATTCATTCATGGCCT

Gene	Accession	Sequence	
IL12 (Il12p35)	NM_008351	Forward:	CTAGACAAGGGCATGCTGGT
		Reverse:	GCTTCTCCCACAGGAGGTTT
IL12 (Il12p40)	NM_008352	Forward:	AGCAGTAGCAGTTCCTGA
		Reverse:	AGTCCCTTTGGTCCAGTGTG
Mrc1	NM_008625	Forward:	ATATATAACAAGAATGGTGGGCAGT
		Reverse:	TCCATCCAAATGAATTTCTTATCC
Nos2 (iNos)	NM_010927	Forward:	TTCTGTGCTGTCCCAGTGAG
		Reverse:	TGAAGAAAACCCCTTGTGCT
Nphs1 (nephrin)	NM_019459	Forward:	TTAGCAGACACGGACACAGG
		Reverse:	CTCTTTCTACCGCCTCAACG
Nphs2 (podocin)	NM_130456	Forward:	TGACGTCCCTTTTTCCATC
		Reverse:	CAGGAAGCAGATGTCCCAGT
Tgf- β 1	NM_011577	Forward:	GGAGAGCCCTGGATACCAAC
		Reverse:	CAACCAGGTCCTTCCTAAA
Tnf- α	NM_013693	Forward:	CCACCACGCTCTTCTGTCTAC
		Reverse:	AGGGTCTGGGCCATAGAACT
Ym1 (Chi3l3)	NM_009892	Forward:	TCTGGGTACAAGATCCCTGAA
		Reverse:	TTTCTCCAGTGTAGCCATCCTT

3.1.4 Solutions

Anesthesia mixture

Isoflurane

Harvard Anesthesia System, UK

Genotyping

1x PBND buffer

50 mM KCL

10 mM Tris-HCL, pH 8.3

2.5 mM MgCl₂

0.01 % w/v gelatin

0.45 % v/v Nonidet P40

0.45 % v/v Tween20

H₂O

Proteinase K

Merck

MACS Buffer

PBS pH 7.2

0.5 % bovine serum albumin

2 mM EDTA

10x PBS, pH 7.4

1.37 M NaCl

27 mM KCl

0.1 M KH₂PO₄18 mM Na₂HPO₄**FACS analysis****FACS-buffer**

500 ml D-PBS + 0.2 % BSA + 0.1 % Na Azide

Paris-buffer, pH 7.4

20 mM Tris-HCl

125 mM NaCl

10 mM KCl

10 mM Na-Acetate

5 mM Glucose

10x HBSS (Hank's balanced saline solution) with Ca, Mg, pH 7.4

54 mM KCl

4.4 mM KH₂PO₄

1.37 M NaCl

3.5 mM Na₂HPO₄·2H₂O42 mM NaHCO₃13 mM CaCl₂4.9 mM MgCl₂·6H₂O4.1 mM MgSO₄·7H₂O

55 mM D-Glucose

10x HBSS without Ca, Mg

54 mM KCl

4.4 mM KH₂PO₄

1.37 M NaCl

3.5 mM Na₂HPO₄·2H₂O

DNase-stock solution (1 mg/ml)

DNase (Type IV) 15.000 U/6 mg, Sigma-Aldrich, Steinheim, Germany

Reconstitute 6 mg of DNase with 6 ml of 50 % glycerol solution.

50 % (w/v) glycerol solution in 20 mM Tris/HCl, pH 7.5, 1 mM MgCl₂

40 mM Tri-buffer in 100 ml H₂O, pH 7.4

50 mM Glycerol 100 % + 20 mM Tris-buffer

1 M MgCl₂

Collagenase/DNase solution

1 mg/ml Collagenase (Type I, Sigma-Aldrich, Steinheim, Germany), 0.1 mg/ml DNase
in 1x HBSS (with Ca, Mg)

10 mg Collagenase

1 ml DNase-stock (1 mg/ml)

9 ml 1x HBSS (with Ca, Mg)

- Warm in waterbath at 37 °C

Collagenase solution

10 mg Collagenase

10 ml 1x HBSS (with Ca, Mg)

- Warm in waterbath at 37 °C

2 mM EDTA

7.44 mg EDTA + 10 ml 1x HBSS (w/o Ca, Mg)

Or 100 µl of 0.2 M EDTA solution + 10 ml 1x HBSS

- Warm in waterbath at 37 °C

3.2 Methods

3.2.1 Animal studies

3.2.1.1 Homing conditions and animal procedures

Col4a3-deficient and wildtype littermate mice in identical 129/SvJ genetic backgrounds were selected from the available Alport disease models because of their consistent phenotype leading to uremic death at about 10 weeks of age (Cosgrove et al., 1996). Mice were housed in filter top cages with a 12 hour dark/light cycle and unlimited access to food (Sniff, Soest, Germany) and water for the duration of the study. Cages, bedding, food, and water were sterilized by autoclaving before use and genotyped as described (Ninichuk et al., 2005). All experimental procedures were performed according to the German animal care and ethics legislation and were approved by the local government authorities.

3.2.1.2 Study design and experimental procedures

For a first study, 4-week-old *Col4a3*-deficient and wildtype mice were treated with intraperitoneal injections of etanercept at 100 µg/mouse 3 days per week for 5 weeks and the other mice were treated with either saline or the same amount of human IgG as a vehicle or a control, respectively. One cohort of *Col4a3*-deficient mice (n=9) was monitored to determine life span and another cohort was sacrificed at 9-week-old for histopathological evaluation.

For a second study, at the age of 4 weeks groups of *Col4a3*-deficient and wildtype mice were started to receive seven intraperitoneal injections on alternate days of either 100 µl normal saline (vehicle), 10 µg of ultrapure LPS (Invivogen, San Diego, CA) in vehicle or 40 µg endotoxin-free CpG-phosphothioate oligonucleotide 1668 (5'-TCG ATG ACG TTC CTG ATG CT-3', TIB-Molbiol, Berlin, Germany) in vehicle. The doses of both TLR agonists were selected because they induced identical serum levels of IL-6 and CCL2/MCP-1 6 hours after intraperitoneal injection. One cohort of mice was bled and sacrificed at 6 weeks of age. Another cohort was followed until death in order to determine life span. An additional cohort of CpG-DNA-treated *Col4a3*-deficient mice was intraperitoneally injected with either saline or 100 µg etanercept (Wyeth, Taplow,

Maidendead, UK) every other day from week 4 to 6 to block TNF- α (Karkar et al., 2001; Lech et al., 2009).

Urine and plasma samples from all mice were collected at weekly intervals and used for renal function estimations.

3.2.1.3 Plasma and urine sample analysis

Blood samples were collected under isoflurane anesthesia by retroorbital bleeding using heparinised capillaries. Plasma was separated using EDTA (10 μ l of 0.5 M solution per 200 μ l of blood) by centrifugation at 8000 rpm for 5 minutes and stored at -20 °C until used for different cytokine estimations.

Urine samples were collected every alternate week or at study termination from each mouse in microcentrifuge tubes and were stored at -20 °C until used for different biochemical estimations as described (Anders et al., 2003b; Sayyed et al., 2009).

Urinary albumin

Urinary albumin levels were determined using albumin ELISA kit from Bethyl laboratories following manufacturer's instructions. Urine samples from mice were diluted 1000 times with assay diluent before estimation. In brief, immuno 96 well solid plate (Nunc, Wiesbaden, Germany) was coated with capture antibody (Anti-Mouse albumin, 1:100 dilution) diluted in carbonate-bicarbonate (pH 9.6) coating buffer and incubated overnight at 4 °C. The plate was washed 3 times with wash buffer (Tris NaCl with 0.05 % Tween 20) and blocked with blocking solution (Tris NaCl with 1 % BSA, pH 8) at room temperature for 1 hour. Blocked plate was washed 5 times with wash buffer and then diluted samples/standards were transferred into assigned wells and further incubated for 1 hour. After incubation the plate was again washed 5 times and diluted HRP-conjugated detection antibody (using the suggested dilution) was added and the plate was incubated in the dark for further 1 hour. After HRP-conjugate incubation was over each well was washed 5 times and 100 μ l of Substrate Solution (1:1, Teteramethylbenzidine (TMB):Hydrogen Peroxide, TMB Substrate reagent, BD Biosciences, Heidelberg, Germany) was added to each well and incubated without plate sealer for about 30 minutes at room temperature in the dark. The reaction was stopped

by addition of stop solution (2 N H₂SO₄). The absorbance was read at 450 nm within 10 minutes of stop solution addition. The albumin content in each sample was determined using the equation of regression line generated by plotting absorbance of different standards against their known concentrations.

Urinary creatinine measurement

Urinary creatinine levels were measured using enzymatic reaction (Jaffe' reaction using biochemical kit from Diasys Diagnostic Systems, Holzheim, Germany). Urine samples were diluted 10 times with distilled water. Different dilutions of standard were prepared using the stock provided with the kit. Working monoreagent was prepared by mixing 4 parts of reagent 1 (R1) and 1 part of reagent 2 (R2) provided with the kit. 10 µl of each of the diluted samples and standards were added to a 96 well plate with flat bottom (Nunc maxisorb plate). 200 µl of monoreagent was added to each well and absorbance was read at 490 nm immediately after and 1 (A1) and 2 (A2) minutes of addition using ELISA plate reader. The change in absorbance (ΔA) was calculated as $\Delta A = [(A2 - A1) \text{ sample or standard}] - [(A2 - A1) \text{ blank}]$. Creatinine content of samples was calculated as:

$$\text{Creatinine (mg/dl)} = \Delta A \text{ sample} / \Delta A \text{ standard} * \text{Concentration of standard (mg/dl)}$$

Urinary albumin to creatinine ratio (UACR)

Urinary albumin to creatinine ratio was calculated after converting values for albumin and creatinine to similar units (mg/dl). Albumin content for each sample calculated (mg/dl) was divided by creatinine content (mg/dl) for the same sample.

Plasma creatinine and blood urea nitrogen determination

Blood urea nitrogen (BUN) in plasma was measured using a commercially available kit (DiaSys Diagnostic Systems). Plasma samples and standard were added to a 96 well plate and 200 µl of monoreagent was added and absorbance of A1 and A2 was read at

360 nm using ELISA plate reader. The change in absorbance (ΔA) was calculated as $\Delta A = [(A1 - A2) \text{ sample or standard}] - [(A1 - A2) \text{ blank}]$. And BUN content of samples was converted from urea content calculated as:

$$\text{Urea (mg/dl)} = \Delta A \text{ sample} / \Delta A \text{ standard} * \text{concentration of standard (mg/dl)}$$

$$\text{BUN (mg/dl)} = \text{Urea (mg/dl)} * 0.467$$

Glomerular filtration rate

Glomerular filtration rate in conscious mice was determined using fluorescein Isothiocyanate-inulin (FITC-inulin) clearance from plasma after single bolus intravenous injection (Ninichuk et al., 2008). In short, 5 % FITC-inulin was dissolved in 0.9 % NaCl facilitated by heating at 65 °C and dialyzed through the 1 kDa dialysis membrane (Spectra/Pro 6, Spectrum Laboratories Inc., Rancho Dominguez, CA) in 0.9 % NaCl overnight at room temperature. Prior to use, the dialyzed solution was filtered through a 0.22 μm filter. Animals were anesthetized using isoflurane for short duration, and 5 % FITC-inulin solution was rapidly injected retroorbitally (3.74 $\mu\text{l/g}$ body weight). Blood samples were drawn at different time point (5, 10, 15, 20, 35, 60 and 90 minutes post inulin injection). Blood samples were centrifuged at 8000 rpm for 5 minutes and plasma was separated. Each plasma sample was buffered to pH 7.4 by mixing 10 μl of plasma with 40 μl of 500 mM HEPES buffer (pH 7.4) in 96 well plates. Fluorescence was determined using excitation filter having wave length of 485 nm while read filter was set at wave length of 535 nm.

For GFR calculation two-compartment clearance was employed. In two compartment model the initial, rapid decay phase represents redistribution of tracer from the intravascular compartment to extracellular fluid. Later, slower decay in concentration of the tracer due to systemic clearance from plasma predominates. At any given time (tx), the plasma concentration of the tracer (Y) can be calculated as

$$\mathbf{Y = Ae^{-\alpha tx} + Be^{-\beta tx} + Plateau}$$

Where,

Y is plasma concentration of tracer

A is y-intercept of fast decay rate (SPAN1)

B is y-intercept of slow decay rate (SPAN2)

α is fast decay rate constant

β is slow decay rate constant

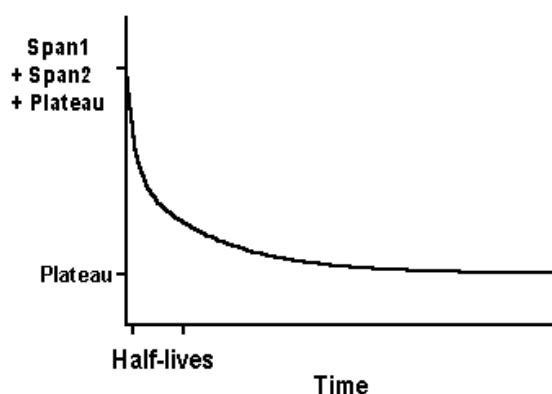


Figure 12. Representation two phase regression curve

These parameters were calculated using non-linear curve-fitting program (GraphPad Prism, GraphPad Software Inc, San Diego, CA, USA) followed by exponential two-phase decay with plateau set as zero.

GFR was calculated as:

$$\text{GFR} = I / (A/\alpha + B/\beta)$$

Calculated GFR was reported as ml/min and was expressed as mean \pm SEM for each group.

3.2.1.4 Immunohistochemical methods and histopathological evaluation

Parts of the kidneys were fixed in 10 % formalin in phosphate-buffered saline (PBS) and embedded in paraffin. 2 μ m sections were cut and processed for staining with periodic acid-Schiff reagent. Glomerular sclerotic lesions were assessed using a semiquantitative score by a blinded observer as follows: 0 = no lesion, 1 = <25 % sclerotic, 2 = 25-49 % sclerotic, 3 = 50-74 % sclerotic, 4 = 75-100 % sclerotic, respectively. 15 glomeruli were analysed per section (Ninichuk et al., 2006).

All immunohistological studies were performed after deparaffinisation. Dehydration was carried out by incubating the sections in xylene, 100 % absolute ethanol, 95 %, 80 % and 50 % ethanol followed by rinsing with PBS (2 changes, 3 minutes each). The following antibodies were used as primary antibodies: rat anti-Mac2 (glomerular macrophages, Cederlane, Ontario, Canada, 1:50), rat anti-F4/80 (interstitial macrophages, Serotec, Oxford, UK, 1:50), rat anti-CD45 (leukocytes, Dianova, Hamburg, Germany, 1:25), rat anti-Wilms Tumor (WT)-1 (podocytes, Santa Cruz, Santa Cruz, CA, USA, 1:25), goat anti-mTNF- α (R&D Systems, Minneapolis, MN, USA, 1:200). For immunofluorescence staining, rat anti-Wilms Tumor (WT)-1 and guinea pig anti-nephrin (Acris Antibodies, Herford, Germany, 1:100) were used as primary staining. Cy3® goat anti-rat IgG (H+L) (Invitrogen), for WT-1 detection and Alexa Fluor® 488 goat anti-guinea pig IgG (H+L) (Invitrogen) for nephrin detection were used as secondary antibodies. Glomerular cell counts evaluated only cells of the tuft from 50 glomeruli and interstitial cells were counted in 15 high power fields (hpf, 400x).

3.2.1.4 Electron microscopy

For ultrastructural analysis, kidney specimens of 6-week-old treated and control mice were dissected and fixed in 0.1 M PBS buffer (pH 7.4) supplemented with 0.4 % paraformaldehyde and 2 % glutaraldehyde. Polymerisation (using fresh Epon resin) was carried out at 60 °C for 24 hours as described (Miosge et al., 1999).

3.2.1.5 TUNEL assay

A terminal deoxynucleotidyl transferase dUTP nick end labeling (TUNEL) assay was performed to quantify apoptotic podocytes. Paraffin sections of the kidney were stained with *In Situ* Cell Death Detection Kit (Roche, Mannheim, Germany) according to the manufacturer's instruction. Nephrin (Acris Antibodies, Herford, Germany, 1:50) was costained as a podocyte marker and Alexa Fluor® 555 goat anti-guinea pig IgG (H+L) (Invitrogen) was used as a secondary antibody.

3.2.2 Cytokines

All cytokine levels in plasma samples obtained from mice or supernatant collected from *in vitro* cell stimulations were estimated using ELISA kits following the manufacturer's instructions.

CCL2/MCP-1 or IL-6 levels in samples were measured using a commercially available ELISA kit (BD Biosciences). Immuno 96 well solid plate (Nunc) was coated with 100 μ l of capture antibody using coating buffer (Phosphate buffer, pH 6.5) and incubated overnight at 4 °C. The plate was washed 3 times with wash buffer (PBS with 0.05 % Tween 20) and was blocked using assay diluent (PBS with 10 % FCS) for further 1 hour at room temperature. After blocking the plate was washed 3 times and 100 μ l of standard and diluted samples in assay diluent were added to respective well and incubated at room temperature for 2 hours. After washing 5 times with wash buffer, 100 μ l of HRP-Conjugated detection antibody (1:250 times diluted in assay diluent) was added and incubated at room temperature in the dark for 1 hour. Final washing step with 7 times was followed and 100 μ l of TMB substrate solution (freshly prepared) was added and incubated for 20 to 30 minutes followed by addition of stop solution (2 N H₂SO₄) and absorbance was read at 450 nm within 10 minutes of stop solution addition. The absorbance in each sample was calculated using the equation of regression line generated with by plotting absorbance of different standards against their known concentrations.

3.2.3 RNA analysis

A small piece of kidney from each mouse was preserved in RNAlater reagent (QIAGEN, Hilden, Germany) and cells for *in vitro* study were collected with lysis buffer containing 1 % of β -Mercaptoethanol using scraper and stored at -20 °C before RNA isolation. Total RNA was isolated from kidney or cells using an RNA extraction kit (QIAGEN) according to the manufacturer's instructions. In brief, 20-30 mg of kidney stabilized in RNAlater reagent was disrupted in 600 μ l of lysis buffer containing 1 % of β -Mercaptoethanol using a conventional rotor-stator homogenizer for 30-40 seconds. The cleared lysate collected by centrifugation at 8000 rpm for 5 minutes was mixed with equal volume of 70 % ethanol. The sample mixture was transferred to a RNA column and centrifuged at 11,000 rpm for 15 seconds. After the lysate was washed with a half

volume of wash buffer I, DNase I mixed in buffer RDD (10 µl DNase I in 70 µl RDD, RNase free-DNase set, QIAGEN) was added and incubated at room temperature for 15 minutes to remove DNase. Remained half volume of wash buffer I was added and further procedures were performed. The RNA was finally eluted in 32 µl of RNase-free water by centrifugation.

The concentration of RNA was determined by measuring the absorbance at 260 nm in a spectrophotometer. RNA samples were diluted in DEPC water (2 µl of RNA + 98 µl of RNase-free water, 50 times dilution) and absorbance was measured at two wavelengths as 260 nm and 280 nm.

$$\text{Amount of RNA } (\mu\text{g}/\mu\text{l}) = \text{O.D. at 260 nm} * 40 * 50 (\text{dilution factor}) / 1000$$

The ratio of optical densities at 260 nm and 280 nm is an indicator for RNA purity (indicative of protein contamination in the RNA samples). Only samples with a ratio of 1.8 or more were considered to be of acceptable quality.

By using NanoDrop spectrophotometer, 2 µl of RNA sample was used to detect its concentration indicating as ng/µl.

The quality of isolated RNA was determined by agarose gel electrophoresis. RNA samples were mixed with RNA loading buffer containing ethidium bromide (Sigma-Aldrich) and were heated at 65 °C for 10 minutes, then were loaded on the 1.5 % agarose gel. After running gel the RNA bands were visualized by UV light and documented. RNA samples showing a single bright band were considered to be of good quality. Loss of RNA integrity could be detected as smear formation in the agarose gel.

3.2.4 cDNA synthesis and real-time RT-PCR (SYBR Green)

After isolation of RNA, cDNA was synthesized using reverse transcriptase (Superscript II; Invitrogen, Carlsbad, CA, USA). 1-2 µg of RNA samples were diluted in DEPC water and incubated at 65 °C for 5 minutes for denaturation. The RNA samples placed on ice were mixed with master mix¹⁾. The samples were incubated at 42 °C for 90 minutes on thermal shaker and the reaction was stopped by heat-inactivation at 85 °C for 5 minutes.

The synthesized cDNA samples were mixed with 2x SYBR Green master mix²⁾, gene-specific forward and reverse primer pair (each primer concentration is 10 pmol/μl), and Taq polymerase

1) Master mix: 5x F_s buffer (Invitrogen), 25 mM dNTPs (Invitrogen), 0.1 M DTT (Invitrogen), RNasin (Promega, Mannheim, Germany), Hexanucleotide (Roche, Mannheim, Germany), Superscript II (Invitrogen) or DEPC water in the case of the control cDNA (RT minus).

2) 2x SYBR Green master mix: 10x Taq buffer without detergent (Fermentas, St. Leon-Rot, Germany), dNTPs (Invitrogen), PCR Optimizer (Bitop, Berlin, Germany), BSA PCR grade (Fermentas), SYBR Green I (Fluka), 25 mM MgCl₂ (Fermentas), and DEPC water.

SYBR Green Dye detection system was used for quantitative real-time PCR on Light Cycler 480 (Roche) using 18s rRNA as a housekeeper gene. Gene-specific primers (300 nM, Metabion, Martinsried, Germany) were used as listed in material part. Controls consisting of DEPC water were negative for target and housekeeper genes. To reduce the risk of false positive crossing point (C_p) the high confidence algorithm was used. The melting curves profiles were analyzed for every sample to detect eventual unspecific products or primer dimers.

For RT-PCR following protocol was used.

Pre-incubation was carried out for 5 minutes at 95 °C so as to activate the polymerase and complete de-naturation of cDNA samples. Followed by amplification for 40 cycles, each comprising of 15 seconds incubation at 95 °C and 45 seconds incubation at 60 °C. For melting curve initial 95 °C for 5 seconds followed by 65 °C for 1 minute with continuous heating was used. The RT-PCR for the reference genes (18S rRNA) was carried out under similar conditions. The C_p values were calculated using the Light Cycler480 and the results were normalized with respective reference gene expression for each sample. In all cases controls consisting of DEPC water were negative for target or reference genes. All designed SYBR green primers for all genes evaluated were obtained from Metabion (Martinsried, Germany).

3.2.5 Flow cytometry

Renal cell suspensions were prepared and stained for flow cytometry using a FACScalibur machine as previously described (Vielhauer et al., 2003). In brief, kidneys were mechanically disrupted and incubated in 1x Hanks' balanced salt solution (HBSS) containing 1 mg/ml collagenase type I and 0.1 mg/ml deoxyribonuclease type I (Sigma-Aldrich) for 20 minutes at 37°C. After washes tissues were incubated in 5 ml 2 mmol/L EDTA in 1x HBSS (without calcium and magnesium) for 20 minutes at 37°C. The supernatant containing isolated cells was kept on ice and for a second enzyme step the remaining pellet was incubated in 5 ml of 1 mg/ml collagenase I in 1x HBSS for 20 minutes at 37°C. The suspension was subsequently passed through a 19-gauge, 27-gauge needle, and pooled with the first supernatant from the EDTA incubation. Cells were filtered through a 70-µm cell strainer (BD, Heidelberg, Germany) and washed twice in PBS. All washing steps were performed in FACS buffer (PBS containing 0.2 % of BSA and 0.1 % of NaAzide). Renal leukocytes were characterized by using the following antibodies: PE-conjugated anti-CD45 (clone 30-F11, BD), PE- or allophycocyanin-conjugated anti-CD11b (clone M1/70, BD), FITC-conjugated anti-CD3ε (clone 145-2C11, BD), anti-CD11c (clone N418, Serotec, Oxford, UK), anti-Ly6G (clone 1A8), anti-Ly6C (clone AL-21, BD), allophycocyanin-conjugated anti-CD4 (clone RM4-5, BD), F4/80 (clone CL:A3-1, Serotec, Oxford, UK), anti-Ly6G and C (clone RB6-8C5, BD), and PerCp-conjugated anti-CD8a (clone 53-6.7, BD).

3.2.6 Isolation of renal macrophages

In brief, kidneys were finely minced and digested for 30 minutes at 37°C with 1 mg/ml collagenase type I and 0.1 mg/ml deoxyribonuclease type I (Sigma-Aldrich) in HBSS. The digested tissues were washed and filtered through 30 µm nylon mesh filter to remove debris and cell segments. Renal CD11b⁺ macrophages were isolated using microbead-conjugated antibodies (Miltenyi Biotech, Bergisch-Gladbach, Germany). Magnetic bead separation was done according to the manufacturer's instructions.

3.2.7 Protein isolation and Western blotting

Protein from kidney tissues was extracted with lysis buffer (50 mM Tris HCL, 150 mM NaCl, 100 μ M sodium ortovanadate, 0.5% sodium deoxycholate, 4 % NP 40, 2 % Triton X-100, 5 mM EDTA, 300 mM sucrose and protease inhibitors). After determination of protein concentrations, 50 μ g of the protein was mixed with 5x SDS loading buffer (100 mM Tris-HCl, 4% SDS, 20% glycerol, and 0.2% bromophenol blue) for Western blot analysis. Samples were heated at 95°C for 5 minutes. Proteins were separated by SDS PAGE and then transferred to a polyvinylidene difluoride membrane. Nonspecific binding to the membrane was blocked for 2 h at room temperature with 5% BSA in Tris-buffered saline buffer (20 mM Tris-HCl, 150 mM NaCl, and 0.1% Tween 20). The membranes were then incubated overnight at 4°C with goat anti-mouse TNF- α (R&D systems) or rabbit anti- β actin (Cell Signaling, Danvers, MA). After washing, the membrane was incubated with a peroxidase-conjugated donkey anti-goat IgG (Dianova, Hamburg, Germany) in Tris buffered saline buffer. The signals were visualized by an enhanced chemiluminescence system (Amersham, Buckinghamshire, UK).

3.2.8 *In vitro* studies

Isolation of renal interstitial fibroblasts

Renal fibroblasts were prepared as previously described (Clayton et al., 1997). In brief, kidneys were harvested from 129/SvJ wild type mice. Minced kidneys were passed through cell strainers (70 and 30 μ m) and incubated in normal cell culture medium at 37 °C, 5 % CO₂ for 1 to 2 hr to deplete monocytic cells or lymphocyte-like cells. The cells were cultured in Duplecco's modified Eagle medium (DMEM) supplemented with 10 % fetal calf serum (FCS) and 1 % penicillin-streptomycin 100 U/ml and 100 μ g/ml. After several passages until overgrowing of fibroblasts, positive selection of fibroblasts was isolated by magnetic cell sorting technique (MACS separation, Miltenyi Biotec, Bergish Gladbach, Germany). Cells were stained with primary PE-conjugated antibody (monoclonal anti-mouse CD90, Clone 30-H12, Acris Antibodies, Hiddenhausen, Germany) in 100 μ l buffer containing PBS pH 7.2, 0.5 % BSA and 2 mM EDTA at 4 °C for 10 minutes in the dark. The cells were washed by adding 1-2 ml of buffer and centrifuged twice. Pellets were resuspended in buffer mixed with anti-PE microbeads and incubated at 4 °C for 15 minutes in the dark. The collection of labeled cells was

carried out by passing through MACS LS column. After separation cells were characterized by FACS analysis.

Cells were treated with either medium or various stimuli; Pam3CysSK4 (Invivogen, San Diego, CA), ultrapure LPS (Invivogen), CpG-ODN 1668 (TIB Molbiol, Berlin, Germany), and TNF- α (ImmunoTools, FireSoythe, Germany). Total RNA and cell culture supernatants were harvested after 24 or 48 hours for real time RT-PCR and ELISA, respectively.

Isolation of bone marrow-derived macrophages

Bone marrow-derived macrophages were prepared from 129/SvJ wild type or *col4a3*-deficient mice as described (Davies and Gordon, 2005; Zhang et al., 2008) with some modifications. Bone marrow from tibia and femur was collected by flushing with DMEM and red blood cells were removed by incubating in 0.155 M NH₄Cl. Washed cells were resuspended in 1x HBSS and cultured in DMEM supplemented with 10 % FCS, 1 % penicillin-streptomycin, and 5 ng/ml of M-CSF (ImmunoTools) or 20 % L929 culture supernatant containing CSF at 37 °C, 5 % CO₂. Every 2 day the medium was changed (Boltz-Nitulescu et al., 1987). After 6-7 days cells were used for stimulation. Macrophages were characterized by flow cytometry using fluorescently labeled antibodies (PE-conjugated anti-CD11b, allophycocyanin-conjugated anti-F4/80). The subset of macrophages were identified by double positive population of CD11b and F4/80 and distinguished from other cell types by using FITC-conjugated anti-CD3 as a T cell marker, PE-conjugated anti-CD11c (clone HL3, BD Biosciences) as a dendritic cell marker, and allophycocyanin-conjugated anti-Ly6G/C as a granulocyte (neutrophils) marker.

Cells were incubated with 2.5 % FCS contained-medium, LPS or CpG-DNA at various concentrations for 24 hours before harvesting total RNA or cell culture supernatants, respectively.

3.2.6 Statistical analysis

Paired Student's t-test was used for the comparison of single groups. A value of $p < 0.05$ was considered to indicate statistical significance. Survival curves were compared by Kaplan-Meier analysis by log-rank two-tailed testing.

4. Results

4.1 Endogenous factors contributing to Alport nephropathy

4.1.1 Leukocyte infiltration of Alport nephropathy in *Col4a3*^{-/-} mice

Alport disease is characterized by progressive glomerulosclerosis and subsequent progressive tubulointerstitial injury, leading to ESRD. In 6-week-old *Col4a3*-deficient mice, CD45⁺ leukocytes accumulate in the glomerular and in the tubulointerstitial compartment during the progression of Alport nephropathy (Figure 13).

Hence, we first determined the leukocyte accumulation of Alport nephropathy during aging and then characterized the leukocyte subsets of kidney cell suspensions by flow cytometry (Figure 14A). The number of renal CD45⁺ leukocytes increased from 4-week-old *Col4a3*-deficient mice and the leukocytes were remarkably detected at 6 and 9 weeks of age (Figure 14B). The leukocyte subsets in CD45⁺ gated cells were characterized by using additional surface markers. F4/80⁺/CD11c⁺ and F4/80⁻/CD11c⁺ dendritic cells as well as F4/80⁺/CD11c⁻ macrophages were the largest leukocyte populations in kidneys of *Col4a3*-deficient mice. CD3⁺/CD4⁺ and CD4⁺/CD8⁺ T cells and Gr-1⁺/Ly6G⁺ neutrophils were also present in kidneys of *Col4a3*-deficient mice (Figure 14C). Thus, the progression of Alport nephropathy is associated with leukocytes infiltrates, especially of macrophages and dendritic cells.

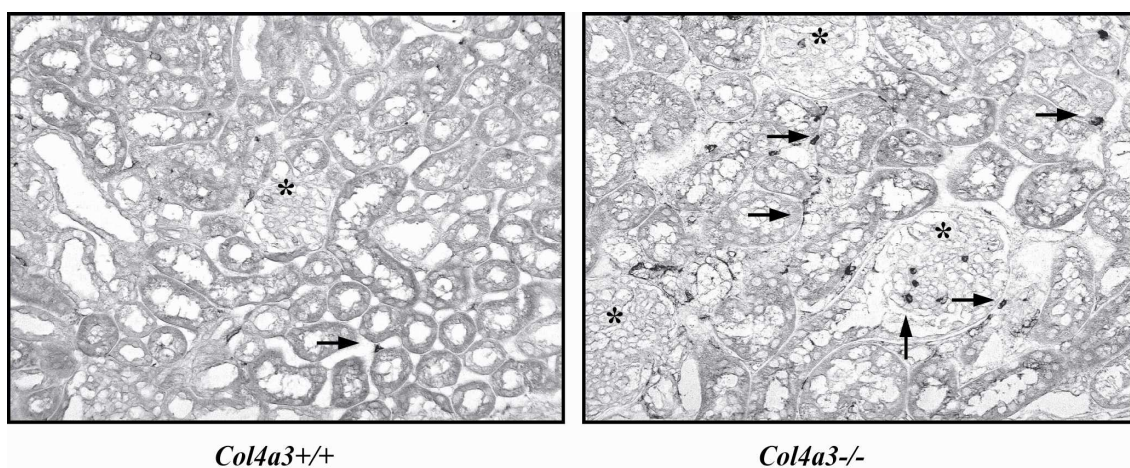
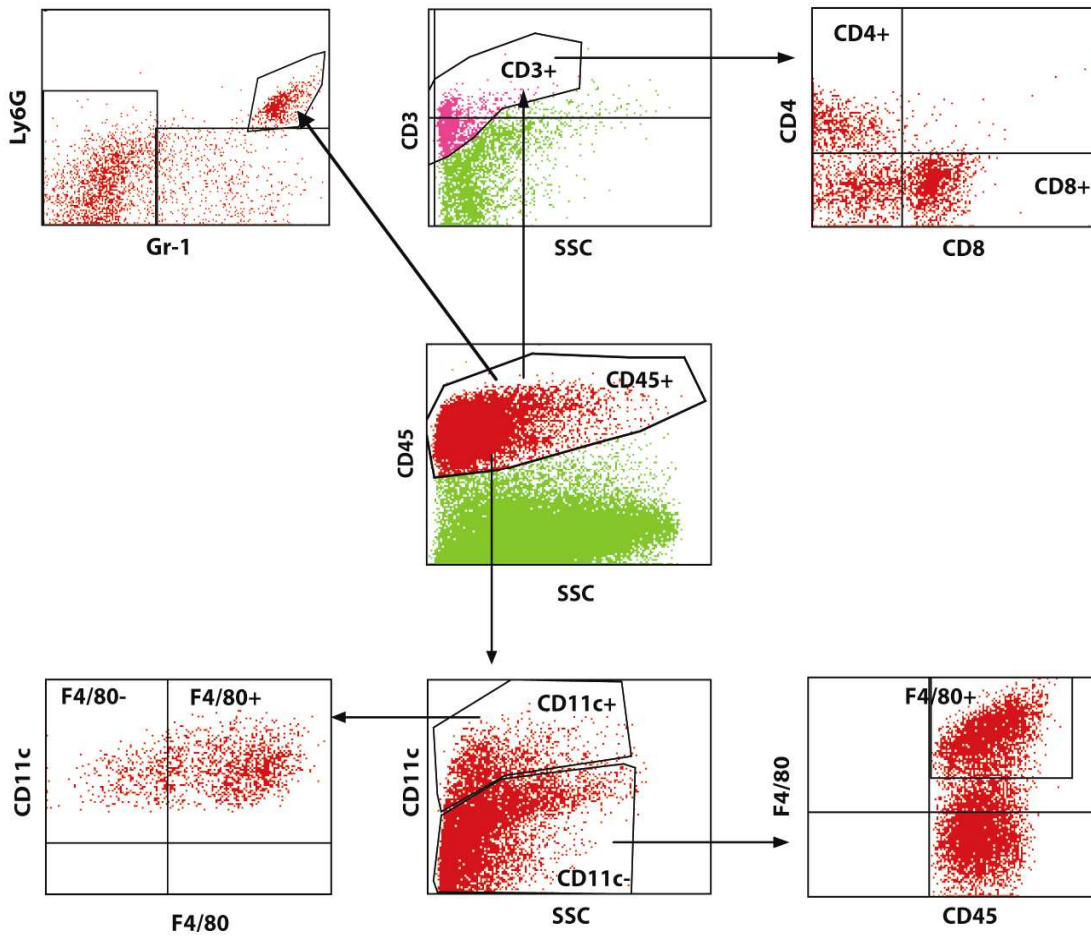
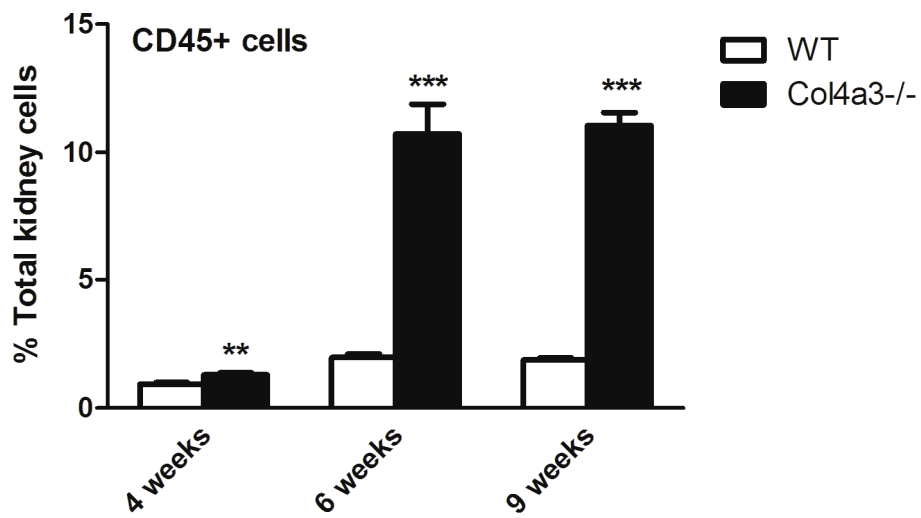


Figure 13. Histopathology of *Col4A3*-deficient mice.

Renal sections were obtained from 6-week-old wildtype and *Col4a3*-deficient mice and stained for CD45 to identify infiltrating leukocytes. Representative images are shown and glomeruli are indicated by asterisks and CD45⁺ cells are indicated by arrows. Note that CD45⁺ cells infiltrate glomeruli and the interstitial compartment of *Col4a3*-deficient mice. Original magnification x200.

A**B**

C

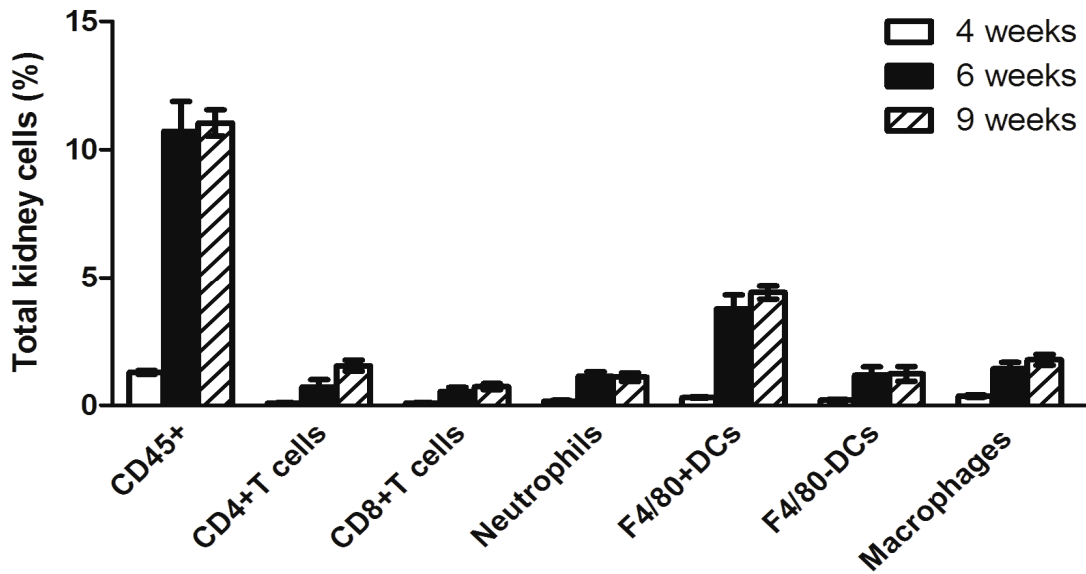


Figure 14. Infiltrating leukocytes in murine Alport nephropathy.

Renal cell suspensions were prepared for leukocyte flow cytometry from 4, 6, and 9-week-old wildtype and *Col4a3*-deficient mice as described in Methods. (A) Examples of flow cytometry dot plots to characterize individual CD45+ cell populations in total renal cell suspension. CD4+ T cells: CD45+/CD3+/CD4+/CD8-, CD8+ T cells: CD45+/CD3+/CD4-/CD8+, Neutrophils: CD45+/Ly6G+/Gr-1+, F4/80+ DCs: CD45+/CD11c+/F4/80+, F4/80-DCs: CD45+/CD11c+/F4/80-, Macrophages: CD45+/CD11c-/F4/80+. (B) The proportion of CD45+ cell population in total renal cells from 4, 6, and 9 week-old wildtype and *Col4a3*-deficient mice. (C) Intrarenal leukocyte subsets were characterized by additional surface markers as described. Data represent the percentage of all kidney cells \pm SEM from 5-7 mice in each group. * $p < 0.05$, ** $p < 0.01$, *** $p < 0.001$ versus wildtype mice.

4.1.2 TNF- α expression in *Col4a3*^{-/-} mice with Alport nephropathy

The increased leukocyte influx indicates the presence of tissue injury and inflammation in many of progressive kidney diseases and progressive inflammatory responses result in a massive proinflammatory cytokine/chemokine production such as IL-6, CCL2/MCP-1, and TNF- α . TNF- α has inflammatory and apoptotic functions (Varfolomeev and Ashkenazi, 2004), and it is a candidate protein that may be involved in the regulation of renal parenchymal cells, e.g. podocyte. Whether TNF- α is at all expressed during the progression of ‘non-inflammatory’ types of glomerulosclerosis is not known, hence, a functional role of TNF- α for the progression of diseases like Alport nephropathy is at all speculative. We therefore first studied the mRNA and protein expression of TNF- α throughout the progression of Alport nephropathy in *Col4a3*-deficient mice.

To address the expression of TNF- α in Alport nephropathy, we first quantified TNF- α mRNA expression levels in total kidney mRNA on different ages (4, 6, and 9 week) of wildtype (*Col4a3*^{+/+}) and *Col4a3*-deficient mice. While TNF- α mRNA was hardly detectable in wildtype kidneys, *Col4a3*-deficient kidneys significantly upregulated TNF- α mRNA expression (Figure 15A). Western blot confirmed the induction of intrarenal TNF- α at the protein level (Figure 15B). Next we performed immunostaining in order to observe the localization of intrarenal TNF- α expression in 9-week-old *Col4a3*-deficient mice. Staining intensity was most prominent in the glomerular compartment where the predominant TNF-positivity was localized to the mesangium as well as to podocytes (Figure 15C). Together, TNF- α is increasingly expressed during the progression of Alport nephropathy of *Col4a3*-deficient mice, e.g. in glomerular cells including podocytes.

4.1.3 TNF- α expression in intrarenal leukocytes of *Col4a3*^{-/-} mice

Leukocytes have been described as an important source of intrarenal TNF- α expression in other types of kidney diseases (Vielhauer and Mayadas, 2007). To address this issue in Alport nephropathy, we analyzed renal cell suspensions of *Col4a3*-deficient mice by multicolour flow cytometry. The number of intrarenal CD45⁺ leukocytes was markedly elevated from 6 weeks of age and did not increase any further up to 9 weeks of age (Figure 14B). On flow cytometry an increased number of TNF- α expressing cells was positive for mostly CD45⁺ leukocytes in total kidney cell suspension from *Col4a3*-deficient mice as compared to less percent in wild-type mice (Figure 16A) which had much intrarenal leukocyte numbers (Figure 14B). Additional surface staining data indicates that CD45⁺TNF- α ⁺ cells from *Col4a3*-deficient mice was present in all leukocyte subsets including T cells, neutrophils, CD11⁺ dendritic cells and renal macrophages as compared to age-matched wildtype mice (Figure 16B). Together, Alport nephropathy is associated with intrarenal TNF- α expression which originates from renal parenchymal cells, e.g. podocytes, as well as from infiltrating immune cells.

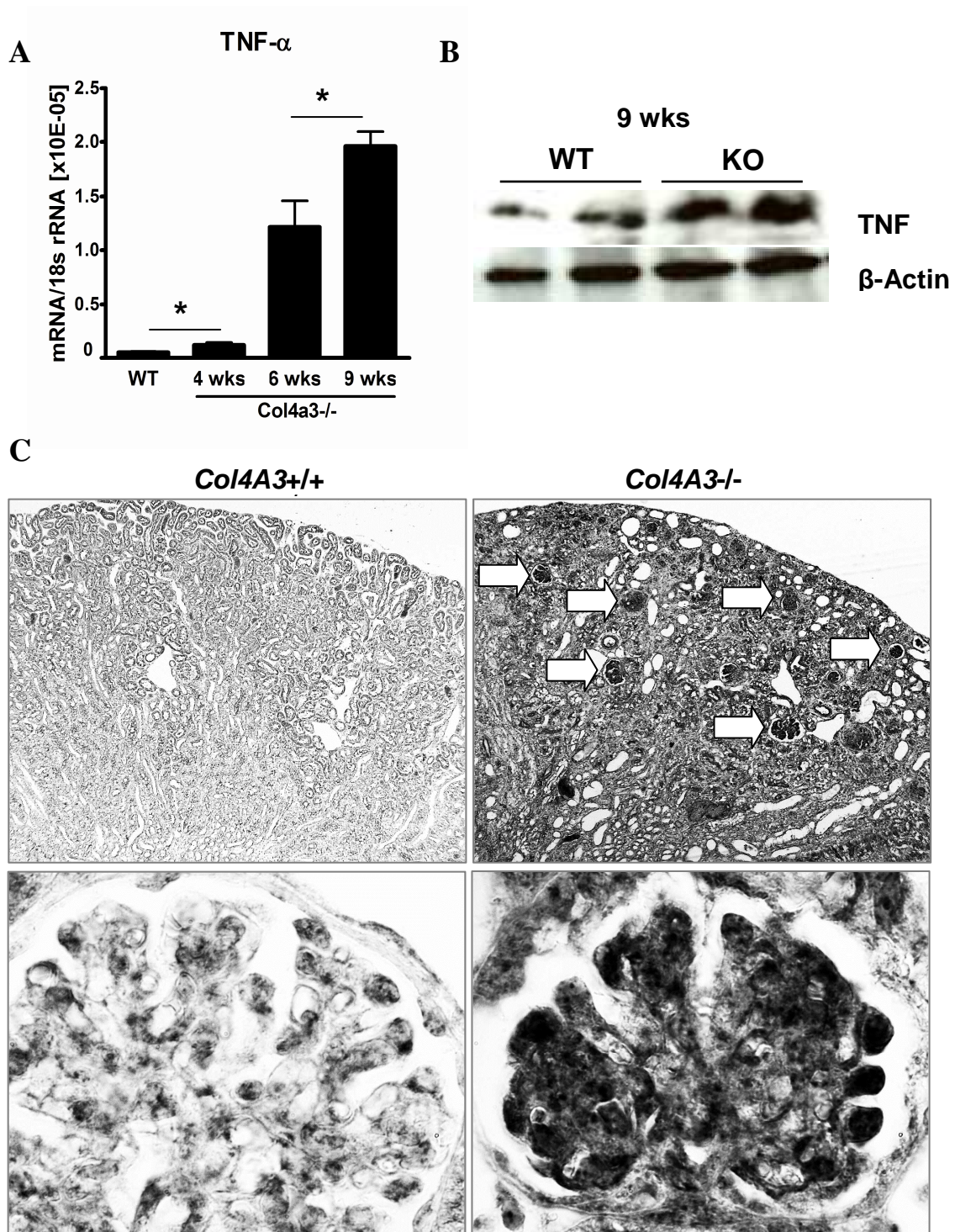


Figure 15. TNF- α expression in murine Alport nephropathy. (A) TNF- α mRNA levels were quantified by real time RT-PCR from renal samples of 4, 6, and 9-week-old wildtype and *Col4a3*-deficient mice as indicated. Data are mean ratios \pm SEM to the respective 18s rRNA. (B) TNF- α protein expression was determined by Western blot on renal protein extracts from 9-week-old wildtype and *Col4a3*-deficient mice, accordingly. Respective β -actin stains are shown as loading control. (C) TNF- α immunostaining in kidneys of wildtype and *Col4a3*-deficient mice illustrated positive staining signals in glomeruli (white arrows in the upper panel, original magnification $\times 100$). At higher magnification (lower panel, original magnification $\times 1000$) TNF- α positivity localizes to the mesangium and to podocytes in *Col4a3*-deficient mice only.

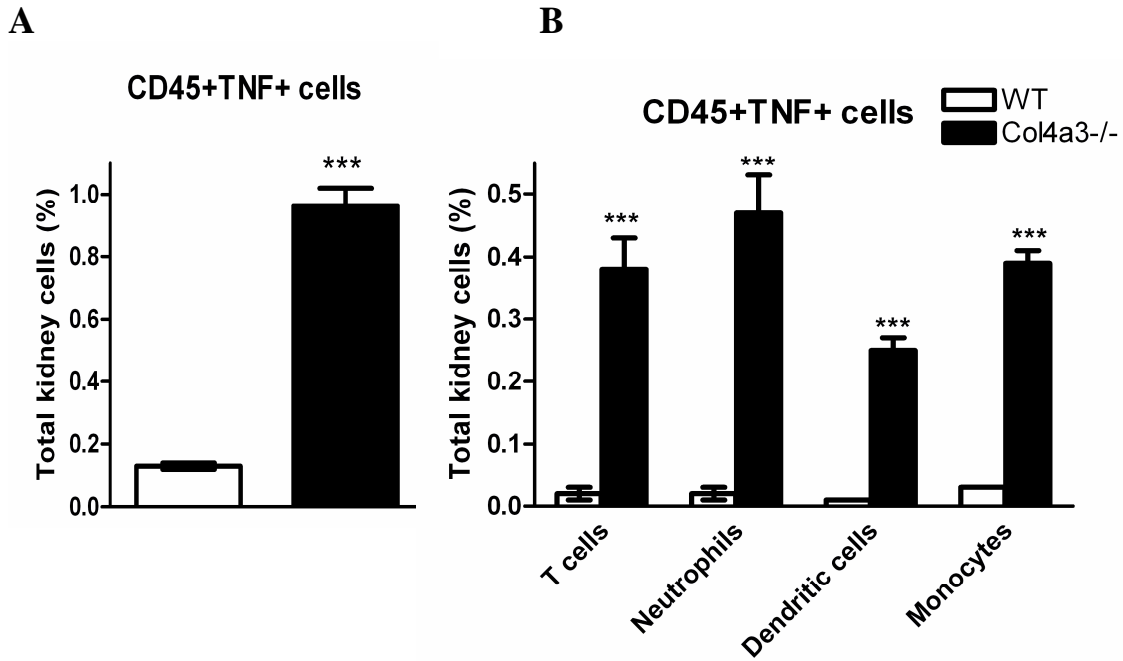


Figure 16. TNF- α -secreting leukocytes in murine Alport nephropathy. Renal leukocytes were identified by flow cytometry for CD45 in kidney cell suspensions of 4, 6, and 9-week-old wildtype and *Col4a3*-deficient mice. (A) Intracellular staining for TNF- α was used to quantify the amount of TNF- α -producing leukocytes. (B) Leukocyte subsets were characterized by additional surface markers. Data represent the percentage of means \pm SEM from 5-7 mice in each group. *** $p < 0.001$ wildtype versus *Col4a3*-deficient mice.

4.1.4 TNF- α blockade prolongs life span of *Col4a3*-/- mice

Given the renal TNF- α expression during the progression of Alport nephropathy, we questioned whether TNF- α itself contributes to renal pathology and renal failure. To address this issue, we randomized 4-week-old *Col4a3*-deficient mice into three groups that either received injections of saline, of 100 μ g etanercept or 100 μ g of human IgG for a period of five weeks. The latter group served as a control group because etanercept is a TNF- α antagonist that consists of a TNFR binding domain linked to the Fc part of human IgG1. The dose of etanercept was chosen by additional experiments with two groups: low dose (50 μ g) for 5 weeks and same dose (100 μ g) for 3 weeks. Finally, best dose and period for longest prolonged life span was selected (data not shown). In a first experiment, all groups were followed to monitor overall survival, which serves as a robust readout parameter for ESRD and uremic death in this model. Etanercept treatment significantly prolonged life span by two weeks, i.e. 20% of total life span of *Col4a3*-deficient mice as documented by a mean survival of 81 days versus 68 days in IgG- or untreated *Col4a3*-deficient mice (Figure 17). Thus, TNF- α blockade with etanercept from 4 weeks of age prolongs the life span of *Col4a3*-deficient mice.

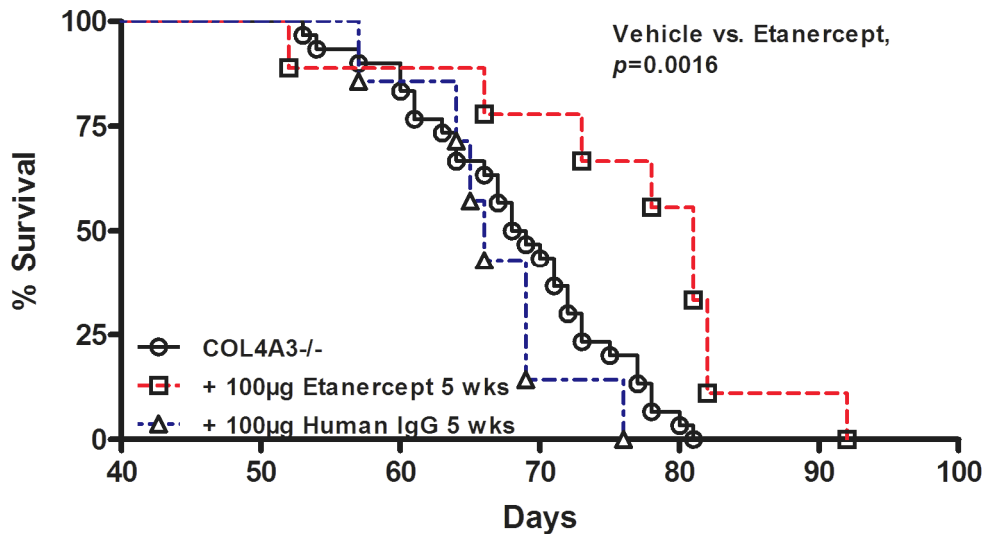


Figure 17. TNF blockade and life span of *Col4a3*-deficient mice. 4-week-old *Col4a3*-deficient mice were received either saline, human IgG or etanercept injections for 5 weeks. Survival time is illustrated as Kaplan-Meier curve. Mean survival is indicated for vehicle and etanercept groups.

4.1.5 TNF- α blockade improves renal function in *Col4a3*^{-/-} mice

To test whether the effect of etanercept on overall survival relates to its effect on renal function, we measured GFR as a marker of the kidney's excretory function at the age of 4, 6, and 8 weeks in mice of all groups. GFR measurements after 2 and 4 weeks of treatment revealed a progressive decline of renal function in untreated *Col4a3*-deficient mice, while TNF- α blockade with etanercept significantly improved GFR compared to their untreated *Col4a3*-deficient mice controls, albeit not reaching the level of wildtype mice (Figure 18A). Consistent with this finding, the progressive increase of plasma creatinine and BUN levels seen in untreated *Col4a3*-deficient mice were significantly reduced by etanercept treatment (Figures 18B and 18C). Proteinuria, a marker of renal barrier function, was determined as urinary albumin-creatinine ratio (UACR). There was a trend towards lower UACR in etanercept treated mice which, however, did not reach statistical significance (Figure 18D). Together, TNF- α blockade with etanercept, prolongs life span of *Col4a3*-deficient mice in association with improved excretory renal function.

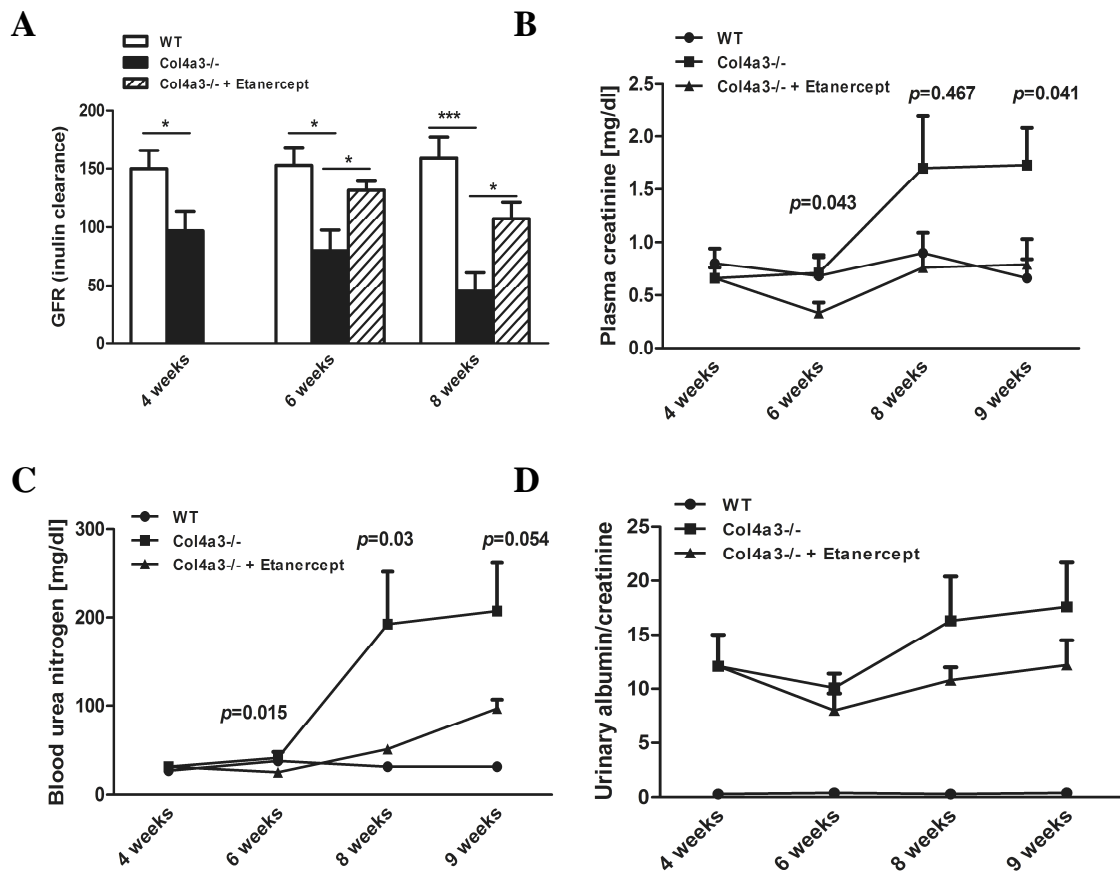


Figure 18. TNF- α blockade and renal function of *Col4a3*-deficient mice. (A) GFR was determined as a functional marker of the glomerular filtration barrier at week 4, 6, and 8 weeks in mice of all groups. Note that etanercept treatment significantly increased GFR as compared to saline-treated *Col4a3*-deficient mice. Plasma creatinine (B), blood urea nitrogen (C), and urinary albumin/creatinine ratios (D) were also determined throughout the study as indicated. Data represent means \pm SEM, * $p < 0.05$, *** $p < 0.001$.

4.1.6 TNF- α blockade protects *Col4a3*-/- mice from glomerulosclerosis

Does the effect of etanercept on the life span and renal function of *Col4a3*-deficient mice relate to renal pathology? To answer this question, we treated a second cohort of mice and performed a cross sectional analysis of all groups at 9 weeks of age. Renal sections from mice of all groups were stained with Periodic acid-Schiff stain (PAS) and the extent of glomerulosclerosis was quantified by a semiquantitative sclerosis score ranging from 0 to 4, describing sclerosis in 0, 1-25%, 26-50%, 51-75%, and 76-100% of glomeruli, respectively. 9-week-old *Col4a3*-deficient mice displayed a significant percentage of glomeruli with scores 3 and 4 indicating severe diffuse glomerulosclerosis. TNF- α blockade with etanercept significantly reduced the percentages of glomeruli with a sclerosis score of 3 or 4 and increased those with a score of 1 and 2 indicating a shift towards less severe glomerular lesions (Figure 19). At the ultrastructural level the

Glomerular ultrastructure

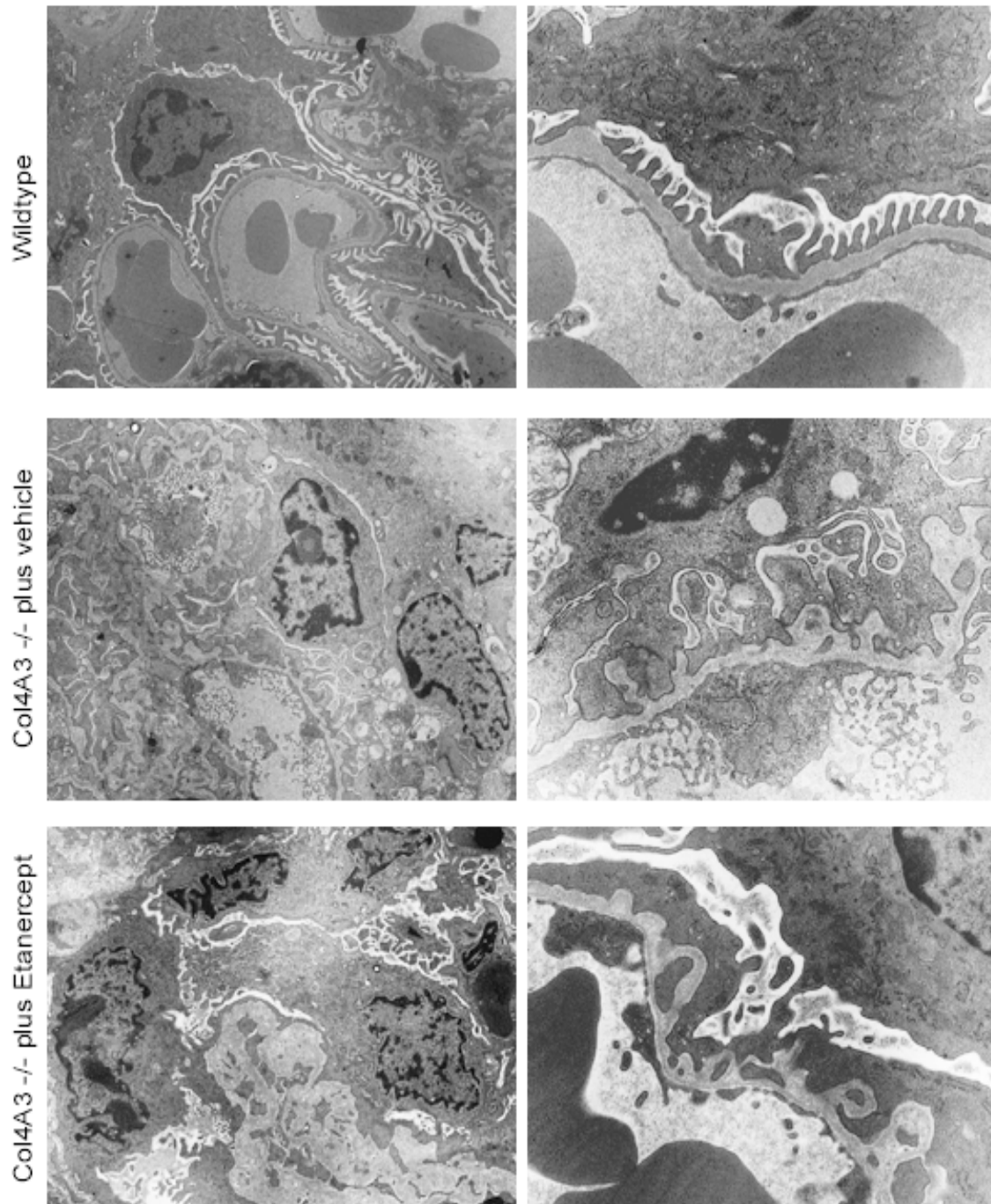


Figure 20. Glomerular ultrastructure in 9-week-old *Col4a3*-deficient mice. The glomerular ultrastructure was assessed by transmission electron microscopy in 9-week-old wildtype and *Col4a3*-deficient mice as indicated. Note that lack of *Col4a3* is associated with irregular GBM thickness and podocyte foot process effacement as compared to age-matched wild-type mice. In addition, collapse of glomerular capillaries and diffuse glomerular matrix expansion indicates advanced glomerulosclerosis. Etanercept treatment reduced glomerular scarring but did not affect the GBM abnormalities and podocyte foot process effacement as noted at high magnification.

4.1.7 TNF- α blockade prevents podocyte loss in *Col4a3*^{-/-} mice

Podocyte loss is the central pathomechanism that drives the progression of glomerular diseases towards diffuse glomerulosclerosis (Kriz and Lemley, 1999; Wharram et al., 2005). Therefore, we questioned whether the progression of Alport nephropathy in *Col4a3*-deficient mice is associated with quantifiable podocyte loss and whether the protective effect of etanercept is associated with increases podocyte numbers. We first used WT-1 immunostaining to quantify glomerular podocytes, a method that has been successfully used in other disease models such as diabetic nephropathy db/db mice. However, we found faint WT-1 positivity also in parietal epithelial cells of mildly affected glomeruli and strong positivity of overgrowing parietal epithelial cells in severely sclerotic glomeruli which did not allow a reliable quantitative assessment of glomerular podocyte numbers (not shown). We therefore used double immunofluorescence for WT-1 and nephrin to identify and quantify glomerular podocytes. Figure 21A illustrates podocytes as nephrin-WT-1 positive cells at their typical location in wild-type mice. In 9-week-old *Col4a3*-deficient mice such nephrin-WT-1 positive podocytes were less frequent and large sclerotic parts of many glomeruli were overgrown by nephrin negative cells (Figures 21B and 21C). Occasionally, nephrin and WT-1 positive intratubular casts were seen, indicating that detached podocytes can become a component of cellular casts (Figure 21D). TNF- α blockade with etanercept significantly increased the numbers of nephrin/WT-1 positive podocytes in that ways that focal sclerosis was far more common as globally sclerotic glomeruli (Figures 21E and 21F). Next we quantified TUNEL/nephrin positive cells in glomeruli to assess apoptotic podocytes. Alport nephropathy was associated with the occurrence of TUNEL positive podocytes which could not be detected in age-matched wildtype control mice (Figure 22). Etanercept treatment significantly reduced the numbers of TUNEL/nephrin positive glomerular cells (Figure 22), indicating that etanercept protected from Alport mice from podocyte apoptosis. Analyzing renal mRNA expression profiles of nephrin and podocin confirmed that TNF- α blockade with etanercept had a podocyte-protective effect as untreated *Col4a3*-deficient mice had decreased expression levels of podocyte markers which were prevented by TNF- α blockade (Figure 23A). By contrast, the mRNA expression levels of proinflammatory genes such as IL-6, CCL2, CCL5, and TNF- α itself were not significantly reduced with TNF- α blockade (Figure 23A). Accordingly, etanercept treatment did not affect renal leukocyte counts in *Col4a3*-deficient mice at the end of the study (Figure 23B). Thereby it limits an essential downstream pathomechanism for progressive glomerulosclerosis of *Col4a3*-deficient mice with Alport nephropathy.

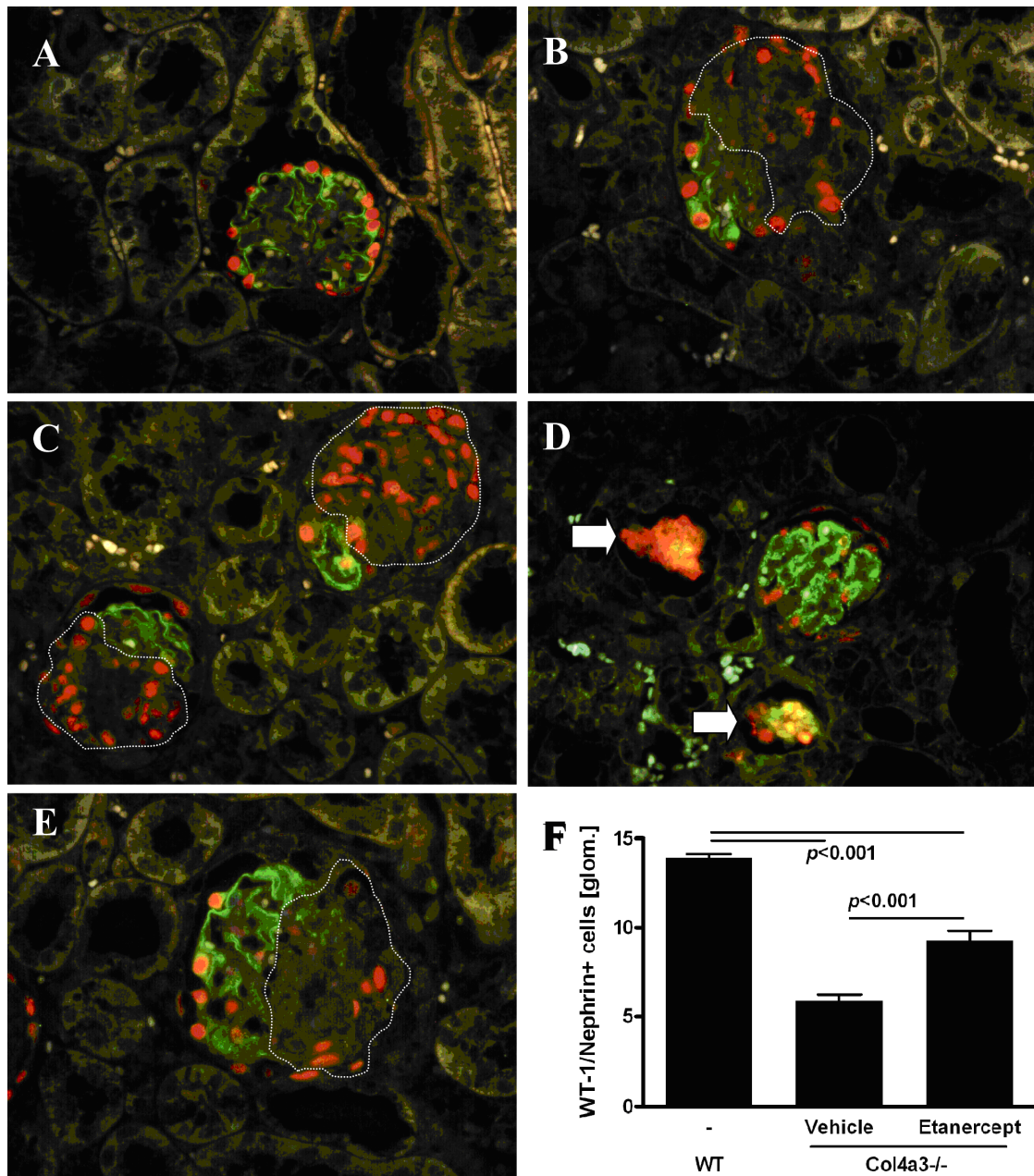


Figure 21. Podocytes in *Col4a3*-deficient mice. WT-1/nephrin immunofluorescence was used to quantify differentiated podocytes in kidneys of 9-week-old mice from all genotypes. (A) Note nuclear WT-1 and cytoplasmic nephrin double positive podocytes in a normal glomerulus of a wildtype mouse. Faint WT-1 staining is occasionally observed in parietal epithelial cells. (B) Age-matched *Col4a3*-deficient mice display a different glomerular staining pattern with only few WT-1/nephrin double positive cells and predominant WT-1+/nephrin- cells (encircled). (C) This image illustrates that these WT-1+/nephrin- cells overgrow the glomeruli in a crescent-like fashion. (D) WT-1/nephrin double positive cells form intratubular casts (white arrows) indicating that podocyte detachment from the GBM, i.e. podocyte loss. (E) TNF- α blockade with etanercept partially restored normal glomerular architecture and only segmental loss of WT-1/nephrin double positive podocytes (encircled). (F) Quantitative analysis of WT-1/nephrin double positive differentiated podocytes in 9-week-old mice from all genotypes. Data represent means \pm SEM.

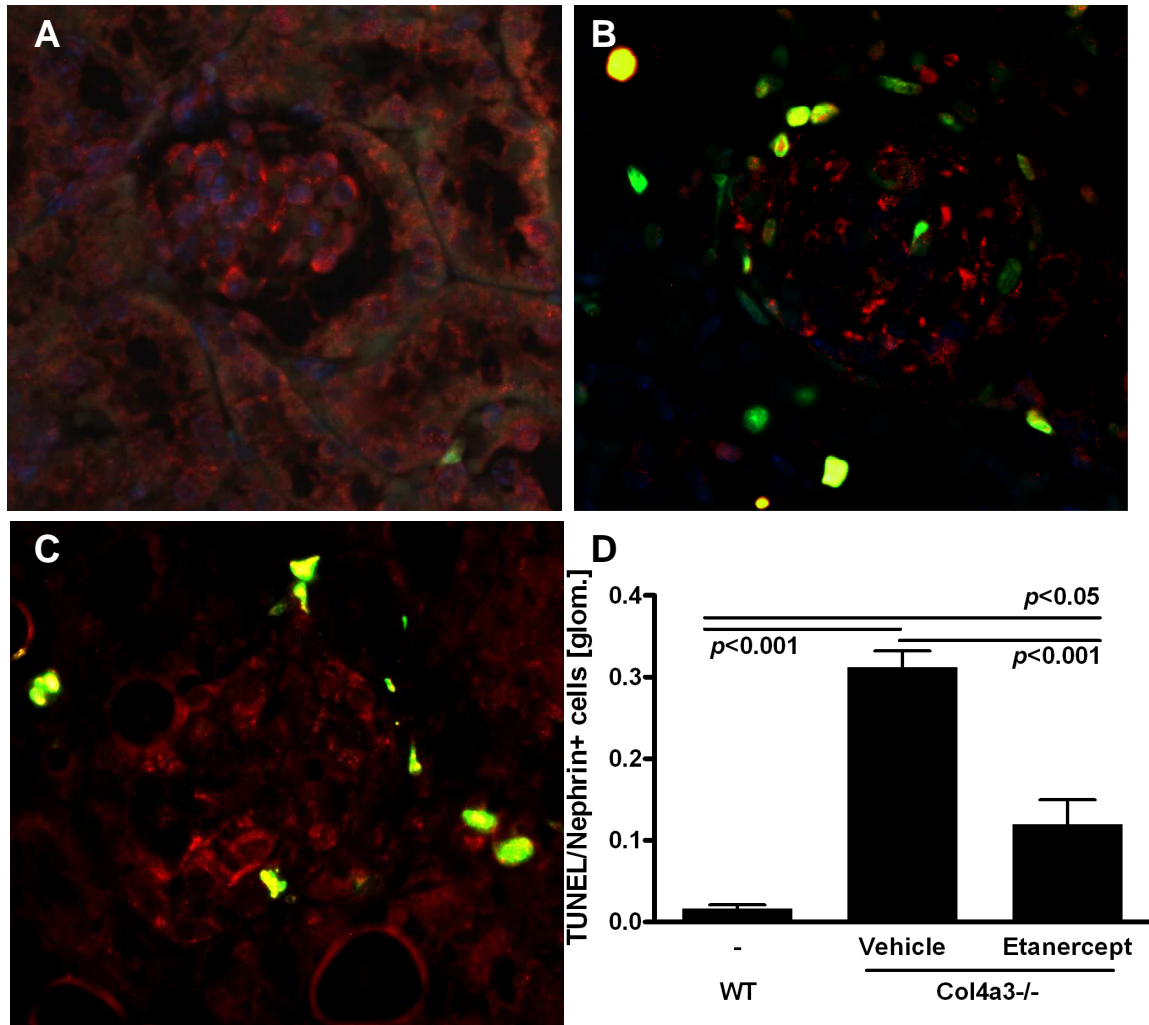
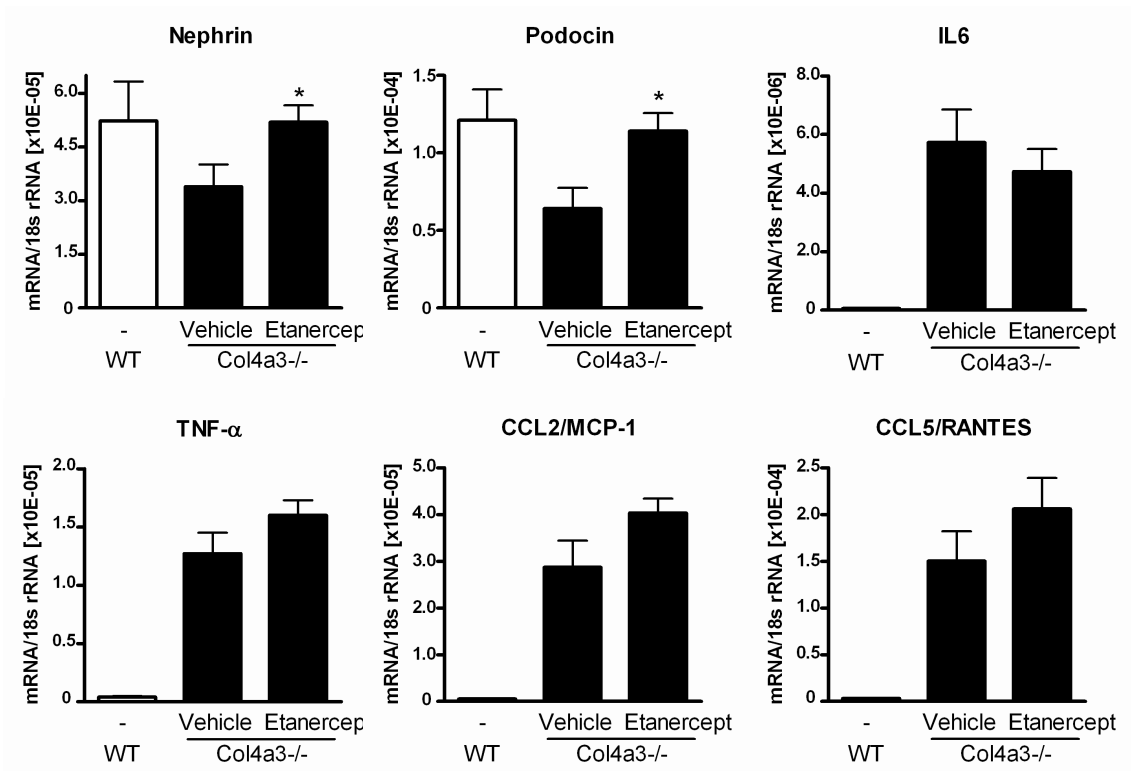


Figure 22. TUNEL+podocytes in *Col4a3*-deficient mice. TUNEL/nephrin costaining was used to quantify apoptotic podocytes in kidneys of 9-week-old mice of all groups in 50 glomeruli per mouse section. TUNEL staining (green) identified apoptotic renal cells, and red staining identified nephrin-positive podocytes. (A) wildtype, (B) saline-treated *Col4a3*-deficient mice, (C) etanercept-treated *Col4a3*-deficient mice, (D) quantitative analysis of lead to nephrin/TUNEL double positive apoptotic podocytes. Data represent means \pm SEM.

A



B

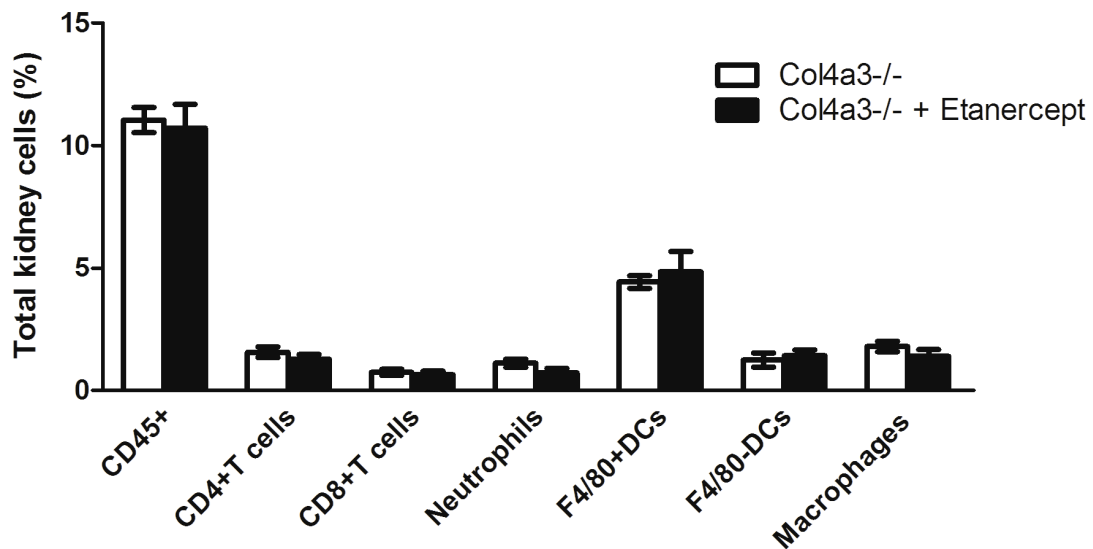


Figure 23. Renal mRNA expression and leukocyte counts in *Col4a3*-deficient mice. (A) Total kidney mRNA was prepared from mice of all groups for real-time RT-PCR. Renal mRNA expression levels were calculated as ratio per respective 18s rRNA expression. Data represent means \pm SEM from 6-8 mice. (B) Renal leukocytes were quantified by flow cytometry in kidney cell suspensions of 9-week-old *Col4a3*-deficient mice as described in methods. Data represent the percentage of all kidney cells \pm SEM from 5-7 mice in each group. Note that TNF- α blockade with etanercept did not affect any leukocyte subset. * $p < 0.05$ saline- versus etanercept-treated *Col4a3*-deficient mice.

4.2 Exogenous factors that accelerate the progression of Alport nephropathy

4.2.1 Effect of innate immunity on renal parenchymal cells

Numerous factors such as toxic, metabolic, infectious or traumatic types may be involved in pathomechanisms that aggravate progressive renal disease. For example, intrinsic renal cells including mesangial cells, endothelial cells, tubular epithelial cells, and podocytes express several types of TLRs and these cells by TLR activation are sufficient to release proinflammatory cytokines and chemokines aggravating renal injury (Anders, 2007). We speculated that TLR activation of intrinsic renal cells in response to PAMP-like molecules such as LPS, lipopeptides or bacterial DNA also triggered the secretion of proinflammatory and profibrotic mediators.

To address this issue, we isolated CD90⁺ renal fibroblasts from 6-week-old mice and stimulated them with agonists for TLR2 (Pam3Cys lipopeptide), TLR4 (LPS), TLR9 (CpG-DNA) and with TNF- α . TLR2 and TLR4 stimulation activated renal fibroblasts and induced IL-6 and CCL2/MCP-1 mRNA expression (Figure 24A), while TGF- β , collagen-1 α , and smooth muscle actin expression remained unchanged (Figure 24B). The CpG-DNA had no significant effect on CCL2/MCP-1 mRNA expression because renal fibroblasts do not express TLR9 (data not shown). Finally, the protein levels of CCL2/MCP-1 and TGF- β as detected by ELISA in collected supernatant from renal fibroblast cultures was also shown to remain unchanged (Figure 24C). Thus, TLR activation in renal fibroblasts triggers proinflammatory mediators, like CCL2/MCP-1 and IL-6, but does not induce the production of profibrotic molecules like TGF- β , collagen-1 α , and smooth muscle actin in renal fibroblasts.

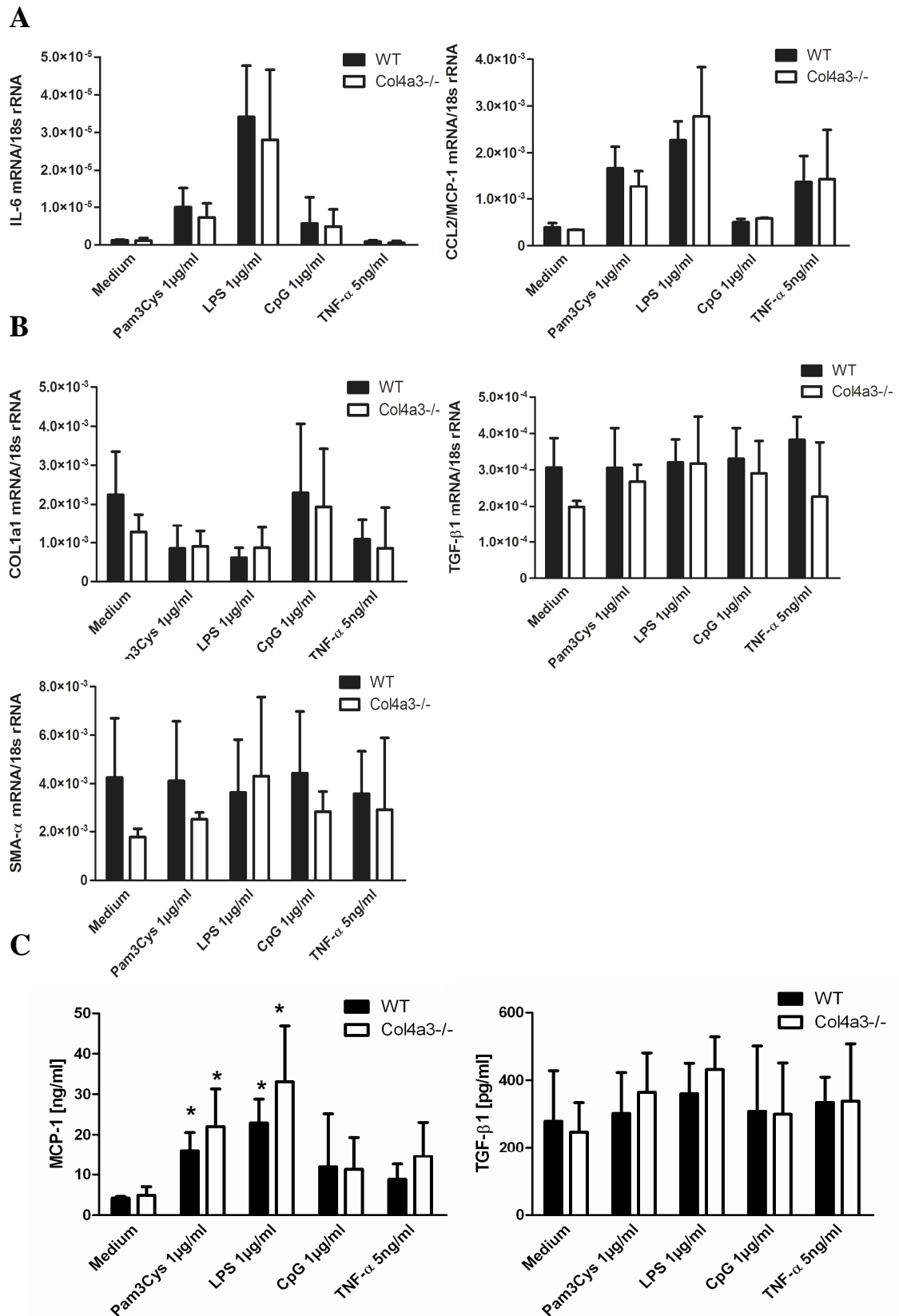


Figure 24. TLR-induced expression of cytokines and profibrotic mediators in renal fibroblasts. CD90⁺ fibroblasts were prepared from mice and cultured as described in methods. The cells were stimulated with either Pam3Cys lipopeptide (TLR2 agonist), LPS (TLR4 agonist), CpG-DNA (TLR9 agonist) or TNF α . (A), (B) After 24 h cells were harvested and the mRNA expression was quantified by real-time PCR and normalized to the 18S rRNA level. (C) Cell culture supernatants were obtained after 48h stimulation. MCP-1 and TGF- β levels were measured by ELISA. Data represent means \pm SD from three independent experiments. * $p < 0.05$ versus medium.

4.2.2 Macrophage activation via TLRs in Alport nephropathy

Glomerulosclerosis is a major cause of ESRD in patients with Alport nephropathy, albeit tubulointerstitial fibrosis with interstitial leukocytes also contributes to the disease progression. As described above, leukocyte cell infiltration is associated with disease progression. Previous studies with *Col4a3*-deficient mice show that the blockade of chemokine receptor CCR1 reduces renal fibrosis and prolonged life span, whereas the blockade of CCL2/MCP-1 has no effect (Clauss et al., 2009; Ninichuk et al., 2005). Macrophages in Alport kidneys might therefore have a non-inflammatory phenotype by displaying low expression of CCR2. In fact, the phenotype or activation state of renal macrophages is thought to significantly affect the extent of renal inflammation and tissue damage (Ricardo et al., 2008). M1 macrophage infusion aggravated renal damage and dysfunction, whereas M2 macrophage infusion reduced renal pathology and improved renal function (Anders et al., 2003a; Anders et al., 2003b; Huang et al., 2000; Wang et al., 2007).

Therefore, we hypothesized that the activation state of renal macrophages would affect disease progression of Alport nephropathy in *Col4a3*-deficient mice. We speculated that classically-activated macrophages by e.g. TLR activation would increase renal inflammation and accelerate the progression of Alport nephropathy. To address this issue, we induced TLR activation with TLR agonists in *Col4a3*-deficient mice. Mice received a series of injections with LPS or with unmethylated CpG-ODNs. CpG-DNA was selected because it mimicks the potential of bacterial DNA to selectively activate macrophages and dendritic cells via TLR9 (Anders, 2007). LPS mimicks infection with Gram-negative bacteria and activates macrophages via TLR4. With this study design, we also addressed the question whether infections affect the progression of Alport nephropathy, e.g. by modulating intrarenal inflammation.

4.2.2.1 Effect of LPS or CpG-DNA on life span of *Col4a3*^{-/-} mice

CpG-DNA and LPS are known triggers of leukocyte activation. CpG-DNA activates murine B cells, macrophages, and dendritic cells via the endosomal TLR9/MyD88 signaling pathway (Hemmi et al., 2000). By contrast, LPS stimulates leukocytes as well as non-immune cells via TLR4, which in turn activates MyD88 and

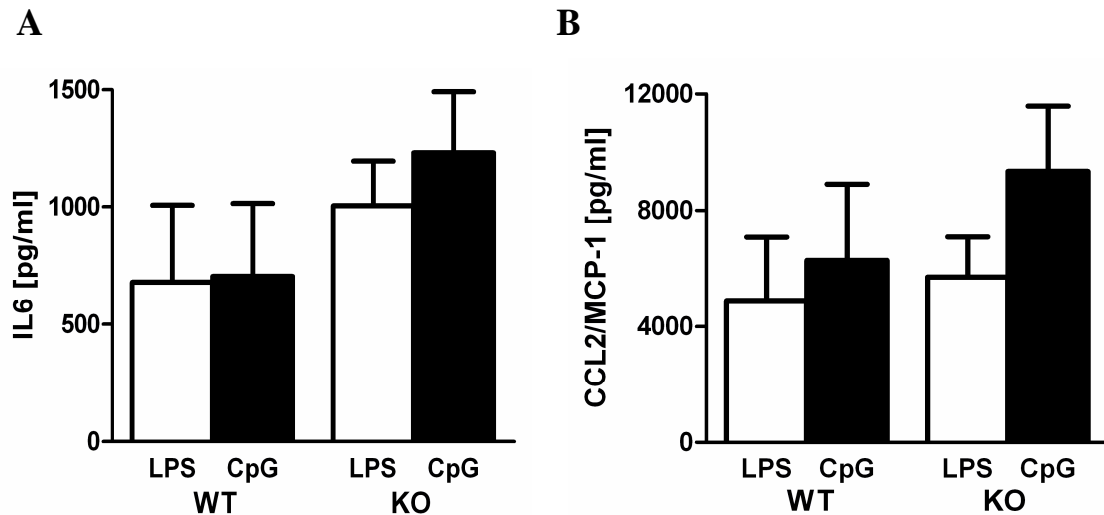


Figure 25. Plasma cytokine levels in *Col4a3*-deficient mice. Plasma cytokine levels of interleukin (IL)-6 and CCL2/MCP-1 from 4-week-old wildtype and *Col4a3*-deficient mice treated with saline, LPS or CpG-DNA. Before and after 6 h of injection, plasma was obtained and cytokines were measured by ELISA. (A) IL6 and (B) CCL2/MCP-1 levels in 4-week-old of *Col4a3*-deficient mice injected with 10 μ g of LPS and 40 μ g of CpG-DNA as indicated. Data represent as \pm SEM from 4-6 mice in each group.

TRIF signaling (Poltorak et al., 1998). *Col4a3*-deficient and wildtype mice received seven injections of CpG-DNA or LPS on alternate days starting from 4 weeks of age at a dose of 40 μ g or 10 μ g, respectively. These doses were selected because they induced similar plasma levels of IL-6 and CCL2/MCP-1 at 6 hours after single injection into 4-week-old *Col4a3*-deficient mice (Figure 25). Studies of the mice until death revealed that CpG-DNA significantly reduced the life span of *Col4a3*-deficient mice as documented by a mean survival of 46 days versus 76 days in saline-treated *Col4a3*-deficient mice (Figure 26). By contrast, LPS had no effect on the survival of *Col4a3*-deficient mice. In addition, CpG-DNA or LPS injections did not affect the survival in wildtype mice until 150 days of age. Thus, systemic exposure to CpG-DNA, but not to LPS, shortens the life span of *Col4a3*-deficient mice.

4.2.2.2 CpG-DNA, but not LPS, aggravates Alport nephropathy

Does the effect of CpG-DNA on the life span of *Col4a3*-deficient mice cause acceleration of Alport nephropathy? To answer this question, we treated a second cohort of mice and performed a cross-sectional analysis of all groups at 6 weeks of age. Renal sections from mice of all groups were stained with PAS and the extent of glomerulosclerosis was quantified by a semiquantitative sclerosis score ranging from 0 to 4 as described in the Methods section. In *Col4a3*-deficient mice, CpG-DNA

significantly increased the percentages of glomeruli with a sclerosis score of 3 or 4 and reduced those with a score of 0 and 2 indicating a shift towards more severe glomerular lesions (Figure 27). This was associated with a significant reduction in the number of podocytes per glomerulus (Figure 28). By contrast, LPS did not affect the aforementioned glomerular abnormalities in *Col4a3*-deficient mice (Figure 27 and 28). Neither CpG-DNA nor LPS injections affected the normal glomerular structure in wildtype mice (Figure 27). At the ultrastructural level the characteristic abnormalities of Alport nephropathy, i.e. GBM irregularities and podocyte foot process effacement became evident in *Col4a3*-deficient mice (Figure 29A). Additionally, extensive accumulation of extracellular matrix and podocyte damage was seen in CpG-DNA-injected *Col4a3*-deficient mice (Figure 29B). By contrast, LPS caused activation of glomerular endothelial cells as illustrated by luminal tubular extensions of endothelial cells (Figure 29B). Silver staining sections also showed the severe glomerular lesion by CpG-DNA (Figure 30). These morphological changes were associated with an increase of albuminuria and blood urea nitrogen levels in CpG-DNA treated *Col4a3*-deficient mice (Figure 31). Taken together, the effects of CpG-DNA on life span are associated with an acceleration of Alport nephropathy.

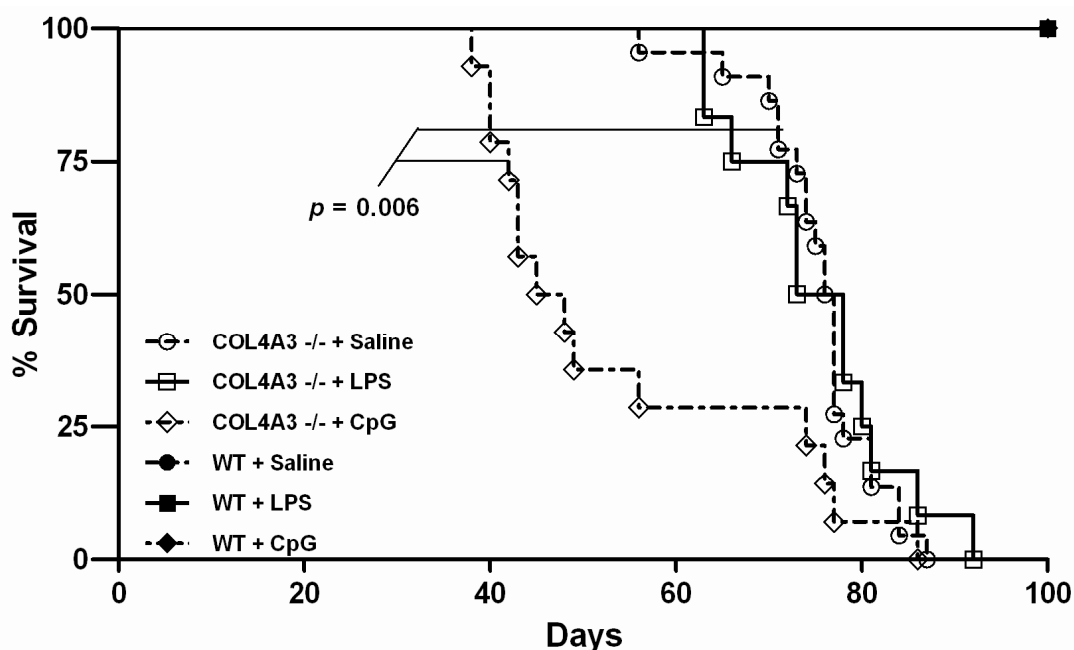


Figure 26. Life span of *Col4a3*-deficient mice. Wildtype and *Col4a3*-deficient mice were treated with saline, LPS or CpG-DNA from week 4 to 6 of age as indicated. Survival time is illustrated as Kaplan-Meier curve.

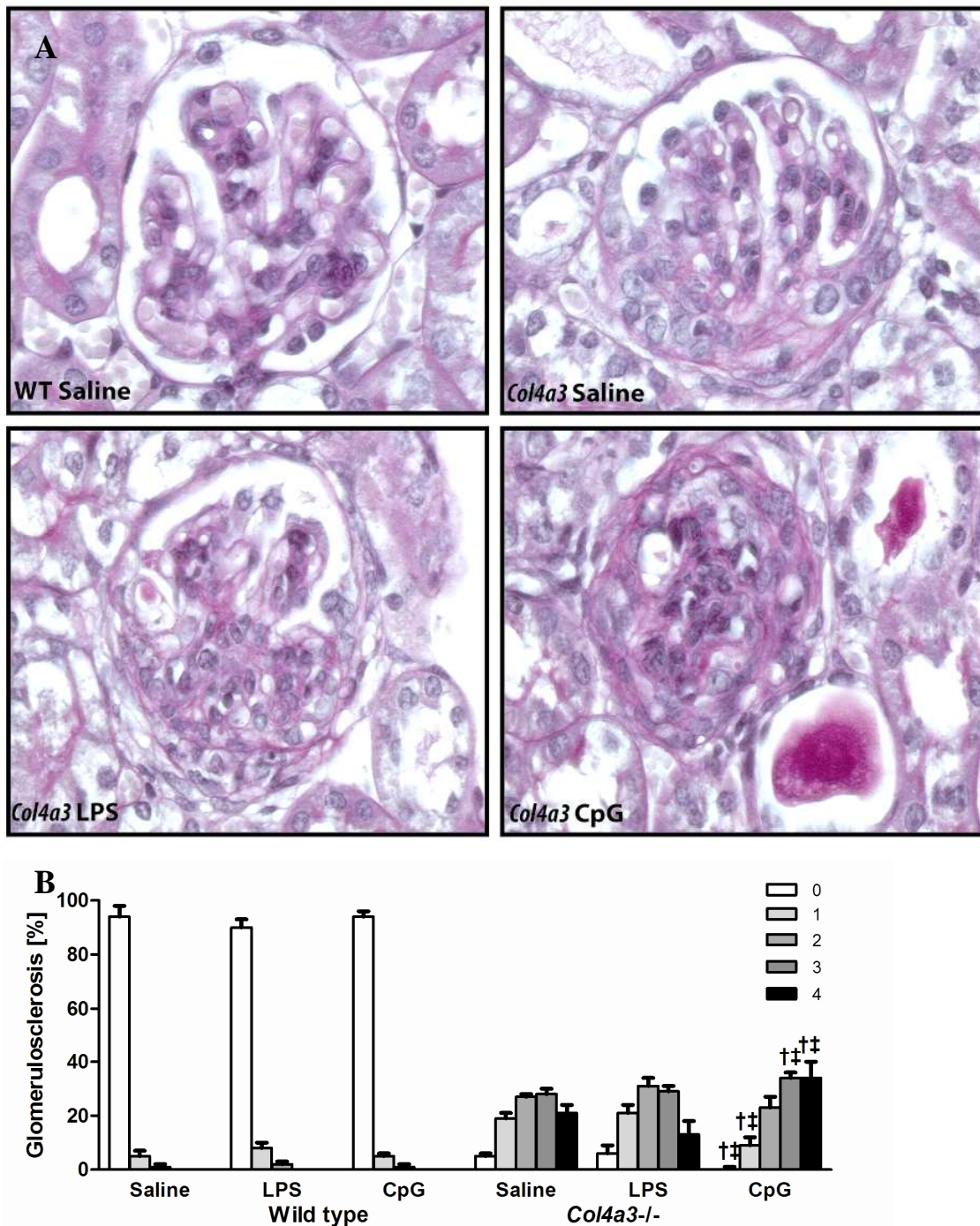


Figure 27. Renal histopathology in 6-week-old wildtype and *Col4a3*-deficient mice. (A) Renal sections of wild-type and *Col4a3*-deficient mice were stained with periodic acid Schiff solution (B) The extent of glomerulosclerosis was evaluated in mice of all groups by using a semiquantitative sclerosis score ranging from 0 (no sclerosis) to 4 (global sclerosis) as described in the Methods part. Data represent means \pm SEM. † $p < 0.05$ /‡ $p < 0.01$ versus saline-treated mice of the same genotype. Data represent means \pm SEM, * $p < 0.05$ versus wildtype, † $p < 0.05$ versus saline-treated mice of the same genotype. The figure includes representative images of single glomeruli from mice of all groups as indicated, original magnification x400.

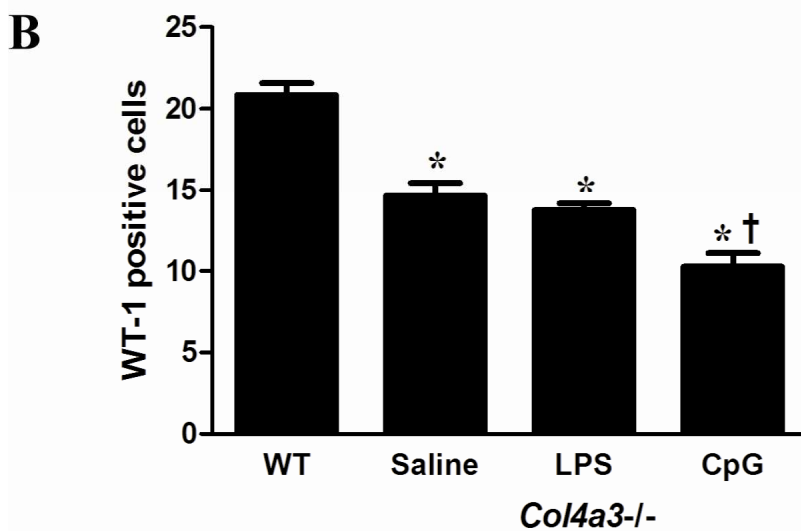
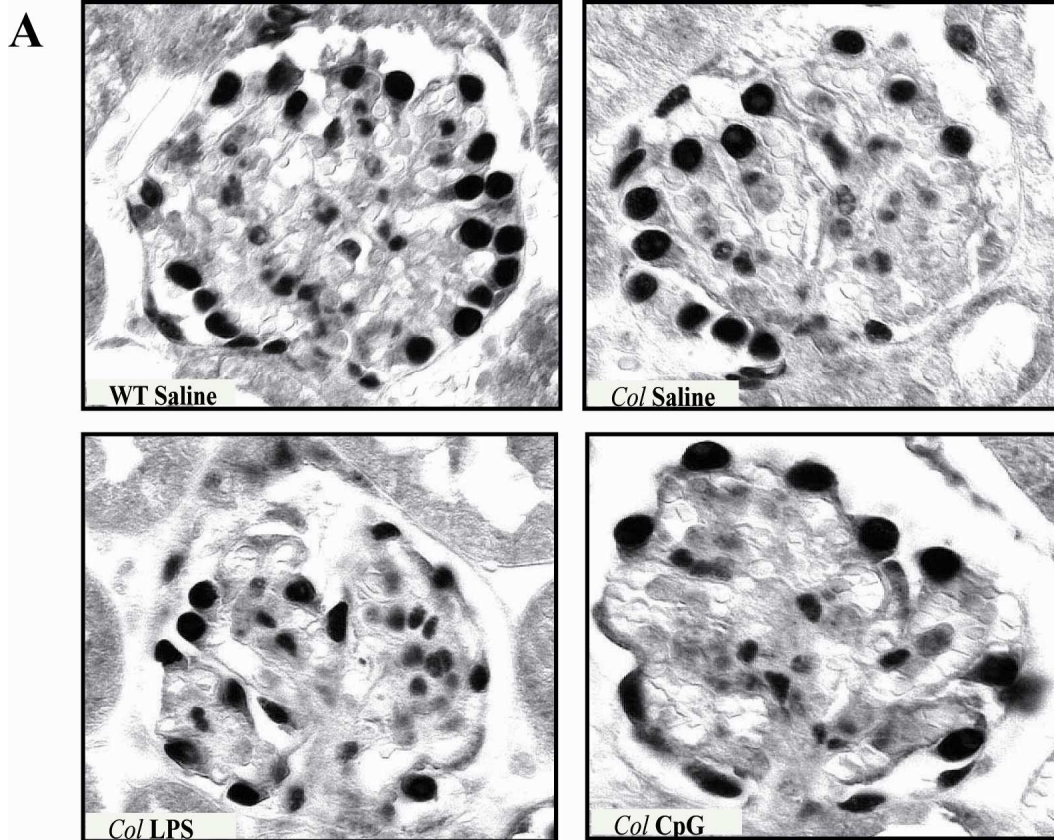


Figure 28. Renal histopathology in 6-week-old wildtype and *Col4a3*-deficient mice. (A) Renal sections of wild-type and *Col4a3*-deficient mice were stained with anti-WT-1. (B) The number of glomerular podocytes was quantified by counting WT-1+ cells in 15 glomeruli per section. Data represent means ± SEM, * $p < 0.05$ versus wildtype, † $p < 0.05$ versus saline-treated mice of the same genotype. The figure includes representative images of single glomeruli from mice of all groups as indicated, original magnification x400.

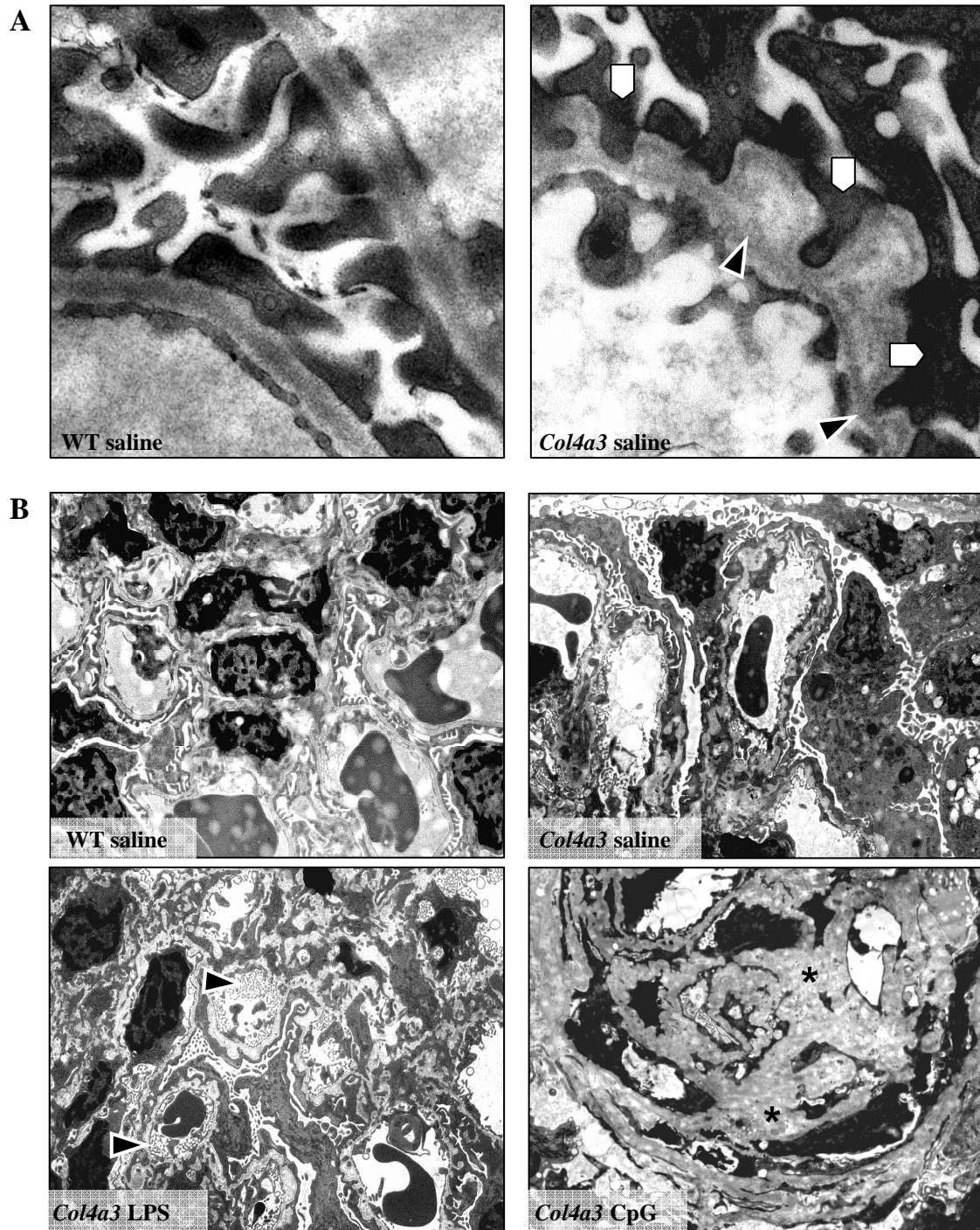


Figure 29. Glomerular ultrastructure in 6-week-old *Col4a3*-deficient mice. Electron microscopy was applied to assess the glomerular ultrastructure of 6-week-old wild-type and *Col4a3*-deficient mice. (A) Note that lack of *Col4a3* is associated with irregular GBM thickness (▶) and podocyte foot process effacement (△) as compared to age-matched wild-type mice (original magnification x25000). (B) At lower magnification (x3150) changes in glomerular matrix and capillary structure between wild-type and *Col4a3*-deficient mice become visible. Note that exposure of *Col4a3*-deficient mice to CpG-DNA caused extensive accumulation of extracellular matrix (*) with major capillary and podocyte abnormalities, i.e. glomerulosclerosis. By contrast, LPS exposure caused activation of glomerular endothelial cells, evident by tubular extensions into the capillary lumen (▶).

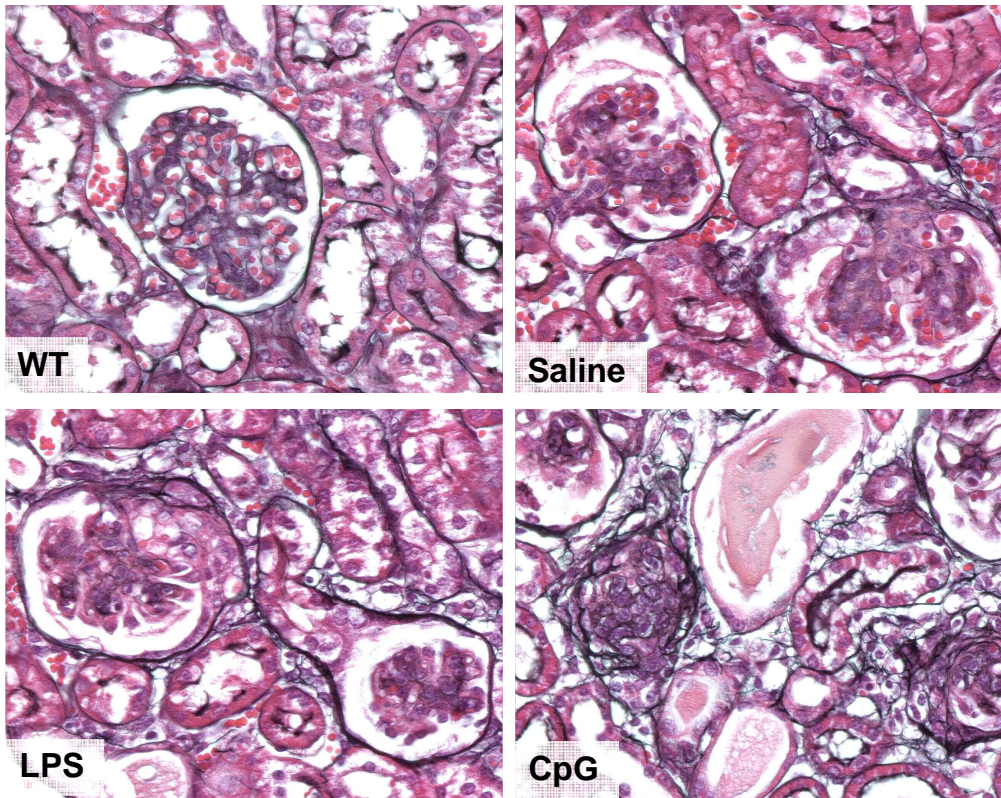


Figure 30. Renal lesion in *Col4a3*-deficient mice. Renal sections of wild-type and *Col4a3*-deficient mice were stained with silver. Images illustrate representative sections of kidneys from the respective groups at week 6 of age (original magnification 100x).

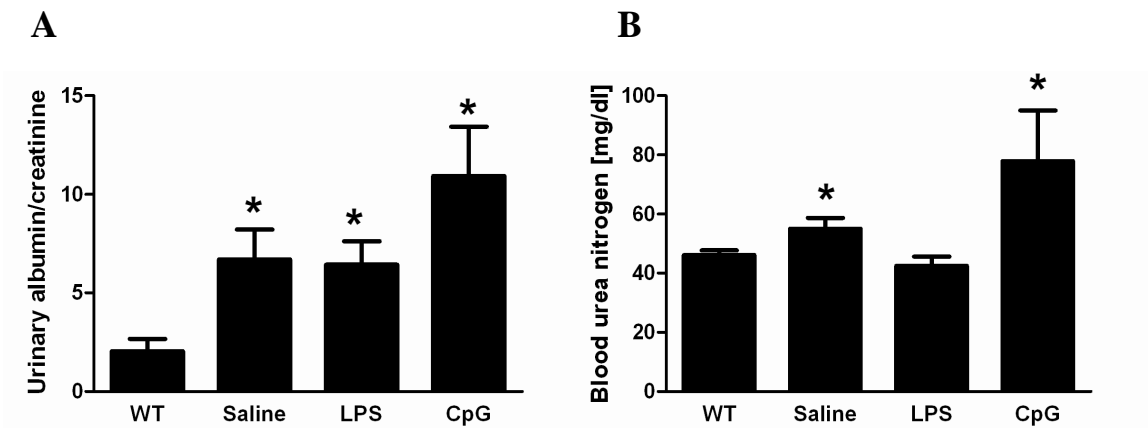


Figure 31. Proteinuria and blood urea nitrogen in wildtype and *Col4a3*-deficient mice. Proteinuria (A) and blood urea nitrogen (B) were determined from 6-week-old of wildtype and *Col4a3*-deficient mice from all groups and calculated as described in *Methods*. Data represent means \pm SEM. * $p < 0.05$ versus wildtype mice.

4.2.2.3 CpG-DNA increases activated renal macrophages in *Col4a3*^{-/-} mice

Among those cells that infiltrate the kidney in Alport nephropathy, only macrophages and dendritic cells express TLR9 (Hemmi et al., 2000). Hence, we speculated that CpG-DNA injections may aggravate Alport nephropathy by altering the numbers of leukocytes in kidneys of *Col4a3*-deficient mice. To address this issue, we performed quantitative flow cytometry of renal cell suspensions from mice of all groups at 6 weeks of age. CpG-DNA significantly increased the amount of renal F4/80⁺/CD11c⁻ macrophages (and CD8⁺ T cells) but not those of renal CD11c⁺ dendritic cells in *Col4a3*-deficient mice (Figure 32). This was consistent with increased numbers of interstitial F4/80⁺ cells as well as Mac2⁺ glomerular macrophages in renal sections of *Col4a3*-deficient mice as determined by immunostaining (Figure 33). By contrast, LPS injections did not affect renal leukocyte numbers in *Col4a3*-deficient mice (Figures 32 and 33). Similarly, neither CpG-DNA nor LPS injection affected the numbers of renal leukocytes in wildtype mice (data not shown). Next, we asked whether CpG-DNA injections also affected the functional phenotype of intrarenal macrophages. We addressed this question in various ways. We used, for example, flow cytometry to quantify the numbers of Ly6C^{hi} intrarenal macrophages, which represent a classically-activated proinflammatory (M1) phenotype (Mantovani et al., 2005; Mosser and Edwards, 2008). CpG-DNA injections significantly increased the numbers of intrarenal Ly6C^{hi} positive macrophages as compared to LPS- or saline-treated *Col4a3*-deficient mice (Figure 32B). In summary, CpG-DNA accelerates kidney disease in *Col4a3*-deficient mice in association with increased numbers of classically-activated renal macrophages.

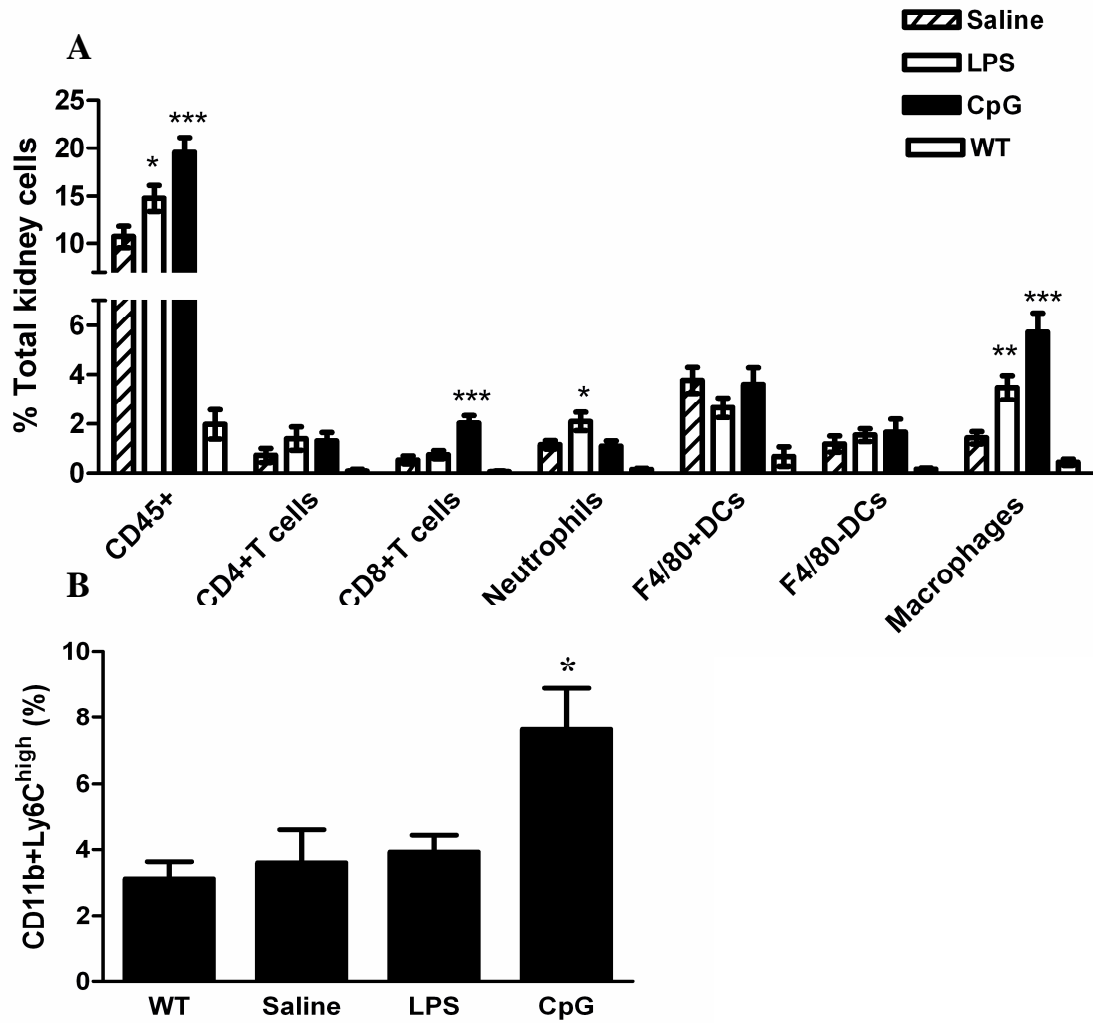


Figure 32. CpG-DNA alters renal leukocyte infiltration in 6-week-old *Col4a3*-deficient mice. (A) Renal cell suspensions were prepared for leukocyte flow cytometry from 6-week-old wildtype and *Col4a3*-deficient mice in all groups. The marker CD11c⁺ identified DCs, macrophages were F4/80⁺/CD11c⁻. Data represent the percentage of all kidney cells \pm SEM from 5-7 mice in each group. * $p < 0.05$, ** $p < 0.01$, *** $p < 0.001$, LPS- or CpG-DNA- versus saline-treated *Col4a3*-deficient mice. (B) The percentage of Ly6C^{high} cells gated on CD11b⁺ population in kidney. * $p < 0.05$ CpG-DNA versus all groups.

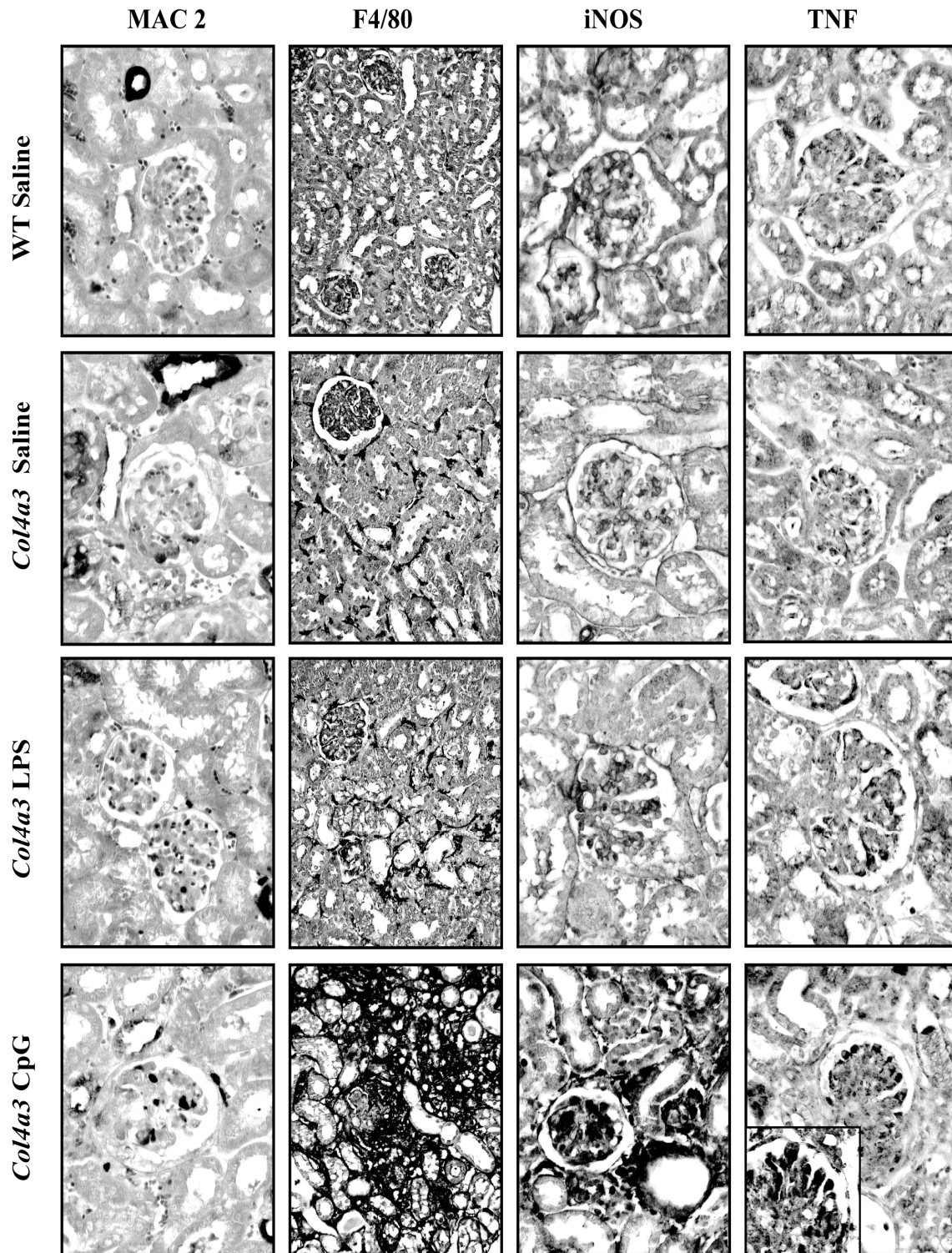


Figure 33. Immunostaining of renal sections. Renal sections of wild-type and *Col4a3*-deficient mice were stained with appropriate antibodies as indicated. The figure includes representative images of mice from all groups, original magnification x200 or x400.

4.2.2.4 CpG-DNA and LPS modulate the expression of macrophage markers

In an alternative approach to characterize macrophage polarization we quantified a number of macrophage activation markers by real-time PCR using renal RNA extracts from mice of all treatment groups. All primers for macrophage phenotypes were previously tested using bone marrow-derived macrophages stimulated with different TLR agonists (data not shown). In *Col4a3*-deficient mice, CpG-DNA injection increased renal mRNA levels of the following M1 (classically-activated) macrophage markers: TNF- α , iNOS, IL-12, CXCL10 (Figure 34A). All of these markers were down-regulated in LPS -treated *Col4a3*-deficient mice. CpG-DNA injections also induced some of the markers that refer to M2 (alternatively-activated) macrophage such as arginine-1, TGF- β , and Fizz-1 (Figure 34B). All aforementioned results were confirmed by real-time PCR analysis of mRNA isolates from CD11b⁺ cells that we isolated by magnetic beads from mice of all groups (Figure 35). The predominant intrarenal induction of TNF- α and iNOS mRNA by CpG-DNA was consistent with an increased glomerular (and interstitial) staining intensity by anti-iNOS IgG and anti-TNF IgG on renal sections of CpG-DNA- but not of saline- or LPS- treated *Col4a3*-deficient mice (Figure 33). Interestingly, TNF- α immunostaining was also positive on glomerular podocytes (Figure 33). Taken together, mRNA profiling and immunostaining support that CpG-DNA accelerates kidney disease in *Col4a3*-deficient mice by modulating the phenotype of renal macrophages.

4.2.2.5 Effect of CpG-DNA on Alport nephropathy is mediated by TNF- α

Because the effects of CpG-DNA on kidney disease in *Col4a3*-deficient mice were associated with a marked induction of TNF- α , we questioned whether this accounts for the aggravation of Alport nephropathy. Thus, we treated additional *Col4a3*-deficient mice with CpG-DNA together with or without the TNF- α antagonist etanercept. Etanercept completely abrogated the effect of CpG-DNA on the acceleration of glomerulosclerosis as glomerular sclerosis scores were similar or even lower as compared to saline-treated *Col4a3*-deficient mice (Figures 36A and B). Similarly, etanercept significantly increased the numbers of WT-1⁺ podocytes in glomerular tufts (Figures 36C and D) and significantly reduced the albumin-creatinine ratio in CpG-DNA-treated *Col4a3*-deficient mice (Figure 37A). The premature mortality of CpG-

DNA-treated *Col4a3*-deficient mice was also improved from a mean lethality at 46 days to 77 days by etanercept-treatment which was identical to saline-treated *Col4a3*-deficient mice (Figure 37B). Thus, CpG-DNA accelerates Alport nephropathy in *Col4a3*-deficient mice via activating renal macrophages to secrete TNF- α .

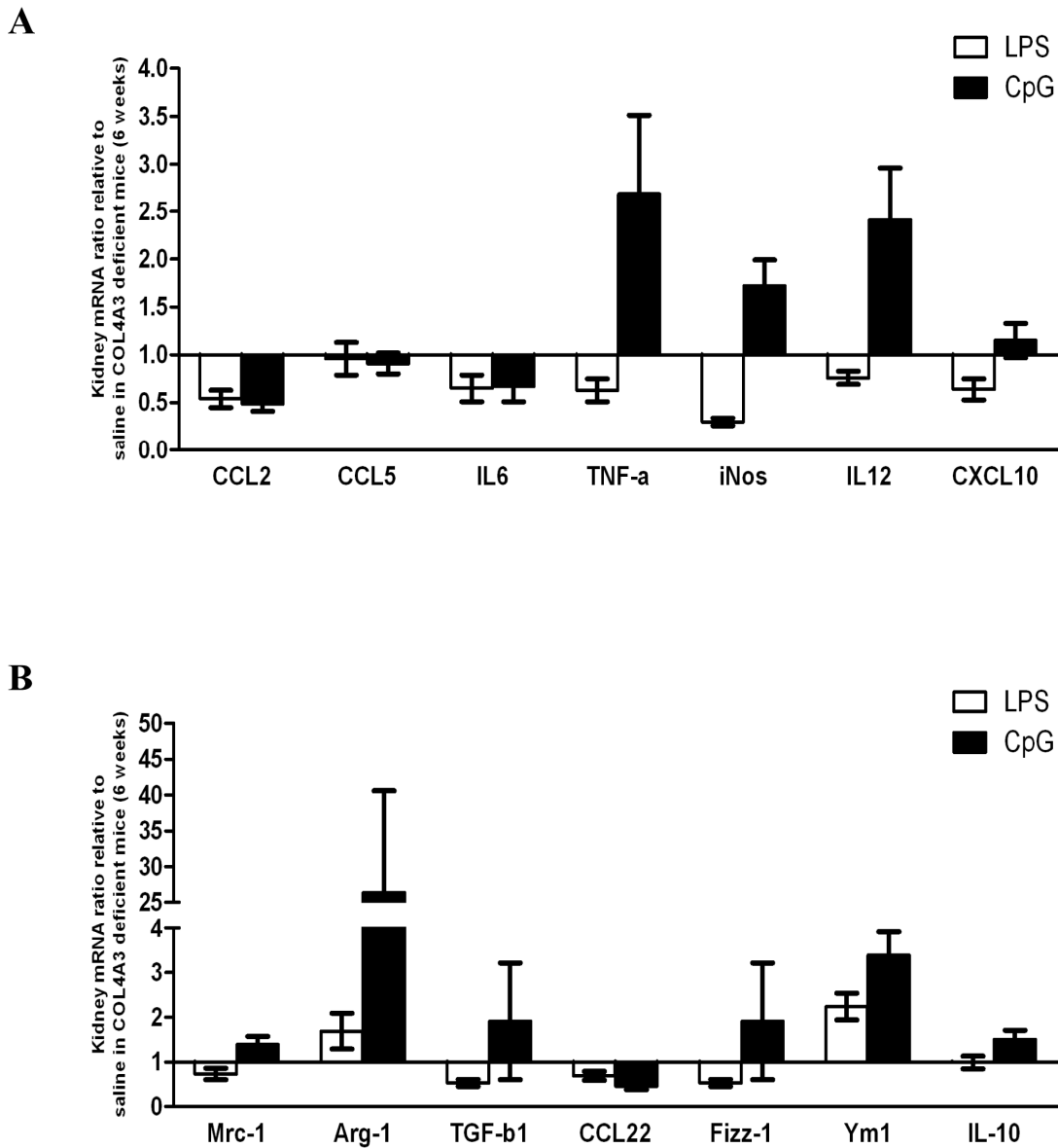


Figure 34. Renal mRNA expression of macrophage phenotype markers in *Col4a3*-deficient mice. Total kidney mRNA was prepared from mice of all groups for real-time RT-PCR. Markers of M1 (A) or M2 (B) macrophages were quantified and were calculated as ratio per respective 18s rRNA expression. The graph shows the mRNA levels of LPS- (white bars) or CpG-DNA-injected mice (black bars) relative to the levels of saline-treated mice to indicate induction or suppression of each marker.

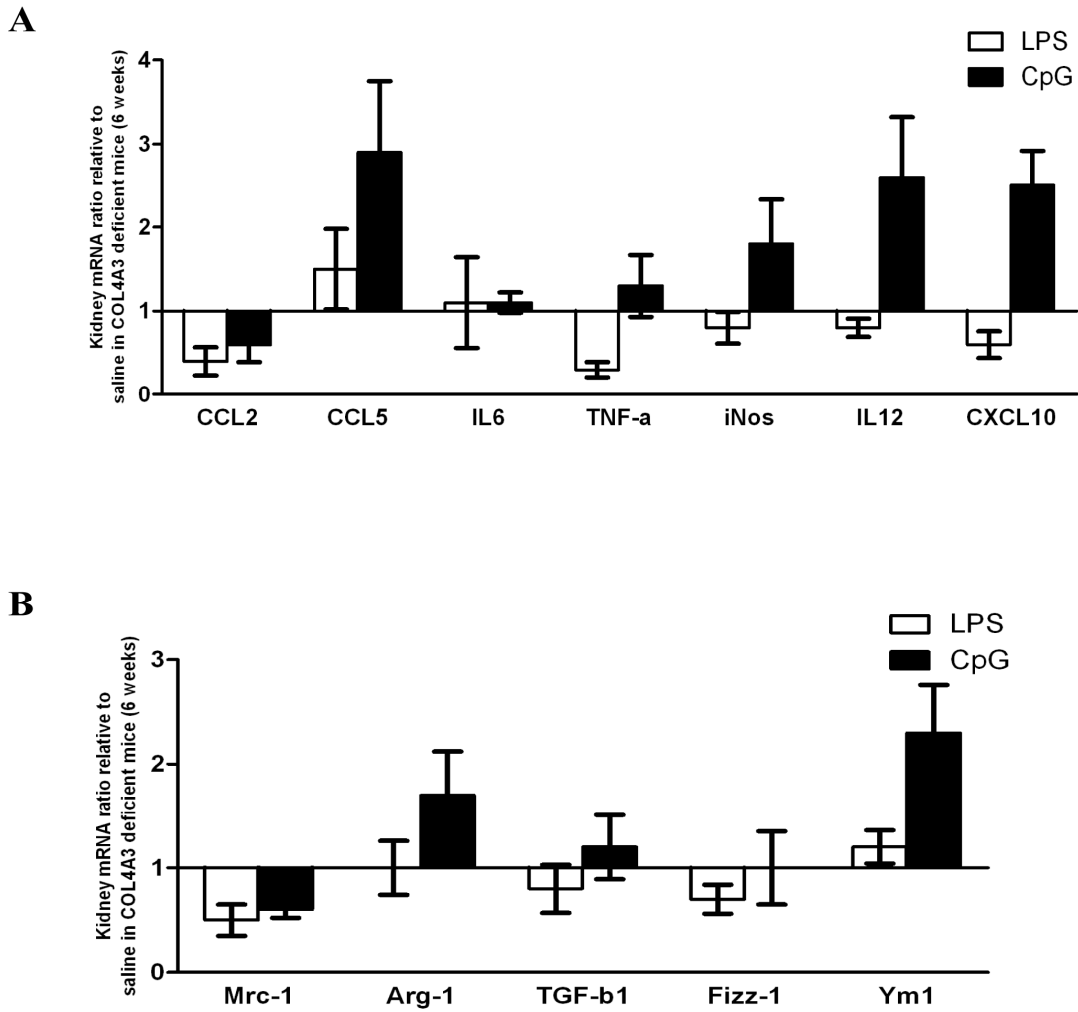


Figure 35. mRNA profile of renal CD11b+ macrophage in *Col4a3*-deficient mice. mRNA of CD11b+ cells isolated from kidney of all groups was prepared for real-time RT-PCR. Markers of M1 (A) or M2 (B) macrophages were quantified and were calculated as ratio per respective 18s rRNA expression. The graph shows the mRNA levels of LPS- (white bars) or CpG-DNA-injected mice (black bars) relative to the levels of saline-treated mice to indicate induction or suppression of each marker.

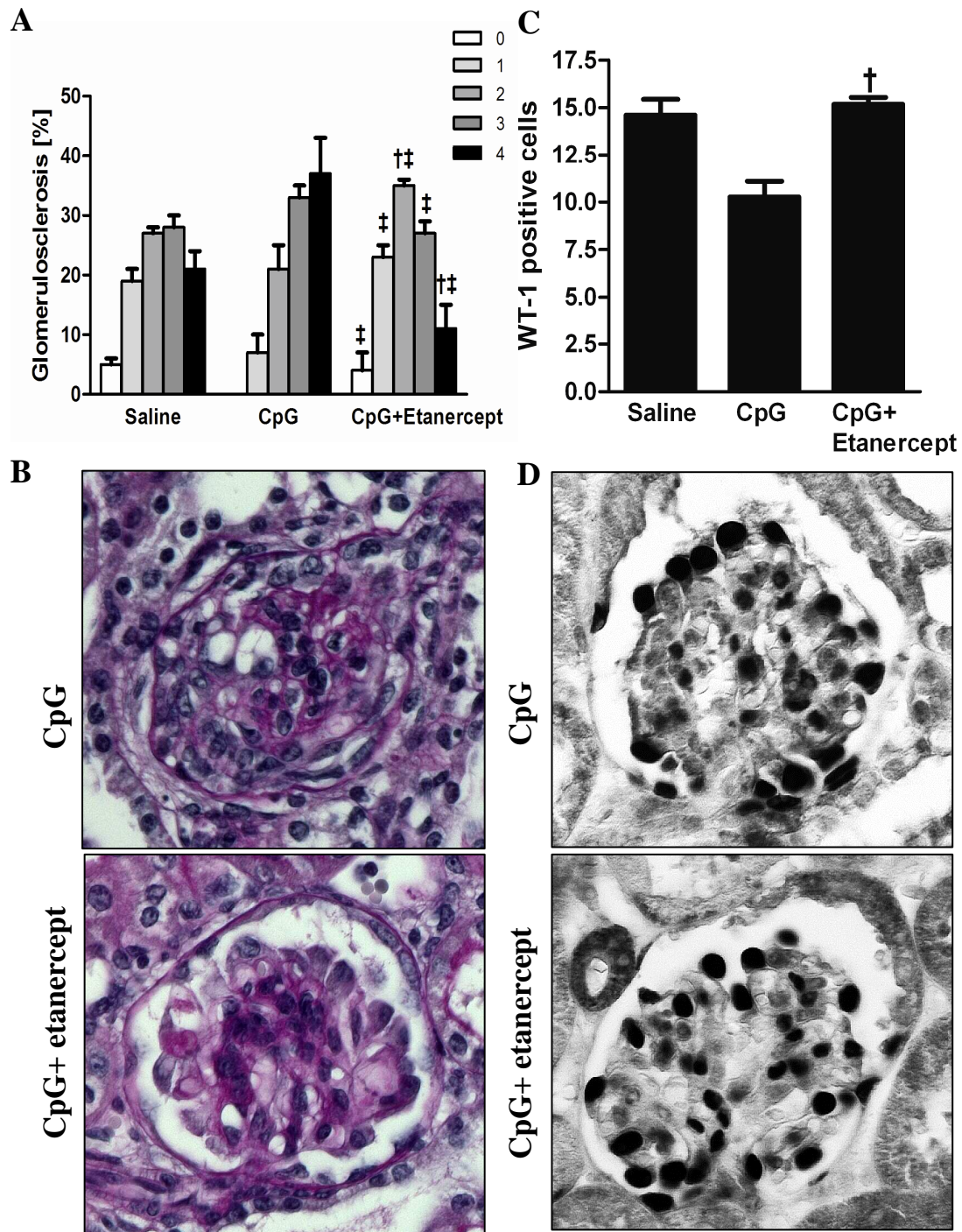


Figure 36. Effect of TNF- α blockade with etanercept on CpG-DNA-induced aggravation of Alport nephropathy. (A) The extent of glomerulosclerosis was evaluated in mice of all groups by using a semiquantitative sclerosis score ranging from 0 (no sclerosis) to 4 (global sclerosis) as described in the Methods part. Data represent means \pm SEM. $\dagger p < 0.05$ versus saline-/ $\ddagger p < 0.05$ versus CpG-DNA-treated *Col4a3*-deficient mice. (B) Renal sections of *Col4a3*-deficient mice were stained with periodic acid Schiff solution. The figure illustrates representative images of single glomeruli from mice of all groups as indicated, original magnification $\times 400$. (C) The number of glomerular podocytes was quantified by counting WT-1+ cells in 15 glomeruli per section. Data represent means \pm SEM, $\dagger p < 0.05$ versus CpG-DNA-treated *Col4a3*-deficient mice. (D) Renal sections of *Col4a3*-deficient mice were stained with anti-WT-1. The figure illustrates representative images of single glomeruli from mice of all groups as indicated, original magnification $\times 400$.

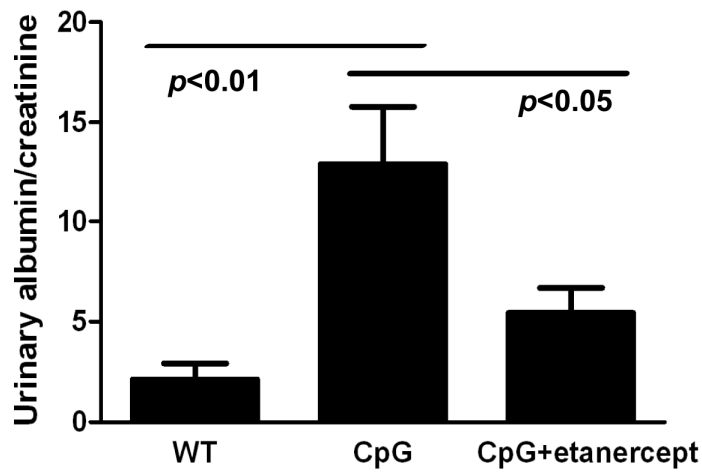
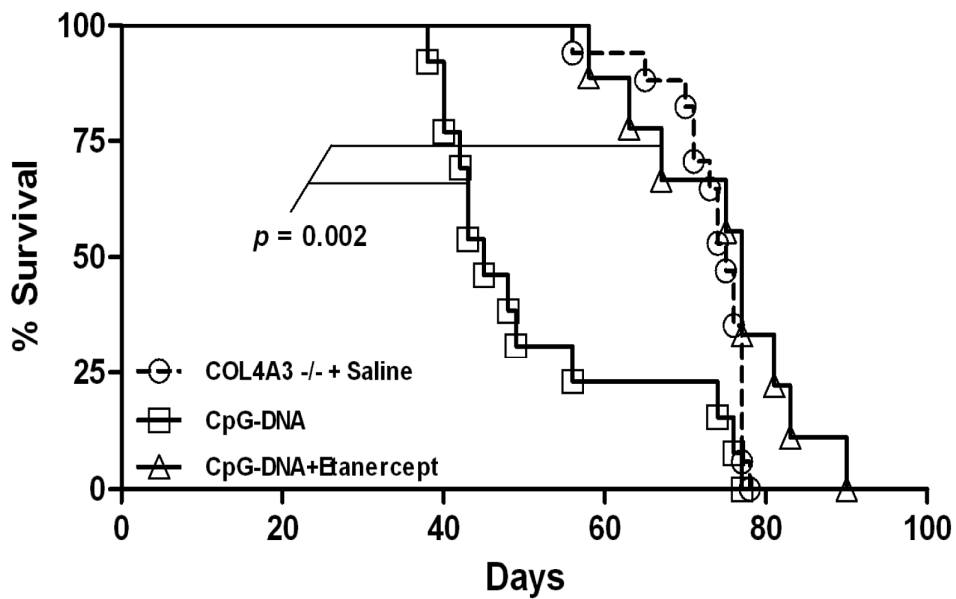
A**B**

Figure 37. Effect of TNF- α blockade on proteinuria and life span of CpG-DNA-accelerated Alport nephropathy. (A) Proteinuria was determined in 6-week-old wildtype and *Col4a3*-deficient mice the latter being treated either with CpG-DNA only or CpG-DNA and etanercept. Data represent means of urinary albumin/creatinine ratios \pm SEM. (B) CpG-DNA treated *Col4a3*-deficient mice were injected with etanercept from week 4 to 6 of age as indicated. Survival time is illustrated as Kaplan-Meier curve.

5. Discussion

Chronic renal failure involves progressive loss of renal parenchymal cells and fibrosis, which is accompanied by an infiltration of immune cells such as macrophages and T cells, followed by progressive glomerulosclerosis. A comprehensive understanding of the pathomechanisms of CKD still remains elusive. For example, the factors contributing to tissue damage and remodeling in the disease progression have not fully been defined yet. In the current study, we used *Col4a3*-deficient mice, which reflect the genetic and phenotypical characteristics of human Alport syndrome (Cosgrove et al., 1996) and, furthermore, represent a suitable model to study the pathomechanisms of the progressive glomerulosclerosis in absence of major inflammatory lesions. Studies using this model have demonstrated that renal cell activation and infiltrating leukocytes both contribute to the progression of renal dysfunction but little is known about how the renal cell activation and leukocytes promote tissue remodeling in Alport syndrome (Jedlicka et al., 2009; Lebleu et al., 2008).

The role of TNF- α in Alport nephropathy

In the first study, we postulated that endogenous molecules, which are synthesized during the progression of Alport nephropathy, can enhance the progressive loss of renal cells. For example, the proapoptotic cytokine, TNF- α would contribute to Alport glomerulosclerosis by promoting podocyte loss.

TNF- α is a multiple functional cytokine of proapoptotic and immunoregulatory functions. The biological function of TNF- α ligand arises via interaction with transmembranous receptors (TNFRs) comprising the recruited intracellular adaptor molecules such as FADD, RIP, TRADD, and TRAF. One pathway leads to induction of NF- κ B-mediated cytokines that elicit proinflammatory or antiinflammatory effects via TNFR1 and TNFR2, whereas the TNFR1-binding pathway triggers an extrinsic apoptosis pathway by activating caspase 8 (Hehlgans and Pfeffer, 2005; Rahman and McFadden, 2006; Wajant et al., 2003). In kidney, TNFRs are expressed by glomeruli and tubular cells in renal injury and, the increased expression and synthesis of TNF receptors and ligand indicate the evidence for glomerular pathology and it has been documented in a number of animal models of severe glomerular inflammation (Ortiz and Egido, 1995; Sanchez-Nino et al., 2010; Vielhauer and Mayadas, 2007). Here, we

confirmed that the expression of proinflammatory and proapoptotic cytokine TNF- α increased over time in glomerular and in tubulointerstitial compartments of *Col4a3*-deficient mice. Data in this thesis also showed that leukocyte accumulation in kidneys from *Col4a3*-deficient mice increased during the progression of Alport nephropathy and the leukocytes were also the source of TNF- α expression. The intrarenal TNF- α expressed by renal parenchymal cells and by infiltrating leukocytes promotes progressive glomerulosclerosis by enhancing podocyte loss.

Loss-of-podocytes is the central pathophysiological element of glomerulosclerosis (Kriz and Lemley, 1999; Wharram et al., 2005). Podocytes are terminally differentiated epithelial cells and their sophisticated structural interaction with other podocytes via the slit membrane is elementary to their functional role at the glomerular filtration barrier. Hence, replacing a detached podocyte may be as difficult as replacing a single piece of a puzzle. Although intraglomerular podocyte progenitors have been reported, their capacity to regenerate dying podocytes in the adult kidney is limited (Appel et al., 2009; Ronconi et al., 2009). Therefore, in chronic forms of glomerulopathies with persistent triggers for podocyte injury, significant podocyte apoptosis is sufficient to cause diffuse glomerulosclerosis and decline of GFR (Kriz and Lemley, 1999; Wharram et al., 2005). In Alport nephropathy, the altered composition of the GBM affects podocytes, which is characterized by podocyte foot process effacement and proteinuria (Cosgrove et al., 1996; Hudson et al., 2003).

The immunohistological data from WT-1 and nephrin co-stained kidneys of *Col4a3*-deficient mice indicate reliable quantification of the number of podocytes. Our finding is that the progression of glomerulosclerosis in *Col4a3*-deficient mice is tightly linked to the loss of nephrin-expressing differentiated podocytes like it has been reported for other forms of glomerulosclerosis (Kriz and Lemley, 1999; Sayyed et al., 2009; Susztak et al., 2006; Wang et al., 2008; Wharram et al., 2005). Our hypothesis on the basis of the first study is that podocyte loss is enhanced by increasing intrarenal TNF- α expression and thus TNF- α blockade would reduce the glomerulosclerosis.

TNF- α is a bifunctional cytokine. Its proinflammatory effects alert and activate other cells for cytokine production. This includes tissue macrophages that produce large amounts of reactive oxygen species upon TNF- α exposure as a dominant trigger for tissue inflammation and damage (Vielhauer and Mayadas, 2007). This fact is evidenced by genetic variants of increased TNF- α signaling, which lead to dwarfism, cachexia, and early death due to systemic and widespread tissue inflammation including the kidney

(Lee et al., 2000; Shembade et al., 2010). As such, TNF- α antagonism, e.g. with etanercept, has proven to be effective in genetic forms of inappropriate TNF- α signaling like TNF receptor-associated periodic syndrome (TRAPS) as well as in chronic inflammatory diseases such as rheumatoid arthritis or Crohn's disease (Weinberg and Montler, 2005). In contrast to proinflammatory cytokines such as IL-6, TNF- α has profound proapoptotic effects as TNFRs activate the extrinsic apoptotic pathway involving caspase-8. As such, TNF- α expression in inflammatory lesions is thought to contribute to tissue damage by enhancing apoptotic cell death of intrinsic parenchymal cells, e.g. tubular cell death in acute kidney injury (Choi et al., 2009; Dong et al., 2007). While apoptotic tubular cells can often rapidly be regenerated after acute kidney injury (Bonventre, 2003), persistent TNF- α expression may contribute to the progressive loss of renal parenchymal cells and tissue atrophy in CKD. TNF- α suppresses nephrin expression and induces podocyte apoptosis in a dose-dependent manner (Doublier et al., 2010; Lai et al., 2009; Saito et al., 2010). We have demonstrated by TUNEL assays that the increased numbers of TUNEL-positive podocytes were observed in *Col4a3*-deficient mice. Furthermore, we document that TNF- α contributes to the progressive loss of podocytes in the glomerular compartment *in vivo*. This suggests that TNF- α at least partially accounts for progressive CKD and renal failure in Alport syndrome. In accordance with our hypothesis, the blockade of the biological activity of TNF- α with etanercept prolonged about 20% of total life span of *Col4a3*-deficient mice and the effect of etanercept was related to the improvement of all aspects of Alport nephropathy involving podocyte loss, proteinuria, glomerulosclerosis, and decline of GFR. This was evidenced by a partial restoration of nephrin-positive, differentiated podocytes in etanercept-treated *Col4a3*-deficient mice. Both mRNA and protein levels of nephrin were recovered and apoptotic podocytes were reduced by etanercept. TNF- α blockade with etanercept was previously shown to have similar protective effects on glomerulosclerosis of hypertensive rodents (Elmarakby et al., 2006), hence, TNF- α -induced podocyte loss is likely to represent a general pathomechanism of glomerulosclerosis.

The effect of macrophage-mediated TNF- α expression on Alport nephropathy

In most types of acute and chronic kidney diseases it has been shown that leukocyte infiltrates contribute to disease progression by secreting proinflammatory and profibrotic

mediators (Boor et al., 2007; Eardley et al., 2008; Wilson et al., 2004). Experimental reduction of renal leukocytes, e.g. by irradiation, targeted deletion, specific toxins or by chemokine antagonism, was shown to protect from renal pathology and to improve the renal function (Anders et al., 2006; Ferenbach et al., 2007; Kitching et al., 2008; Sean Eardley and Cockwell, 2005). These findings are likely to extend to Alport nephropathy, because irradiation and blockade of chemokine receptor CCR1-mediated renal macrophage recruitment both proved to reduce renal fibrosis and prolonged life span in *Col4a3*-deficient mice (Katayama et al., 2008; Ninichuk et al., 2005).

Persistent tissue injury results in recruitment of inflammatory immune cells and activation of non-immune cells including fibroblast and renal cells, which participate in inflammation and extracellular matrix deposition by releasing a variety of proinflammatory and fibrogenetic products. Pathogen- or non-pathogen-derived innate immune responses trigger these processes, ultimately aggravating kidney disease. For example, a pathogen sensor TLR expressed by immune cells as well as by intrinsic renal cells can induce infiltration of inflammatory cells, cell activation, and fibrosis (Anders, 2010; Schlondorff, 2008). Here, we first addressed the question whether renal fibroblasts were a major source of fibrogenetic products causing fibrosis in response to exogenous factors. Our data revealed that TLR-activated renal fibroblasts may be involved in inflammation but not in tissue remodeling. We showed that the expression of proinflammatory cytokines, e.g. IL-6 and CCL-2/MCP-1, was induced, while profibrotic molecules, e.g. collagen 1 α , TGF- β , and smooth muscle actin, remained unchanged in the presence of TLR agonists.

The precise role of intrarenal leukocytes with innate immunity in the pathology of Alport nephropathy however still remains unresolved. The blockade of the proinflammatory CC-chemokine CCL2/MCP-1 has no effect on kidney disease progression and survival of *Col4a3*-deficient mice (Clauss et al., 2009). This is suggesting as CCL2/MCP-1 blockade or CCL2/MCP-1 deficiency prevents macrophage-mediated renal injury in multiple other models of chronic kidney disease (Vielhauer and Anders, 2009). We therefore postulated that CCL2/MCP-1 blockade fails to delay Alport nephropathy because chemokine receptor CCR2⁺ macrophages are relatively less in kidneys from *Col4a3*-deficient mice with non-inflammatory renal disease (Clauss et al., 2009). In fact, CCR2 is expressed by classically-activated (M1) macrophages that are readily recruited from the circulating monocytes into sites of intense inflammation (Mantovani et al., 2004; Mosser and Edwards, 2008). However, the extent of tissue inflammation seems to

be rather low in Alport nephropathy. Hence, macrophages in Alport kidneys might display rather non-inflammatory phenotypes. For some tumors, and in late phases of wound healing, similar tissue macrophage phenotypes lacking CCR2 expression and displaying comparable functional properties, i.e. the alternatively-activated (M2) macrophages and immunoregulatory macrophages, have been reported (Gabrilovich and Nagaraj, 2009; Mantovani et al., 2005; Pollard, 2009; Varin and Gordon, 2009b). In fact, the phenotype or activation state of renal macrophages is thought to significantly affect the extent of renal inflammation and tissue damage (Ricardo et al., 2008). For example, *ex vivo* primed M1 or M2 macrophages maintain their phenotype after adoptive transfer into mice with adriamycin-induced glomerular sclerosis (Wang et al., 2007). Furthermore, M1 macrophage infusion aggravates renal damage and dysfunction, whereas M2 macrophage infusion reduces renal pathology and improves renal function. These studies are consistent with our previous findings that macrophage activation towards the M1 phenotype, e.g. with Met-RANTES or with bacterial DNA, aggravates immune complex glomerulonephritis (Anders et al., 2003a; Anders et al., 2003b).

Here, we show that exposure to CpG-DNA, a synthetic mimic of bacterial DNA ligating TLR9, increased the number and activation state of intrarenal macrophages. This phenomenon was associated with a robust acceleration of renal disease progression. These data suggest first, that the natural course of Alport nephropathy involves a low degree of intrarenal inflammation associated with rather alternatively-activated macrophage infiltrates. Second, environmental stimuli like microbial DNA can drive disease progression by enhancing inflammation via modulating intrarenal macrophage numbers as well as their phenotype. Finally, TNF- α induction is a major element of CpG-DNA-induced acceleration of Alport nephropathy.

The phenotypical diversity of tissue macrophages has evolved as a new research field but the classification of macrophage phenotypes still remains a matter of debate (Mosser and Edwards, 2008; Pollard, 2009; Varin and Gordon, 2009b). Classically-activated (M1) macrophages had been defined as an IL-12, IL-23, and MHCII expressing phenotype upon IFN- γ and TNF- α stimulation (Mantovani et al., 2004). By contrast, IL-4 and/or IL-13 or IL-10 stimulation induce alternatively-activated (M2) macrophages that do not produce the aforementioned proinflammatory mediators but rather express IL-10, Arg-1, Fizz-1, and the mannose receptor (Mantovani et al., 2004). Alternatively-activated macrophages seem to predominate in kidneys of *Col4a3*-deficient mice and may contribute to the remodeling of the extracellular matrix. For example, macrophage

metalloelastase was shown to contribute to the digestive damage of the GBM in *Col4a3*-deficient mice (Rao et al., 2006b). By contrast, we found only very few CD11b⁺/Ly6C^{hi} macrophages in kidneys of *Col4a3*-deficient mice at 6 weeks of age. This may explain why blocking the CC-chemokine CCL2/MCP-1 does not modulate murine Alport nephropathy (Clauss et al., 2009), although CCL2/MCP-1 blockade reduces the progression of most types of experimental kidney diseases by preventing the recruitment and activation of CCR2⁺ M1 macrophages (Mantovani et al., 2004; Ricardo et al., 2008). Our data also demonstrate that systemic exposure to CpG-DNA is more potent than LPS to modulate intrarenal macrophages towards a proinflammatory phenotype as evidenced by increased numbers of CD11b⁺/Ly6C^{hi} macrophages and renal mRNA expression of M1 macrophage markers in CpG-DNA-treated *Col4a3*-deficient mice. These results are consistent with the effects of CpG-DNA on cultured macrophages (Mantovani et al., 2005) and the effects of CpG-DNA injections in murine models of immune complex glomerulonephritis (Anders et al., 2003a; Anders et al., 2004). As a note of caution, such models involve effects of CpG-DNA on humoral immunity that may compromise conclusions on the role of glomerular macrophage phenotypes. A recent study has documented the role of activated macrophages in focal segmental glomerulosclerosis in further detail. Wang, *et al.* observed that the injection of *ex vivo* CpG-DNA-primed macrophages accelerated adriamycin nephropathy, while injection of resting macrophages had no effect (Wang et al., 2007). Our data are consistent with these results albeit we had injected CpG-DNA directly into the mice, thereby mimicking an environmental and systemic trigger of macrophage activation. Interestingly, CpG-DNA also induced M2 macrophage markers like Arg-1, TGF- β , mannose receptor, Fizz-1, and IL-10. Macrophage diversity is obviously more complex in tissue environments and is likely to extend beyond the M1/M2 paradigm (Mosser and Edwards, 2008). Irrespective of such classification issues, our data demonstrate that TNF- α induction is functionally crucial in CpG-DNA-accelerated Alport nephropathy. The TNF- α released by classically-activated macrophages accounts for inflammation and tissue damage in chronic rheumatic diseases, psoriasis, and Crohn's disease. As shown in first study, the increased TNF- α expression by renal cells as well as infiltrated leukocytes was found in rather non-inflammatory type of Alport nephropathy. Furthermore, it has been demonstrated that TNF- α has a pivotal role of contributing to glomerulosclerosis by enhancing podocyte loss. Our key finding reported in the current study is that CpG-DNA switches macrophages towards the M1 phenotype. In turn, they increase renal TNF- α

expression and thus contribute to the acceleration of renal disease progression. Interestingly, our previous data reported in this thesis have shown that the TNF- α blockade with etanercept delayed glomerulosclerosis in *Col4a3*-deficient mice by reducing podocyte loss. This treatment also prevented the acceleration of Alport nephropathy and was consistent with the protective effect of TNF- α inhibitors in renal disease models that are associated with the presence of classically-activated macrophages (Choi et al., 2009; Elmarakby et al., 2006; Karkar et al., 2001; Lech et al., 2009). In addition, macrophage-derived TNF- α mediates podocyte activation and dedifferentiation *in vitro* (Ikezumi et al., 2008). Taken together, our findings are that TNF- α expression in glomeruli promotes podocyte loss by CpG-DNA injection, and TNF- α blockade protects from CpG-DNA-induced acceleration of glomerulosclerosis.

Our data in this thesis suggest that TNF- α plays a pivotal role in the pathogenesis of Alport nephropathy. Therefore, targeting TNF- α could be another novel potential therapy for AS. The TNF- α expression is increased by two possible ways: endogenous expression by renal intrinsic cells (podocytes) as well as infiltrated leukocytes during the progression of Alport nephropathy. It is also enhanced by M1 macrophage stimulated with environmental factors such as bacterial product (CpG-DNA). This represents that activation of TNF- α signaling accelerates podocyte loss contributing to glomerulosclerosis in Alport nephropathy (Figure 38). We show that TNF- α blockade with etanercept has beneficial effects in murine Alport nephropathy. Further studies in humans are demanded to confirm the beneficial effects in human AS. We conclude that, inhibition of the TNF- α signaling may be a novel potential therapeutic target to delay ESRD by reducing glomerulosclerosis in patients with Alport nephropathy.

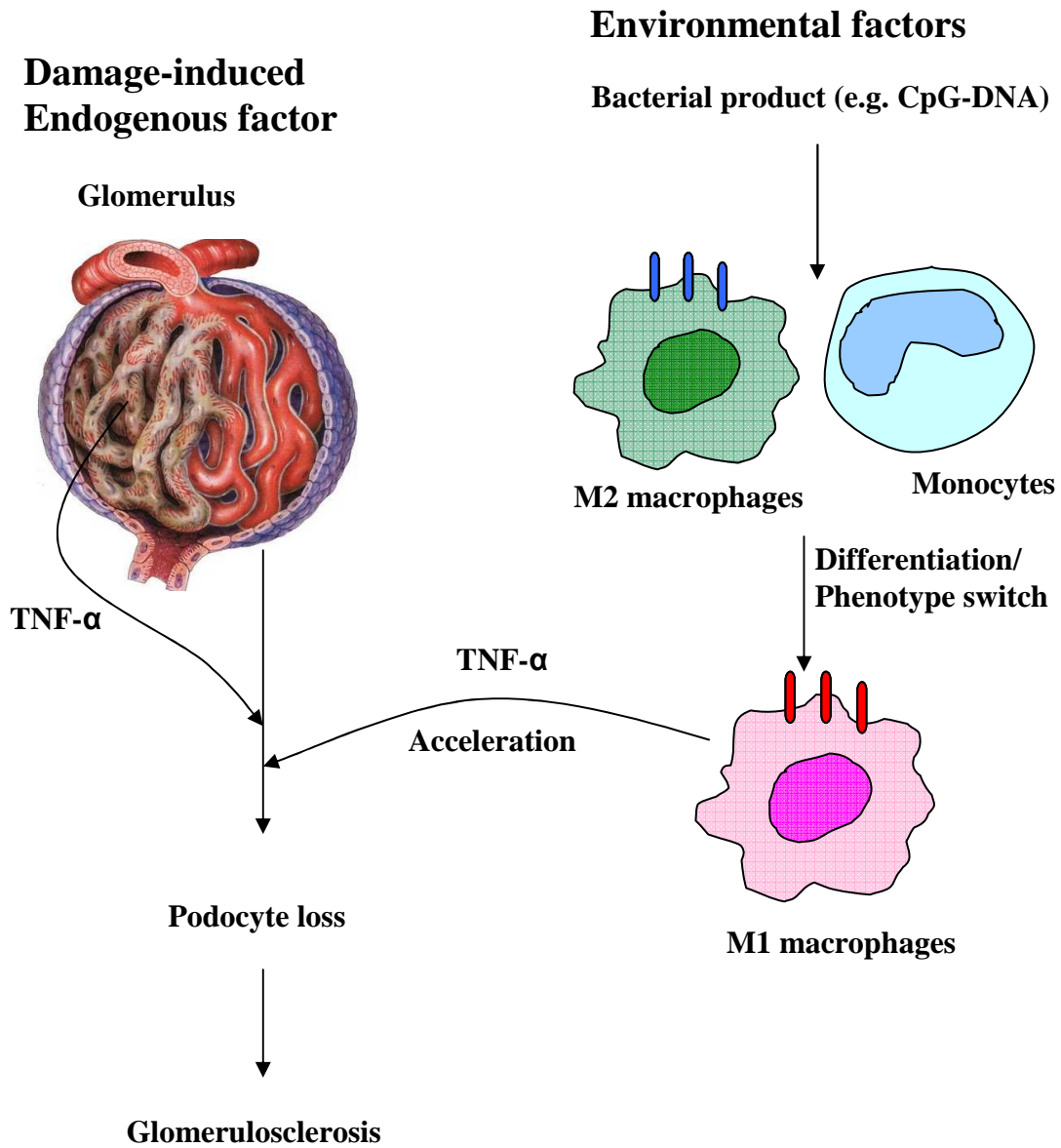


Figure 38. The role of TNF- α on Alport kidney. TNF- α is expressed by both of renal intrinsic cells (e.g. podocytes) and by infiltrating leukocytes (e.g. macrophages). The secretion of TNF- α alone contributes to the Alport glomerulosclerosis by inducing podocyte loss and external signal (e.g. bacterial CpG-DNA) induced-macrophage phenotype switch towards M1 macrophages remarkably increased TNF- α expression leading to the aggravation of glomerulosclerosis by podocyte loss.

6. Summary and conclusion

The pathomechanisms of the progression of chronic kidney diseases involve progressive glomerulosclerosis with renal parenchymal cell loss by proapoptotic factors. Tumor necrosis factor- α (TNF- α) is a proapoptotic cytokine that is produced by macrophages as well as by a variety of cell types. TNF- α signaling regulates cell survival and death. Like in other inflammatory renal diseases, the increased intrarenal TNF- α expression contributes to the disease progression of Alport nephropathy, “a non-inflammatory” murine CKD model. I show that TNF- α expressed by podocytes as well as by infiltrating leukocytes progressively activates renal parenchymal cells, inducing apoptotic pathways that can trigger glomerulosclerosis in Alport disease. The blockade of TNF- α by etanercept prolonged mean survival of *Col4a3*-deficient mice. The beneficial effect on life span was associated with a significant improvement of the glomerulosclerosis, proteinuria, and the glomerular filtration rate (GFR). In particular, etanercept treatment significantly increased the number of glomerular podocytes (WT-1 and nephrin co-staining) and the renal mRNA expression of nephrin and podocin without affecting markers of renal inflammation. The increased number of podocytes was consistent with less TUNEL-positive podocytes that undergo apoptosis.

Importantly, exogenous signals, e.g. infections or toxins, have the potential to regulate the influx of immune cells including dendritic cells, macrophages, neutrophils, and T cells. Here I report a large influx of leukocyte subsets that are mostly dendritic cells and macrophages in *Col4a3*-deficient mice as compared to wildtype mice. While bacterial endotoxin treatment had no effect on the renal disease progression, bacterial cytosine-guanine (CpG)-DNA exacerbated all aspects of Alport nephropathy and reduced the overall life span of *Col4a3*-deficient mice. This effect of CpG-DNA was associated with a significant increase of renal CD11b⁺/Ly6C^{high} macrophages, intrarenal production of TNF- α , iNOS, IL-12, and CXCL10. CpG-DNA switched intrarenal macrophages from non-activated phenotype (M2) towards the classically activated form (M1). These M1 macrophages increased the secretion of TNF- α , which accelerated the disease progression of Alport nephropathy by inducing podocyte loss.

Taken together, I demonstrated that TNF- α is a crucial cytokine which induces podocyte loss in the natural course of the progression of Alport nephropathy. Moreover, the expression of TNF- α is enhanced by selective exogenous factors, e.g. TLR9 activation, which alter the phenotype of renal macrophages towards the M1 phenotype. TNF- α blockade might therefore represent a novel therapeutical option to delay the progression of Alport nephropathy and potentially of other forms of glomerulosclerosis in non-inflammatory and inflammatory conditions.

7. Zusammenfassung

Die Pathogenese des chronischen Nierenversagens beinhaltet die progrediente Glomerulosklerose mit dem Verlust von Nierenparenchymzellen durch proapoptotische Faktoren. Tumor-Nekrose-Faktor-alpha (TNF- α) ist ein proapoptotisches Zytokin, das sowohl von Makrophagen als auch von einer Vielzahl anderer Zellen gebildet und freigesetzt wird. Der TNF- α Signalweg reguliert Zellüberleben und Zelltod. Wie in anderen inflammatorischen Nierenerkrankungen trägt die gesteigerte intrarenale TNF- α -Expression zum Fortschreiten der Alport-Nephropathie, einer "nicht-inflammatorischen" chronischen Nierenerkrankung, im Mausmodell bei. TNF- α , das in Podozyten und infiltrierenden Leukozyten experimentiert wird, aktiviert Nierenparenchymzellen über apoptotische Signalwege, was zu Alport-Glomerulosklerose führen kann. In der vorliegenden Dissertation berichte ich, dass die Blockade von TNF- α durch Etanercept die Lebensdauer von *Col4a3*-defizienten Mäusen verlängerte. Dieser positive Effekt auf die Lebensspanne war mit einer signifikanten Verbesserung der Glomerulosklerose, der Proteinurie und der glomerulären Filtrationsrate (GFR) verbunden. Vor allem die Etanercept-Behandlung erhöhte signifikant die glomeruläre Podozytenzahl und die renale mRNA-Expression von Nephritin und Podocin, ohne jedoch Marker der renalen Inflammation zu beeinflussen. Die zunehmende Zahl der Podozyten war mit einer Abnahme apoptotischer Podozyten assoziiert.

Desweiteren können exogene Stimuli, wie zum Beispiel Infektionen oder Toxine, die Rekrutierung von Immunzellen (dendritische Zellen, Makrophagen, Neutrophile, T-Lymphozyten) modulieren. Im Vergleich zu Nieren von Wildtyp-Mäusen beobachtete ich eine vermehrte Infiltration von Leukozyten, größtenteils bestehend aus dendritischen Zellen und Makrophagen in *Col4a3*-defizienten Nieren. Während das bakterielle Endotoxin LPS keinen Effekt auf die Progression des Krankheitsgeschehens hatte, führte die Stimulation mit Cytosine-Guanin-reicher DNA (CpG-DNA) zu einer Aggravation in allen Aspekten der Alport-Nephropathie und insbesondere zu einer verkürzten Lebensdauer der *Col4a3*-defizienten Mäuse. Dieser Effekt der CpG-DNA-Stimulation war assoziiert mit einer signifikant erhöhten Anzahl von renalen CD11b⁺/Ly6C^{high}-Makrophagen sowie einer vermehrten intrarenalen Produktion von TNF- α , iNOS, IL-12 und CXCL10. CpG-DNA vermittelte die Makrophagen-Differenzierung vom unaktivierten M2-Phänotyp zum klassisch-aktivierten M1-Phänotyp. Interessanterweise sezernieren diese M1-Makrophagen vermehrt TNF- α , was die Progression der Alport-Nephropathie durch zusätzlichen Verlust von Podozyten beschleunigt. Zusammenfassend konnte ich zeigen, dass TNF- α ein entscheidendes Zytokin bei der Induktion des Podozytenverlustes in der Pathogenese der Alport-Nephropathie ist. Darüber hinaus wird die Expression von TNF- α durch einzelne exogene Stimuli wie z.B. TLR9-Aktivierung hochreguliert, was den Phänotyp der renalen Makrophagen in Richtung M1 verschiebt. Die TNF- α -Blockade könnte daher eine therapeutische Option im Rahmen der Behandlung der Alport-Nephropathie sowie anderer Formen der nicht-inflammatorischen und inflammatorischen Glomerulosklerose darstellen.

8. References

1. Abrahamson, D.R. 1987. Structure and development of the glomerular capillary wall and basement membrane. *Am J Physiol* 253:F783-794.
2. Akira, S., and K. Takeda. 2004. Toll-like receptor signalling. *Nat Rev Immunol* 4:499-511.
3. Akira, S., K. Takeda, and T. Kaisho. 2001. Toll-like receptors: critical proteins linking innate and acquired immunity. *Nat Immunol* 2:675-680.
4. Akira, S., S. Uematsu, and O. Takeuchi. 2006. Pathogen recognition and innate immunity. *Cell* 124:783-801.
5. Alexopoulou, L., A.C. Holt, R. Medzhitov, and R.A. Flavell. 2001. Recognition of double-stranded RNA and activation of NF-kappaB by Toll-like receptor 3. *Nature* 413:732-738.
6. Almand, B., J.I. Clark, E. Nikitina, J. van Beynen, N.R. English, S.C. Knight, D.P. Carbone, and D.I. Gabrilovich. 2001. Increased production of immature myeloid cells in cancer patients: a mechanism of immunosuppression in cancer. *J Immunol* 166:678-689.
7. Alport, A.C. 1927. Hereditary Familial Congenital Haemorrhagic Nephritis. *Br Med J* 1:504-506.
8. Anders, H.J. 2007. Innate pathogen recognition in the kidney: toll-like receptors, NOD-like receptors, and RIG-like helicases. *Kidney Int* 72:1051-1056.
9. Anders, H.J. 2010. Toll-like receptors and danger signaling in kidney injury. *J Am Soc Nephrol* 21:1270-1274.
10. Anders, H.J., B. Banas, Y. Linde, L. Weller, C.D. Cohen, M. Kretzler, S. Martin, V. Vielhauer, D. Schlondorff, and H.J. Grone. 2003a. Bacterial CpG-DNA aggravates immune complex glomerulonephritis: role of TLR9-mediated expression of chemokines and chemokine receptors. *J Am Soc Nephrol* 14:317-326.
11. Anders, H.J., M. Frink, Y. Linde, B. Banas, M. Wornle, C.D. Cohen, V. Vielhauer, P.J. Nelson, H.J. Grone, and D. Schlondorff. 2003b. CC chemokine ligand 5/RANTES chemokine antagonists aggravate glomerulonephritis despite reduction of glomerular leukocyte infiltration. *J Immunol* 170:5658-5666.
12. Anders, H.J., V. Ninichuk, and D. Schlondorff. 2006. Progression of kidney disease: blocking leukocyte recruitment with chemokine receptor CCR1 antagonists. *Kidney Int* 69:29-32.
13. Anders, H.J., V. Vielhauer, V. Eis, Y. Linde, M. Kretzler, G. Perez de Lema, F. Strutz, S. Bauer, M. Rutz, H. Wagner, H.J. Grone, and D. Schlondorff. 2004. Activation of toll-like receptor-9 induces progression of renal disease in MRL-Fas(lpr) mice. *Faseb J* 18:534-536.
14. Appel, D., D.B. Kershaw, B. Smeets, G. Yuan, A. Fuss, B. Frye, M. Elger, W. Kriz, J. Floege, and M.J. Moeller. 2009. Recruitment of podocytes from glomerular parietal epithelial cells. *J Am Soc Nephrol* 20:333-343.
15. Barker, D.F., S.L. Hostikka, J. Zhou, L.T. Chow, A.R. Oliphant, S.C. Gerken, M.C. Gregory, M.H. Skolnick, C.L. Atkin, and K. Tryggvason. 1990. Identification of mutations in the COL4A5 collagen gene in Alport syndrome. *Science* 248:1224-1227.
16. Bellini, A., and S. Mattoli. 2007. The role of the fibrocyte, a bone marrow-derived mesenchymal progenitor, in reactive and reparative fibroses. *Lab Invest* 87:858-870.

17. Beutler, B. 2004. Inferences, questions and possibilities in Toll-like receptor signalling. *Nature* 430:257-263.
18. Bhoj, V.G., and Z.J. Chen. 2009. Ubiquitylation in innate and adaptive immunity. *Nature* 458:430-437.
19. Boltz-Nitulescu, G., C. Wiltshcke, C. Holzinger, A. Fellingner, O. Scheiner, A. Gessl, and O. Forster. 1987. Differentiation of rat bone marrow cells into macrophages under the influence of mouse L929 cell supernatant. *J Leukoc Biol* 41:83-91.
20. Bonventre, J.V. 2003. Dedifferentiation and proliferation of surviving epithelial cells in acute renal failure. *J Am Soc Nephrol* 14 Suppl 1:S55-61.
21. Bonventre, J.V., and A. Zuk. 2004. Ischemic acute renal failure: an inflammatory disease? *Kidney Int* 66:480-485.
22. Boor, P., K. Sebekova, T. Ostendorf, and J. Floege. 2007. Treatment targets in renal fibrosis. *Nephrol Dial Transplant* 22:3391-3407.
23. Borza, D.B., O. Bondar, Y. Ninomiya, Y. Sado, I. Naito, P. Todd, and B.G. Hudson. 2001. The NC1 domain of collagen IV encodes a novel network composed of the alpha 1, alpha 2, alpha 5, and alpha 6 chains in smooth muscle basement membranes. *J Biol Chem* 276:28532-28540.
24. Bowie, A.G., and L. Unterholzner. 2008. Viral evasion and subversion of pattern-recognition receptor signalling. *Nat Rev Immunol* 8:911-922.
25. Bucala, R., L.A. Spiegel, J. Chesney, M. Hogan, and A. Cerami. 1994. Circulating fibrocytes define a new leukocyte subpopulation that mediates tissue repair. *Mol Med* 1:71-81.
26. Choi, D.E., J.Y. Jeong, B.J. Lim, K.R. Na, Y.T. Shin, and K.W. Lee. 2009. Pretreatment with the tumor necrosis factor-alpha blocker etanercept attenuated ischemia-reperfusion renal injury. *Transplant Proc* 41:3590-3596.
27. Chow, F., E. Ozols, D.J. Nikolic-Paterson, R.C. Atkins, and G.H. Tesch. 2004a. Macrophages in mouse type 2 diabetic nephropathy: correlation with diabetic state and progressive renal injury. *Kidney Int* 65:116-128.
28. Chow, F.Y., D.J. Nikolic-Paterson, R.C. Atkins, and G.H. Tesch. 2004b. Macrophages in streptozotocin-induced diabetic nephropathy: potential role in renal fibrosis. *Nephrol Dial Transplant* 19:2987-2996.
29. Clauss, S., O. Gross, O. Kulkarni, A. Avila-Ferrufino, E. Radomska, S. Segerer, D. Eulberg, S. Klussmann, and H.J. Anders. 2009. Ccl2/Mcp-1 blockade reduces glomerular and interstitial macrophages but does not ameliorate renal pathology in collagen4A3-deficient mice with autosomal recessive Alport nephropathy. *J Pathol* 218:40-47.
30. Clayton, A., R. Steadman, and J.D. Williams. 1997. Cells isolated from the human cortical interstitium resemble myofibroblasts and bind neutrophils in an ICAM-1--dependent manner. *J Am Soc Nephrol* 8:604-615.
31. Coban, C., Y. Igari, M. Yagi, T. Reimer, S. Koyama, T. Aoshi, K. Ohata, T. Tsukui, F. Takeshita, K. Sakurai, T. Ikegami, A. Nakagawa, T. Horii, G. Nunez, K.J. Ishii, and S. Akira. 2010. Immunogenicity of whole-parasite vaccines against *Plasmodium falciparum* involves malarial hemozoin and host TLR9. *Cell Host Microbe* 7:50-61.
32. Coban, C., K.J. Ishii, T. Kawai, H. Hemmi, S. Sato, S. Uematsu, M. Yamamoto, O. Takeuchi, S. Itagaki, N. Kumar, T. Horii, and S. Akira. 2005. Toll-like receptor 9 mediates innate immune activation by the malaria pigment hemozoin. *J Exp Med* 201:19-25.

33. Coffelt, S.B., R. Hughes, and C.E. Lewis. 2009. Tumor-associated macrophages: effectors of angiogenesis and tumor progression. *Biochim Biophys Acta* 1796:11-18.
34. Coresh, J., B.C. Astor, T. Greene, G. Eknoyan, and A.S. Levey. 2003. Prevalence of chronic kidney disease and decreased kidney function in the adult US population: Third National Health and Nutrition Examination Survey. *Am J Kidney Dis* 41:1-12.
35. Cosgrove, D., R. Kalluri, J.H. Miner, Y. Segal, and D.B. Borza. 2007. Choosing a mouse model to study the molecular pathobiology of Alport glomerulonephritis. *Kidney Int* 71:615-618.
36. Cosgrove, D., D.T. Meehan, J.A. Grunkemeyer, J.M. Kornak, R. Sayers, W.J. Hunter, and G.C. Samuelson. 1996. Collagen COL4A3 knockout: a mouse model for autosomal Alport syndrome. *Genes Dev* 10:2981-2992.
37. Cosgrove, D., K. Rodgers, D. Meehan, C. Miller, K. Bovard, A. Gilroy, H. Gardner, V. Kotelianski, P. Gotwals, A. Amatucci, and R. Kalluri. 2000. Integrin alpha1beta1 and transforming growth factor-beta1 play distinct roles in alport glomerular pathogenesis and serve as dual targets for metabolic therapy. *Am J Pathol* 157:1649-1659.
38. Davies, J.Q., and S. Gordon. 2005. Isolation and culture of human macrophages. *Methods Mol Biol* 290:105-116.
39. Dehmel, S., S. Wang, C. Schmidt, E. Kiss, R.P. Loewe, S. Chilla, D. Schlondorff, H.J. Grone, and B. Luckow. 2010. Chemokine receptor Ccr5 deficiency induces alternative macrophage activation and improves long-term renal allograft outcome. *Eur J Immunol* 40:267-278.
40. Dong, X., S. Swaminathan, L.A. Bachman, A.J. Croatt, K.A. Nath, and M.D. Griffin. 2007. Resident dendritic cells are the predominant TNF-secreting cell in early renal ischemia-reperfusion injury. *Kidney Int* 71:619-628.
41. Doublier, S., E. Lupia, P. Catanuto, S. Periera-Simon, X. Xia, K. Korach, M. Berho, S.J. Elliot, and M. Karl. 2010. Testosterone and 17beta-estradiol have opposite effects on podocyte apoptosis that precedes glomerulosclerosis in female estrogen receptor knockout mice. *Kidney Int*
42. Duffield, J.S., L.P. Erwig, X. Wei, F.Y. Liew, A.J. Rees, and J.S. Savill. 2000. Activated macrophages direct apoptosis and suppress mitosis of mesangial cells. *J Immunol* 164:2110-2119.
43. Duffield, J.S., P.G. Tipping, T. Kipari, J.F. Cailhier, S. Clay, R. Lang, J.V. Bonventre, and J. Hughes. 2005. Conditional ablation of macrophages halts progression of crescentic glomerulonephritis. *Am J Pathol* 167:1207-1219.
44. Eardley, K.S., C. Kubal, D. Zehnder, M. Quinkler, J. Lepenies, C.O. Savage, A.J. Howie, K. Kaur, M.S. Cooper, D. Adu, and P. Cockwell. 2008. The role of capillary density, macrophage infiltration and interstitial scarring in the pathogenesis of human chronic kidney disease. *Kidney Int* 74:495-504.
45. Elmarakby, A.A., J.E. Quigley, D.M. Pollock, and J.D. Imig. 2006. Tumor necrosis factor alpha blockade increases renal Cyp2c23 expression and slows the progression of renal damage in salt-sensitive hypertension. *Hypertension* 47:557-562.
46. Feldmann, M., and R.N. Maini. 2003. Lasker Clinical Medical Research Award. TNF defined as a therapeutic target for rheumatoid arthritis and other autoimmune diseases. *Nat Med* 9:1245-1250.
47. Ferenbach, D., D.C. Kluth, and J. Hughes. 2007. Inflammatory cells in renal injury and repair. *Semin Nephrol* 27:250-259.

48. Gabrilovich, D.I., and S. Nagaraj. 2009. Myeloid-derived suppressor cells as regulators of the immune system. *Nat Rev Immunol* 9:162-174.
49. Gao, B., and M.F. Tsan. 2003. Endotoxin contamination in recombinant human heat shock protein 70 (Hsp70) preparation is responsible for the induction of tumor necrosis factor alpha release by murine macrophages. *J Biol Chem* 278:174-179.
50. Gordon, S. 2003. Alternative activation of macrophages. *Nat Rev Immunol* 3:23-35.
51. Gordon, S., and F.O. Martinez. 2010. Alternative activation of macrophages: mechanism and functions. *Immunity* 32:593-604.
52. Gross, O., B. Beirowski, M.L. Koepke, J. Kuck, M. Reiner, K. Addicks, N. Smyth, E. Schulze-Lohoff, and M. Weber. 2003. Preemptive ramipril therapy delays renal failure and reduces renal fibrosis in COL4A3-knockout mice with Alport syndrome. *Kidney international* 63:438-446.
53. Gross, O., D.B. Borza, H.J. Anders, C. Licht, M. Weber, S. Segerer, R. Torra, M.C. Gubler, L. Heidet, S. Harvey, D. Cosgrove, G. Lees, C. Kashtan, M. Gregory, J. Savige, J. Ding, P. Thorner, D.R. Abrahamson, C. Antignac, K. Tryggvason, B. Hudson, and J.H. Miner. 2009. Stem cell therapy for Alport syndrome: the hope beyond the hype. *Nephrol Dial Transplant* 24:731-734.
54. Gross, O., and C.E. Kashtan. 2009. Treatment of Alport syndrome: beyond animal models. *Kidney international* 76:599-603.
55. Gross, O., M.L. Koepke, B. Beirowski, E. Schulze-Lohoff, S. Segerer, and M. Weber. 2005. Nephroprotection by antifibrotic and anti-inflammatory effects of the vasopeptidase inhibitor AVE7688. *Kidney international* 68:456-463.
56. Gross, O., C. Licht, H.J. Anders, B. Hoppe, B. Beck, B. Tonshoff, B. Hocker, S. Wygoda, J.H. Ehrich, L. Pape, M. Konrad, W. Rascher, J. Dotsch, D.E. Muller-Wiefel, P. Hoyer, B. Knebelmann, Y. Pirson, J.P. Grunfeld, P. Niaudet, P. Cochat, L. Heidet, S. Lebbah, R. Torra, T. Friede, K. Lange, G.A. Muller, and M. Weber. 2012. Early angiotensin-converting enzyme inhibition in Alport syndrome delays renal failure and improves life expectancy. *Kidney international* 81:494-501.
57. Gross, O., E. Schulze-Lohoff, M.L. Koepke, B. Beirowski, K. Addicks, W. Bloch, N. Smyth, and M. Weber. 2004. Antifibrotic, nephroprotective potential of ACE inhibitor vs AT1 antagonist in a murine model of renal fibrosis. *Nephrology, dialysis, transplantation : official publication of the European Dialysis and Transplant Association - European Renal Association* 19:1716-1723.
58. Hacker, H., and M. Karin. 2006. Regulation and function of IKK and IKK-related kinases. *Sci STKE* 2006:re13.
59. Hacker, H., V. Redecke, B. Blagoev, I. Kratchmarova, L.C. Hsu, G.G. Wang, M.P. Kamps, E. Raz, H. Wagner, G. Hacker, M. Mann, and M. Karin. 2006. Specificity in Toll-like receptor signalling through distinct effector functions of TRAF3 and TRAF6. *Nature* 439:204-207.
60. Harvey, S.J., K. Zheng, Y. Sado, I. Naito, Y. Ninomiya, R.M. Jacobs, B.G. Hudson, and P.S. Thorner. 1998. Role of distinct type IV collagen networks in glomerular development and function. *Kidney Int* 54:1857-1866.
61. Hayashi, F., K.D. Smith, A. Ozinsky, T.R. Hawn, E.C. Yi, D.R. Goodlett, J.K. Eng, S. Akira, D.M. Underhill, and A. Aderem. 2001. The innate immune response to bacterial flagellin is mediated by Toll-like receptor 5. *Nature* 410:1099-1103.

62. Hehlhans, T., and K. Pfeffer. 2005. The intriguing biology of the tumour necrosis factor/tumour necrosis factor receptor superfamily: players, rules and the games. *Immunology* 115:1-20.
63. Heidet, L., Y. Cai, L. Guicharnaud, C. Antignac, and M.C. Gubler. 2000. Glomerular expression of type IV collagen chains in normal and X-linked Alport syndrome kidneys. *Am J Pathol* 156:1901-1910.
64. Heidet, L., and M.C. Gubler. 2009. The renal lesions of Alport syndrome. *J Am Soc Nephrol* 20:1210-1215.
65. Hemmi, H., O. Takeuchi, T. Kawai, T. Kaisho, S. Sato, H. Sanjo, M. Matsumoto, K. Hoshino, H. Wagner, K. Takeda, and S. Akira. 2000. A Toll-like receptor recognizes bacterial DNA. *Nature* 408:740-745.
66. Hoffmann, J.A. 2003. The immune response of *Drosophila*. *Nature* 426:33-38.
67. Horiuchi, T., H. Mitoma, S. Harashima, H. Tsukamoto, and T. Shimoda. 2010. Transmembrane TNF-alpha: structure, function and interaction with anti-TNF agents. *Rheumatology (Oxford)* 49:1215-1228.
68. Hoshino, K., O. Takeuchi, T. Kawai, H. Sanjo, T. Ogawa, Y. Takeda, K. Takeda, and S. Akira. 1999. Cutting edge: Toll-like receptor 4 (TLR4)-deficient mice are hyporesponsive to lipopolysaccharide: evidence for TLR4 as the Lps gene product. *J Immunol* 162:3749-3752.
69. Huang, X.R., A.R. Kitching, P.G. Tipping, and S.R. Holdsworth. 2000. Interleukin-10 inhibits macrophage-induced glomerular injury. *Journal of the American Society of Nephrology : JASN* 11:262-269.
70. Hudson, B.G. 2004. The molecular basis of Goodpasture and Alport syndromes: beacons for the discovery of the collagen IV family. *J Am Soc Nephrol* 15:2514-2527.
71. Hudson, B.G., S.T. Reeders, and K. Tryggvason. 1993. Type IV collagen: structure, gene organization, and role in human diseases. Molecular basis of Goodpasture and Alport syndromes and diffuse leiomyomatosis. *J Biol Chem* 268:26033-26036.
72. Hudson, B.G., K. Tryggvason, M. Sundaramoorthy, and E.G. Neilson. 2003. Alport's syndrome, Goodpasture's syndrome, and type IV collagen. *N Engl J Med* 348:2543-2556.
73. Ikezumi, Y., R.C. Atkins, and D.J. Nikolic-Paterson. 2003. Interferon-gamma augments acute macrophage-mediated renal injury via a glucocorticoid-sensitive mechanism. *J Am Soc Nephrol* 14:888-898.
74. Ikezumi, Y., T. Suzuki, T. Karasawa, H. Kawachi, D.J. Nikolic-Paterson, and M. Uchiyama. 2008. Activated macrophages down-regulate podocyte nephrin and podocin expression via stress-activated protein kinases. *Biochem Biophys Res Commun* 376:706-711.
75. Jais, J.P., B. Knebelmann, I. Giatras, M. De Marchi, G. Rizzoni, A. Renieri, M. Weber, O. Gross, K.O. Netzer, F. Flinter, Y. Pirson, K. Dahan, J. Wieslander, U. Persson, K. Tryggvason, P. Martin, J.M. Hertz, C. Schroder, M. Sanak, M.F. Carvalho, J. Saus, C. Antignac, H. Smeets, and M.C. Gubler. 2003. X-linked Alport syndrome: natural history and genotype-phenotype correlations in girls and women belonging to 195 families: a "European Community Alport Syndrome Concerted Action" study. *J Am Soc Nephrol* 14:2603-2610.
76. Jais, J.P., B. Knebelmann, I. Giatras, M. De Marchi, G. Rizzoni, A. Renieri, M. Weber, O. Gross, K.O. Netzer, F. Flinter, Y. Pirson, C. Verellen, J. Wieslander, U. Persson, K. Tryggvason, P. Martin, J.M. Hertz, C. Schroder, M. Sanak, S. Krejcova, M.F. Carvalho, J. Saus, C. Antignac, H. Smeets, and M.C. Gubler.

2000. X-linked Alport syndrome: natural history in 195 families and genotype-phenotype correlations in males. *J Am Soc Nephrol* 11:649-657.
77. Janeway, C.A., Jr., and R. Medzhitov. 2002. Innate immune recognition. *Annu Rev Immunol* 20:197-216.
 78. Jedlicka, J., A. Soleiman, D. Draganovici, J. Mandelbaum, U. Ziegler, H. Regele, R.P. Wuthrich, O. Gross, H.J. Anders, and S. Segerer. 2009. Interstitial inflammation in Alport syndrome. *Hum Pathol*
 79. Jiang, Z., P. Georgel, X. Du, L. Shamel, S. Sovath, S. Mudd, M. Huber, C. Kalis, S. Keck, C. Galanos, M. Freudenberg, and B. Beutler. 2005. CD14 is required for MyD88-independent LPS signaling. *Nat Immunol* 6:565-570.
 80. Jo, S.K., S.A. Sung, W.Y. Cho, K.J. Go, and H.K. Kim. 2006. Macrophages contribute to the initiation of ischaemic acute renal failure in rats. *Nephrol Dial Transplant* 21:1231-1239.
 81. Jose, M.D., Y. Ikezumi, N. van Rooijen, R.C. Atkins, and S.J. Chadban. 2003. Macrophages act as effectors of tissue damage in acute renal allograft rejection. *Transplantation* 76:1015-1022.
 82. Kalluri, R., V.H. Gattone, 2nd, and B.G. Hudson. 1998. Identification and localization of type IV collagen chains in the inner ear cochlea. *Connect Tissue Res* 37:143-150.
 83. Kalluri, R., C.F. Shield, P. Todd, B.G. Hudson, and E.G. Neilson. 1997. Isoform switching of type IV collagen is developmentally arrested in X-linked Alport syndrome leading to increased susceptibility of renal basement membranes to endoproteolysis. *J Clin Invest* 99:2470-2478.
 84. Kang, J.S., X.P. Wang, J.H. Miner, R. Morello, Y. Sado, D.R. Abrahamson, and D.B. Borza. 2006. Loss of alpha3/alpha4(IV) collagen from the glomerular basement membrane induces a strain-dependent isoform switch to alpha5alpha6(IV) collagen associated with longer renal survival in Col4a3^{-/-} Alport mice. *J Am Soc Nephrol* 17:1962-1969.
 85. Kang, Y.S., M.H. Lee, H.K. Song, G.J. Ko, O.S. Kwon, T.K. Lim, S.H. Kim, S.Y. Han, K.H. Han, J.E. Lee, J.Y. Han, H.K. Kim, and D.R. Cha. 2010. CCR2 antagonism improves insulin resistance, lipid metabolism, and diabetic nephropathy in type 2 diabetic mice. *Kidney Int* 78:883-894.
 86. Karkar, A.M., J. Smith, and C.D. Pusey. 2001. Prevention and treatment of experimental crescentic glomerulonephritis by blocking tumour necrosis factor-alpha. *Nephrol Dial Transplant* 16:518-524.
 87. Kashtan, C.E. 1998. Alport syndrome and thin glomerular basement membrane disease. *J Am Soc Nephrol* 9:1736-1750.
 88. Kashtan, C.E. 2002. Animal models of Alport syndrome. *Nephrol Dial Transplant* 17:1359-1362.
 89. Kashtan, C.E., J. Ding, M. Gregory, O. Gross, L. Heidet, B. Knebelmann, M. Rheault, and C. Licht. 2012. Clinical practice recommendations for the treatment of Alport syndrome: a statement of the Alport Syndrome Research Collaborative. *Pediatr Nephrol*
 90. Katayama, K., M. Kawano, I. Naito, H. Ishikawa, Y. Sado, N. Asakawa, T. Murata, K. Oosugi, M. Kiyohara, E. Ishikawa, M. Ito, and S. Nomura. 2008. Irradiation prolongs survival of Alport mice. *J Am Soc Nephrol* 19:1692-1700.
 91. Kawagoe, T., S. Sato, K. Matsushita, H. Kato, K. Matsui, Y. Kumagai, T. Saitoh, T. Kawai, O. Takeuchi, and S. Akira. 2008. Sequential control of Toll-like receptor-dependent responses by IRAK1 and IRAK2. *Nat Immunol* 9:684-691.

92. Kawai, T., and S. Akira. 2006a. Innate immune recognition of viral infection. *Nat Immunol* 7:131-137.
93. Kawai, T., and S. Akira. 2006b. TLR signaling. *Cell Death Differ* 13:816-825.
94. Kawai, T., and S. Akira. 2009. The roles of TLRs, RLRs and NLRs in pathogen recognition. *Int Immunol* 21:317-337.
95. Kawai, T., S. Sato, K.J. Ishii, C. Coban, H. Hemmi, M. Yamamoto, K. Terai, M. Matsuda, J. Inoue, S. Uematsu, O. Takeuchi, and S. Akira. 2004. Interferon-alpha induction through Toll-like receptors involves a direct interaction of IRF7 with MyD88 and TRAF6. *Nat Immunol* 5:1061-1068.
96. Kefalides, N.A. 1966. A collagen of unusual composition and a glycoprotein isolated from canine glomerular basement membrane. *Biochemical and biophysical research communications* 22:26-32.
97. Kipari, T., J.F. Cailhier, D. Ferenbach, S. Watson, K. Houlberg, D. Walbaum, S. Clay, J. Savill, and J. Hughes. 2006. Nitric oxide is an important mediator of renal tubular epithelial cell death in vitro and in murine experimental hydronephrosis. *Am J Pathol* 169:388-399.
98. Kitamoto, K., Y. Machida, J. Uchida, Y. Izumi, M. Shiota, T. Nakao, H. Iwao, T. Yukimura, T. Nakatani, and K. Miura. 2009. Effects of liposome clodronate on renal leukocyte populations and renal fibrosis in murine obstructive nephropathy. *J Pharmacol Sci* 111:285-292.
99. Kitching, A.R., S.R. Holdsworth, and M.J. Hickey. 2008. Targeting leukocytes in immune glomerular diseases. *Curr Med Chem* 15:448-458.
100. Kluth, D.C., L.P. Erwig, and A.J. Rees. 2004. Multiple facets of macrophages in renal injury. *Kidney Int* 66:542-557.
101. Kobayashi, T., M.C. Walsh, and Y. Choi. 2004. The role of TRAF6 in signal transduction and the immune response. *Microbes Infect* 6:1333-1338.
102. Koepke, M.L., M. Weber, E. Schulze-Lohoff, B. Beirowski, S. Segerer, and O. Gross. 2007. Nephroprotective effect of the HMG-CoA-reductase inhibitor cerivastatin in a mouse model of progressive renal fibrosis in Alport syndrome. *Nephrology, dialysis, transplantation : official publication of the European Dialysis and Transplant Association - European Renal Association* 22:1062-1069.
103. Kriz, W. 1996. Progressive renal failure--inability of podocytes to replicate and the consequences for development of glomerulosclerosis. *Nephrol Dial Transplant* 11:1738-1742.
104. Kriz, W., M. Elger, P. Mundel, and K.V. Lemley. 1995. Structure-stabilizing forces in the glomerular tuft. *J Am Soc Nephrol* 5:1731-1739.
105. Kriz, W., N. Gretz, and K.V. Lemley. 1998. Progression of glomerular diseases: is the podocyte the culprit? *Kidney Int* 54:687-697.
106. Kriz, W., and K.V. Lemley. 1999. The role of the podocyte in glomerulosclerosis. *Curr Opin Nephrol Hypertens* 8:489-497.
107. Kronenberg, F. 2009. Emerging risk factors and markers of chronic kidney disease progression. *Nat Rev Nephrol* 5:677-689.
108. Kulkarni, O., D. Eulberg, N. Selve, S. Zollner, R. Allam, R.D. Pawar, S. Pfeiffer, S. Segerer, S. Klussmann, and H.J. Anders. 2009. Anti-Ccl2 Spiegelmer permits 75% dose reduction of cyclophosphamide to control diffuse proliferative lupus nephritis and pneumonitis in MRL-Fas(lpr) mice. *J Pharmacol Exp Ther* 328:371-377.
109. Kulkarni, O., R.D. Pawar, W. Purschke, D. Eulberg, N. Selve, K. Buchner, V. Ninichuk, S. Segerer, V. Vielhauer, S. Klussmann, and H.J. Anders. 2007.

- Spiegelmer inhibition of CCL2/MCP-1 ameliorates lupus nephritis in MRL-(Fas)lpr mice. *J Am Soc Nephrol* 18:2350-2358.
110. Kumagai, Y., H. Kumar, S. Koyama, T. Kawai, O. Takeuchi, and S. Akira. 2009. Cutting Edge: TLR-Dependent viral recognition along with type I IFN positive feedback signaling masks the requirement of viral replication for IFN- α production in plasmacytoid dendritic cells. *J Immunol* 182:3960-3964.
 111. Kumar, H., T. Kawai, and S. Akira. 2009. Toll-like receptors and innate immunity. *Biochem Biophys Res Commun* 388:621-625.
 112. Lai, K.N., J.C. Leung, L.Y. Chan, M.A. Saleem, P.W. Mathieson, K.Y. Tam, J. Xiao, F.M. Lai, and S.C. Tang. 2009. Podocyte injury induced by mesangial-derived cytokines in IgA nephropathy. *Nephrol Dial Transplant* 24:62-72.
 113. Lebleu, V.S., H. Sugimoto, C.A. Miller, V.H. Gattone, 2nd, and R. Kalluri. 2008. Lymphocytes are dispensable for glomerulonephritis but required for renal interstitial fibrosis in matrix defect-induced Alport renal disease. *Lab Invest* 88:284-292.
 114. Lech, M., A. Avila-Ferrufino, R. Allam, S. Segerer, A. Khandoga, F. Krombach, C. Garlanda, A. Mantovani, and H.J. Anders. 2009. Resident dendritic cells prevent postischemic acute renal failure by help of single Ig IL-1 receptor-related protein. *J Immunol* 183:4109-4118.
 115. Lee, E.G., D.L. Boone, S. Chai, S.L. Libby, M. Chien, J.P. Lodolce, and A. Ma. 2000. Failure to regulate TNF-induced NF-kappaB and cell death responses in A20-deficient mice. *Science* 289:2350-2354.
 116. Lees, G.E., R.G. Helman, C.E. Kashtan, A.F. Michael, L.D. Homco, N.J. Millichamp, Z.T. Camacho, J.W. Templeton, Y. Ninomiya, Y. Sado, I. Naito, and Y. Kim. 1999. New form of X-linked dominant hereditary nephritis in dogs. *Am J Vet Res* 60:373-383.
 117. Leeuwis, J.W., T.Q. Nguyen, A. Dendooven, R.J. Kok, and R. Goldschmeding. 2010. Targeting podocyte-associated diseases. *Adv Drug Deliv Rev* 62:1325-1336.
 118. Lemmink, H.H., T. Mochizuki, L.P. van den Heuvel, C.H. Schroder, A. Barrientos, L.A. Monnens, B.A. van Oost, H.G. Brunner, S.T. Reeders, and H.J. Smeets. 1994. Mutations in the type IV collagen alpha 3 (COL4A3) gene in autosomal recessive Alport syndrome. *Hum Mol Genet* 3:1269-1273.
 119. Lenda, D.M., E. Kikawada, E.R. Stanley, and V.R. Kelley. 2003. Reduced macrophage recruitment, proliferation, and activation in colony-stimulating factor-1-deficient mice results in decreased tubular apoptosis during renal inflammation. *J Immunol* 170:3254-3262.
 120. Levey, A.S., K.U. Eckardt, Y. Tsukamoto, A. Levin, J. Coresh, J. Rossert, D. De Zeeuw, T.H. Hostetter, N. Lameire, and G. Eknoyan. 2005. Definition and classification of chronic kidney disease: a position statement from Kidney Disease: Improving Global Outcomes (KDIGO). *Kidney Int* 67:2089-2100.
 121. Li, L., L. Huang, S.S. Sung, A.L. Vergis, D.L. Rosin, C.E. Rose, Jr., P.I. Lobo, and M.D. Okusa. 2008. The chemokine receptors CCR2 and CX3CR1 mediate monocyte/macrophage trafficking in kidney ischemia-reperfusion injury. *Kidney Int* 74:1526-1537.
 122. Longo, I., P. Porcedda, F. Mari, D. Giachino, I. Meloni, C. Deplano, A. Brusco, M. Bosio, L. Massella, G. Lavoratti, D. Roccatello, G. Frasca, G. Mazzucco, A.O. Muda, M. Conti, F. Fasciolo, C. Arrondel, L. Heidet, A. Renieri, and M. De Marchi. 2002. COL4A3/COL4A4 mutations: from familial hematuria to autosomal-dominant or recessive Alport syndrome. *Kidney Int* 61:1947-1956.

123. Ma, F.Y., J. Liu, A.R. Kitching, C.L. Manthey, and D.J. Nikolic-Paterson. 2009. Targeting renal macrophage accumulation via c-fms kinase reduces tubular apoptosis but fails to modify progressive fibrosis in the obstructed rat kidney. *Am J Physiol Renal Physiol* 296:F177-185.
124. Macconi, D., F. Sangalli, M. Bonomelli, S. Conti, L. Condorelli, E. Gagliardini, G. Remuzzi, and A. Remuzzi. 2009. Podocyte repopulation contributes to regression of glomerular injury induced by ACE inhibition. *Am J Pathol* 174:797-807.
125. MacGregor, M.S., D.E. Boag, and A. Innes. 2006. Chronic kidney disease: evolving strategies for detection and management of impaired renal function. *Qjm* 99:365-375.
126. Mancuso, G., M. Gambuzza, A. Midiri, C. Biondo, S. Papasergi, S. Akira, G. Teti, and C. Beninati. 2009. Bacterial recognition by TLR7 in the lysosomes of conventional dendritic cells. *Nat Immunol* 10:587-594.
127. Mantovani, A., A. Sica, and M. Locati. 2005. Macrophage polarization comes of age. *Immunity* 23:344-346.
128. Mantovani, A., A. Sica, S. Sozzani, P. Allavena, A. Vecchi, and M. Locati. 2004. The chemokine system in diverse forms of macrophage activation and polarization. *Trends Immunol* 25:677-686.
129. Medzhitov, R. 2007. Recognition of microorganisms and activation of the immune response. *Nature* 449:819-826.
130. Medzhitov, R., and C. Janeway, Jr. 2000. Innate immunity. *N Engl J Med* 343:338-344.
131. Miner, J.H., and J.R. Sanes. 1996. Molecular and functional defects in kidneys of mice lacking collagen alpha 3(IV): implications for Alport syndrome. *J Cell Biol* 135:1403-1413.
132. Miosge, N., C. Klenczar, R. Herken, M. Willem, and U. Mayer. 1999. Organization of the myotendinous junction is dependent on the presence of alpha7beta1 integrin. *Lab Invest* 79:1591-1599.
133. Mochizuki, T., H.H. Lemmink, M. Mariyama, C. Antignac, M.C. Gubler, Y. Pirson, C. Verellen-Dumoulin, B. Chan, C.H. Schroder, H.J. Smeets, and et al. 1994. Identification of mutations in the alpha 3(IV) and alpha 4(IV) collagen genes in autosomal recessive Alport syndrome. *Nat Genet* 8:77-81.
134. Mosser, D.M., and J.P. Edwards. 2008. Exploring the full spectrum of macrophage activation. *Nat Rev Immunol* 8:958-969.
135. Mundel, P., and W. Kriz. 1995. Structure and function of podocytes: an update. *Anat Embryol* 192:385-397.
136. National Kidney Foundation. 2002. K/DOQI clinical practice guidelines for chronic kidney disease: evaluation, classification, and stratification. *Am J Kidney Dis* 39:S1-266.
137. Niedermeier, M., B. Reich, M. Rodriguez Gomez, A. Denzel, K. Schmidbauer, N. Gobel, Y. Talke, F. Schweda, and M. Mack. 2009. CD4+ T cells control the differentiation of Gr1+ monocytes into fibrocytes. *Proc Natl Acad Sci U S A* 106:17892-17897.
138. Ninichuk, V., S. Clauss, O. Kulkarni, H. Schmid, S. Segerer, E. Radomska, D. Eulberg, K. Buchner, N. Selve, S. Klussmann, and H.J. Anders. 2008. Late onset of Ccl2 blockade with the Spiegelmer mNOX-E36-3'PEG prevents glomerulosclerosis and improves glomerular filtration rate in db/db mice. *Am J Pathol* 172:628-637.

139. Ninichuk, V., O. Gross, C. Reichel, A. Khandoga, R.D. Pawar, R. Ciubar, S. Segerer, E. Belemezova, E. Radomska, B. Luckow, G. Perez de Lema, P.M. Murphy, J.L. Gao, A. Henger, M. Kretzler, R. Horuk, M. Weber, F. Krombach, D. Schlondorff, and H.J. Anders. 2005. Delayed chemokine receptor 1 blockade prolongs survival in collagen 4A3-deficient mice with Alport disease. *J Am Soc Nephrol* 16:977-985.
140. Ninichuk, V., O. Gross, S. Segerer, R. Hoffmann, E. Radomska, A. Buchstaller, R. Huss, N. Akis, D. Schlondorff, and H.J. Anders. 2006. Multipotent mesenchymal stem cells reduce interstitial fibrosis but do not delay progression of chronic kidney disease in collagen4A3-deficient mice. *Kidney Int* 70:121-129.
141. Ninichuk, V., O. Kulkarni, S. Clauss, and H.J. Anders. 2007. Tubular atrophy, interstitial fibrosis, and inflammation in type 2 diabetic db/db mice. An accelerated model of advanced diabetic nephropathy. *Eur J Med Res* 12:351-355.
142. Ohashi, K., V. Burkart, S. Flohe, and H. Kolb. 2000. Cutting edge: heat shock protein 60 is a putative endogenous ligand of the toll-like receptor-4 complex. *J Immunol* 164:558-561.
143. Ortiz, A., and J. Egido. 1995. Is there a role for specific anti-TNF strategies in glomerular diseases? *Nephrol Dial Transplant* 10:309-311.
144. Pagtalunan, M.E., P.L. Miller, S. Jumping-Eagle, R.G. Nelson, B.D. Myers, H.G. Rennke, N.S. Coplon, L. Sun, and T.W. Meyer. 1997. Podocyte loss and progressive glomerular injury in type II diabetes. *J Clin Invest* 99:342-348.
145. Park, B.S., D.H. Song, H.M. Kim, B.S. Choi, H. Lee, and J.O. Lee. 2009. The structural basis of lipopolysaccharide recognition by the TLR4-MD-2 complex. *Nature* 458:1191-1195.
146. Pavenstadt, H., W. Kriz, and M. Kretzler. 2003. Cell biology of the glomerular podocyte. *Physiol Rev* 83:253-307.
147. Perico, N., A. Benigni, and G. Remuzzi. 2008. Present and future drug treatments for chronic kidney diseases: evolving targets in renoprotection. *Nat Rev Drug Discov* 7:936-953.
148. Pescucci, C., F. Mari, I. Longo, P. Vogiatzi, R. Caselli, E. Scala, C. Abaterusso, R. Gusmano, M. Seri, N. Miglietti, E. Bresin, and A. Renieri. 2004. Autosomal-dominant Alport syndrome: natural history of a disease due to COL4A3 or COL4A4 gene. *Kidney Int* 65:1598-1603.
149. Pollard, J.W. 2009. Trophic macrophages in development and disease. *Nat Rev Immunol* 9:259-270.
150. Poltorak, A., X. He, I. Smirnova, M.Y. Liu, C. Van Huffel, X. Du, D. Birdwell, E. Alejos, M. Silva, C. Galanos, M. Freudenberg, P. Ricciardi-Castagnoli, B. Layton, and B. Beutler. 1998. Defective LPS signaling in C3H/HeJ and C57BL/10ScCr mice: mutations in Tlr4 gene. *Science* 282:2085-2088.
151. Qi, F., A. Adair, D. Ferenbach, D.G. Vass, K.J. Mylonas, T. Kipari, M. Clay, D.C. Kluth, J. Hughes, and L.P. Marson. 2008. Depletion of cells of monocyte lineage prevents loss of renal microvasculature in murine kidney transplantation. *Transplantation* 86:1267-1274.
152. Rahman, M.M., and G. McFadden. 2006. Modulation of tumor necrosis factor by microbial pathogens. *PLoS Pathog* 2:e4.
153. Rao, V.H., D.T. Meehan, D. Delimont, M. Nakajima, T. Wada, M.A. Gratton, and D. Cosgrove. 2006a. Role for macrophage metalloelastase in glomerular basement membrane damage associated with alport syndrome. *Am J Pathol.* 169:32-46.

154. Rao, V.H., D.T. Meehan, D. Delimont, M. Nakajima, T. Wada, M.A. Gratton, and D. Cosgrove. 2006b. Role for macrophage metalloelastase in glomerular basement membrane damage associated with alport syndrome. *Am J Pathol* 169:32-46.
155. Remuzzi, A., E. Gagliardini, F. Sangalli, M. Bonomelli, M. Piccinelli, A. Benigni, and G. Remuzzi. 2006a. ACE inhibition reduces glomerulosclerosis and regenerates glomerular tissue in a model of progressive renal disease. *Kidney international* 69:1124-1130.
156. Remuzzi, G., A. Benigni, and A. Remuzzi. 2006b. Mechanisms of progression and regression of renal lesions of chronic nephropathies and diabetes. *J Clin Invest* 116:288-296.
157. Remuzzi, G., and T. Bertani. 1998. Pathophysiology of progressive nephropathies. *N Engl J Med* 339:1448-1456.
158. Rheault, M.N., S.M. Kren, B.K. Thielen, H.A. Mesa, J.T. Crosson, W. Thomas, Y. Sado, C.E. Kashtan, and Y. Segal. 2004. Mouse model of X-linked Alport syndrome. *J Am Soc Nephrol* 15:1466-1474.
159. Ribechini, E., V. Greifenberg, S. Sandwick, and M.B. Lutz. 2010. Subsets, expansion and activation of myeloid-derived suppressor cells. *Med Microbiol Immunol* 199:273-281.
160. Ricardo, S.D., H. van Goor, and A.A. Eddy. 2008. Macrophage diversity in renal injury and repair. *J Clin Invest* 118:3522-3530.
161. Romagnani, P. 2009. Toward the identification of a "renopoietic system"? *Stem Cells* 27:2247-2253.
162. Ronconi, E., C. Sagrinati, M.L. Angelotti, E. Lazzeri, B. Mazzinghi, L. Ballerini, E. Parente, F. Becherucci, M. Gacci, M. Carini, E. Maggi, M. Serio, G.B. Vannelli, L. Lasagni, S. Romagnani, and P. Romagnani. 2009. Regeneration of glomerular podocytes by human renal progenitors. *J Am Soc Nephrol* 20:322-332.
163. Saito, Y., M. Okamura, S. Nakajima, K. Hayakawa, T. Huang, J. Yao, and M. Kitamura. 2010. Suppression of nephrin expression by TNF-alpha via interfering with the cAMP-retinoic acid receptor pathway. *Am J Physiol Renal Physiol* 298:F1436-1444.
164. Sanchez-Nino, M.D., A. Benito-Martin, S. Goncalves, A.B. Sanz, A.C. Uceros, M.C. Izquierdo, A.M. Ramos, S. Berzal, R. Selgas, M. Ruiz-Ortega, J. Egido, and A. Ortiz. 2010. TNF superfamily: a growing saga of kidney injury modulators. *Mediators Inflamm* 2010:
165. Sayyed, S.G., H. Hagele, O.P. Kulkarni, K. Endlich, S. Segerer, D. Eulberg, S. Klussmann, and H.J. Anders. 2009. Podocytes produce homeostatic chemokine stromal cell-derived factor-1/CXCL12, which contributes to glomerulosclerosis, podocyte loss and albuminuria in a mouse model of type 2 diabetes. *Diabetologia* 52:2445-2454.
166. Sayyed, S.G., M. Ryu, O.P. Kulkarni, H. Schmid, J. Lichtnekert, S. Gruner, L. Green, P. Mattei, G. Hartmann, and H.J. Anders. 2011. An orally active chemokine receptor CCR2 antagonist prevents glomerulosclerosis and renal failure in type 2 diabetes. *Kidney Int*
167. Schlondorff, D.O. 2008. Overview of factors contributing to the pathophysiology of progressive renal disease. *Kidney Int* 74:860-866.
168. Sean Eardley, K., and P. Cockwell. 2005. Macrophages and progressive tubulointerstitial disease. *Kidney Int* 68:437-455.

169. Shankland, S.J. 2006. The podocyte's response to injury: role in proteinuria and glomerulosclerosis. *Kidney Int* 69:2131-2147.
170. Shembade, N., A. Ma, and E.W. Harhaj. 2010. Inhibition of NF-kappaB signaling by A20 through disruption of ubiquitin enzyme complexes. *Science* 327:1135-1139.
171. Shimazu, R., S. Akashi, H. Ogata, Y. Nagai, K. Fukudome, K. Miyake, and M. Kimoto. 1999. MD-2, a molecule that confers lipopolysaccharide responsiveness on Toll-like receptor 4. *J Exp Med* 189:1777-1782.
172. Sica, A., P. Larghi, A. Mancino, L. Rubino, C. Porta, M.G. Totaro, M. Rimoldi, S.K. Biswas, P. Allavena, and A. Mantovani. 2008. Macrophage polarization in tumour progression. *Semin Cancer Biol* 18:349-355.
173. Smoyer, W.E., and P. Mundel. 1998. Regulation of podocyte structure during the development of nephrotic syndrome. *J Mol Med* 76:172-183.
174. Solinas, G., G. Germano, A. Mantovani, and P. Allavena. 2009. Tumor-associated macrophages (TAM) as major players of the cancer-related inflammation. *J Leukoc Biol* 86:1065-1073.
175. Steffes, M.W., D. Schmidt, R. McCreery, and J.M. Basgen. 2001. Glomerular cell number in normal subjects and in type 1 diabetic patients. *Kidney Int* 59:2104-2113.
176. Stieger, N., K. Worthmann, and M. Schiffer. 2011. The role of metabolic and haemodynamic factors in podocyte injury in diabetes. *Diabetes Metab Res Rev* 27:207-215.
177. Sugimoto, H., T.M. Mundel, M. Sund, L. Xie, D. Cosgrove, and R. Kalluri. 2006. Bone-marrow-derived stem cells repair basement membrane collagen defects and reverse genetic kidney disease. *Proceedings of the National Academy of Sciences of the United States of America* 103:7321-7326.
178. Susztak, K., A.C. Raff, M. Schiffer, and E.P. Bottinger. 2006. Glucose-induced reactive oxygen species cause apoptosis of podocytes and podocyte depletion at the onset of diabetic nephropathy. *Diabetes* 55:225-233.
179. Takeda, K., and S. Akira. 2004. TLR signaling pathways. *Semin Immunol* 16:3-9.
180. Takeuchi, O., and S. Akira. 2010. Pattern recognition receptors and inflammation. *Cell* 140:805-820.
181. Tang, P., M.C. Hung, and J. Klostergaard. 1996. Human pro-tumor necrosis factor is a homotrimer. *Biochemistry* 35:8216-8225.
182. Taylor, P.C. 2010. Pharmacology of TNF blockade in rheumatoid arthritis and other chronic inflammatory diseases. *Curr Opin Pharmacol* 10:308-315.
183. Tesch, G.H., S. Maifert, A. Schwarting, B.J. Rollins, and V.R. Kelley. 1999. Monocyte chemoattractant protein 1-dependent leukocytic infiltrates are responsible for autoimmune disease in MRL-Fas(lpr) mice. *J Exp Med* 190:1813-1824.
184. Trinchieri, G. 2003. Interleukin-12 and the regulation of innate resistance and adaptive immunity. *Nat Rev Immunol* 3:133-146.
185. Uematsu, S., K. Fujimoto, M.H. Jang, B.G. Yang, Y.J. Jung, M. Nishiyama, S. Sato, T. Tsujimura, M. Yamamoto, Y. Yokota, H. Kiyono, M. Miyasaka, K.J. Ishii, and S. Akira. 2008. Regulation of humoral and cellular gut immunity by lamina propria dendritic cells expressing Toll-like receptor 5. *Nat Immunol* 9:769-776.
186. Varfolomeev, E.E., and A. Ashkenazi. 2004. Tumor necrosis factor: an apoptosis JuNKie? *Cell* 116:491-497.

187. Varin, A., and S. Gordon. 2009a. Alternative activation of macrophages: immune function and cellular biology. *Immunobiology* 214:630-641.
188. Varin, A., and S. Gordon. 2009b. Alternative activation of macrophages: Immune function and cellular biology. *Immunobiology*
189. Vielhauer, V., and H.J. Anders. 2009. Chemokines and chemokine receptors as therapeutic targets in chronic kidney disease. *Front Biosci (Schol Ed)* 1:1-12.
190. Vielhauer, V., H.J. Anders, G. Perez de Lema, B. Luckow, D. Schlondorff, and M. Mack. 2003. Phenotyping renal leukocyte subsets by four-color flow cytometry: characterization of chemokine receptor expression. *Nephron Exp Nephrol* 93:e63.
191. Vielhauer, V., and T.N. Mayadas. 2007. Functions of TNF and its receptors in renal disease: distinct roles in inflammatory tissue injury and immune regulation. *Semin Nephrol* 27:286-308.
192. Wada, T., N. Sakai, K. Matsushima, and S. Kaneko. 2007. Fibrocytes: a new insight into kidney fibrosis. *Kidney Int* 72:269-273.
193. Wajant, H., K. Pfizenmaier, and P. Scheurich. 2003. Tumor necrosis factor signaling. *Cell Death Differ* 10:45-65.
194. Wang, Y., Q. Cao, G. Zheng, V.W. Lee, D. Zheng, X. Li, T.K. Tan, and D.C. Harris. 2008. By homing to the kidney, activated macrophages potentially exacerbate renal injury. *Am J Pathol* 172:1491-1499.
195. Wang, Y., Y.P. Wang, G. Zheng, V.W. Lee, L. Ouyang, D.H. Chang, D. Mahajan, J. Coombs, Y.M. Wang, S.I. Alexander, and D.C. Harris. 2007. Ex vivo programmed macrophages ameliorate experimental chronic inflammatory renal disease. *Kidney Int* 72:290-299.
196. Ware, C.F. 2005. Network communications: lymphotoxins, LIGHT, and TNF. *Annu Rev Immunol* 23:787-819.
197. Weinberg, A.D., and R. Montler. 2005. Modulation of TNF receptor family members to inhibit autoimmune disease. *Curr Drug Targets Inflamm Allergy* 4:195-203.
198. Wharram, B.L., M. Goyal, J.E. Wiggins, S.K. Sanden, S. Hussain, W.E. Filipiak, T.L. Saunders, R.C. Dysko, K. Kohno, L.B. Holzman, and R.C. Wiggins. 2005. Podocyte depletion causes glomerulosclerosis: diphtheria toxin-induced podocyte depletion in rats expressing human diphtheria toxin receptor transgene. *J Am Soc Nephrol* 16:2941-2952.
199. Wiggins, R.C. 2007. The spectrum of podocytopathies: a unifying view of glomerular diseases. *Kidney Int* 71:1205-1214.
200. Wilson, H.M., D. Walbaum, and A.J. Rees. 2004. Macrophages and the kidney. *Curr Opin Nephrol Hypertens* 13:285-290.
201. Wright, S.D., R.A. Ramos, P.S. Tobias, R.J. Ulevitch, and J.C. Mathison. 1990. CD14, a receptor for complexes of lipopolysaccharide (LPS) and LPS binding protein. *Science* 249:1431-1433.
202. Yamamoto, M., S. Sato, H. Hemmi, S. Uematsu, K. Hoshino, T. Kaisho, O. Takeuchi, K. Takeda, and S. Akira. 2003. TRAM is specifically involved in the Toll-like receptor 4-mediated MyD88-independent signaling pathway. *Nat Immunol* 4:1144-1150.
203. Yamamoto, M., S. Yamazaki, S. Uematsu, S. Sato, H. Hemmi, K. Hoshino, T. Kaisho, H. Kuwata, O. Takeuchi, K. Takeshige, T. Saitoh, S. Yamaoka, N. Yamamoto, S. Yamamoto, T. Muta, K. Takeda, and S. Akira. 2004. Regulation of Toll/IL-1-receptor-mediated gene expression by the inducible nuclear protein I κ B ζ . *Nature* 430:218-222.

204. Yoshioka, K., S. Hino, T. Takemura, S. Maki, J. Wieslander, Y. Takekoshi, H. Makino, M. Kagawa, Y. Sado, and C.E. Kashtan. 1994. Type IV collagen alpha 5 chain. Normal distribution and abnormalities in X-linked Alport syndrome revealed by monoclonal antibody. *Am J Pathol* 144:986-996.
205. Zeisberg, M., J. Hanai, H. Sugimoto, T. Mammoto, D. Charytan, F. Strutz, and R. Kalluri. 2003. BMP-7 counteracts TGF-beta1-induced epithelial-to-mesenchymal transition and reverses chronic renal injury. *Nat Med* 9:964-968.
206. Zeisberg, M., M. Khurana, V.H. Rao, D. Cosgrove, J.P. Rougier, M.C. Werner, C.F. Shield, 3rd, Z. Werb, and R. Kalluri. 2006. Stage-specific action of matrix metalloproteinases influences progressive hereditary kidney disease. *PLoS Med* 3:e100.
207. Zhang, X., R. Goncalves, and D.M. Mosser. 2008. The isolation and characterization of murine macrophages. *Curr Protoc Immunol* Chapter 14:Unit 14 11.
208. Zheng, K., P.S. Thorner, P. Marrano, R. Baumal, and R.R. McInnes. 1994. Canine X chromosome-linked hereditary nephritis: a genetic model for human X-linked hereditary nephritis resulting from a single base mutation in the gene encoding the alpha 5 chain of collagen type IV. *Proc Natl Acad Sci U S A* 91:3989-3993.

9. Abbreviations

ACE	Angiotensin-converting enzyme
ADAS	Autosomal dominant alport syndrome
ARAS	Autosomal recessive alport syndrome
ARB	AT1-receptor blockade
Arg-1	Arginase-1
AP-1	Activator protein-1
APC	Allophyocyanin
AS	Alport syndrome
AS	Ankylosing spondylitis
AT	Angiotensin
BUN	Blood urea nitrogen
CCL2	Chemokine C-C motif ligand 2
CCR2	Chemokine C-C motif receptor 2
CCR5	Chemokine C-C motif receptor 5
CKD	Chronic kidney disease
CLRs	C-type lectin receptors
COL	Collagen
Cp	Crossing point
CpG	Cytidine-phosphate-guanosine
CSF-1	Colony stimulating factor-1
DCs	Dendritic cells
DD	Death domain
DN	Diabetic nephropathy
Ds	double-stranded
DTR	Diphtheria toxin receptor
ER	Endoplasmic reticulum
ESRD	End-stage renal disease
FADD	FAS-associated death domain
FCS	Fetal calf serum
FITC	Fluorescein Isothiocyanate
FSGS	Focal segmental glomerulosclerosis

GBM	Glomerular basement membrane
GFR	Glomerular filtration rate
GPI	Glycosylphosphatidylinositol
HBSS	Hanks' balanced salt solution
HSP	Heat shock protein
IBD	Inflammatory bowel disease
IFN- γ	Interferon- γ
IKK	I κ B kinase
IL	Interleukin
IL-1RII	IL-1receptor II
IRAK	IL-1R-associated kinase
IRI	Ischemia reperfusion injury
KDIGO	Kidney Disease: Improving Global Outcomes
K/DOQI	Kidney Disease Outcomes Quality Initiative
LBP	LPS binding protein
LPS	Lipopolysaccharides
LRR	Leucin-rich-repeat
LT- α	Lymphotoxin- α
MAL	MyD88 adaptor like
MAPK	Mitogen-activated protein (MAP) kinase
MCD	Minimal change disease
MCP-1	Monocyte chemoattractant protein-1
MDA-5	Melanoma differentiation-associated gene 5
MDP	Muramyl dipeptide
MDSCs	Myeloid-derived suppressor cells
MEKK1	MAPK kinase-1
MHCII	Major histocompatibility complex class II
MET	Mesenchymal-to-epithelial transition
MINCLE	Macrophage-inducible C-type lectin
MMP	Matrix metalloproteinase
MMP	Mitochondrial membrane potential
MMP-12	Matrix metalloproteinase-12
MN	Membranous nephropathy

NF- κ B	Nuclear factor kappa B
NIK	NF- κ B inducing kinase
NK	Natural killer
NLRs	Nucleotide-binding oligomerization domain containing (NOD)-like receptors
NO	Nitric oxide
NOS	Nitric oxide synthase
ODNs	Oligodeoxynucleotides
PAMPs	Pathogen-associated molecular patterns
PAS	Periodic acid-Schiff stain
PBS	Phosphate-buffered saline
pDCs	Plasmacytoid DCs
PRRs	Pattern-recognition receptors
RA	Rheumatoid arthritis
RIP	Receptor interacting protein
RLRs	Retinoic acid-inducible gene (RIG)-I-like receptors
ROS	Reactive oxygen species
SARM	Sterile-alpha and Armadillo motif-containing protein
SLE	Systemic lupus erythematosus
Ss	Single-stranded
TAB1	TAK1-binding protein 1
TACE	TNF-alpha converting enzyme
TAK1	TGF- β -activated kinase 1
TAMs	Tumour associated macrophages
Th	T helper
TGF- β	Transforming growth factor- β
TICAM-1	TIR domain-containing adaptor molecule
TIR	Toll/IL-1R homology
TRAM	TRIF-related adaptor molecule
TIRAP	Toll-interleukin 1 receptor (TIR) domain containing adaptor protein
TLRs	Toll-like receptors

TNF- α	Tumor necrosis factor- α
TNF-R1	TNF-receptor 1
TRADD	TNFR-associated death domain
TRAF	TNF receptor associated factors
TRAPS	TNF receptor-associated periodic syndrome
TRIF	TIR-domain-containing adapter-inducing interferon- β
TUNEL	Terminal deoxynucleotidyl transferase dUTP nick end labeling
UACR	Urinary albumin to creatinine ratio
US	United States
UUO	Unilateral ureteric obstruction
XLAS	X-linked alport syndrome

Curriculum Vitae

Personal details

Surname: Ryu
First name: Mi
Date of Birth: 29, September 1980
Sex & Marital Status: Female, Single
Nationality: South Korea

Nephrological centre, Medical Policlinic,
Ludwig-Maximilians University, Munich,
Schillerstr-42, 80336, Germany.
Phone : +49-(0)89 218075856, +49-(0)176 24336508
Fax : +49-(0)89 218075860
E-mail: mi.ryu@med.uni-muenchen.de
mi.ryu@hotmail.com

ACADEMIC PROFILE

Research fellow, Ph.D. (Since 2008)

Nephrological center, Medical Policlinic, faculty of medicine, Ludwig-Maximilians University, Munich, Germany

Master of Science (“Doppel Diplom”), Biotechnology, September 2007

Technical University of Berlin, Berlin, Germany. DongSeo University, Busan, South Korea. Thesis: “Influence of *Streptococcus pneumoniae* (S.p) on the function of the glucocorticoid receptor pathway in pulmonary epithelial cells”. Department of Internal Medicine/Infectious Diseases and Pulmonary Medicine, Charité-Universitätsmedizin Berlin, Berlin, Germany. Advisor: Prof. Dr. rer. nat. Roland Lauster

Bachelor of Science, Biology (minor: Biochemistry), February 2003

ChangWon National University, ChangWon, South Korea. Thesis: “The effect of the action of HrK and IGFBP-6 by TCDD (2,3,7,8-tetrachlorodibenzo-*p*-dioxin)”. Advisor: Prof. Joo-Hung Park

Publications

- Kulkarni OP, Sayyed SG, Kantner C, **Ryu M**, Schnurr M, Sárdy M, Leban J, Jankowsky R, Ammendola A, Doblhofer R, Anders HJ. 4SC-101, a novel small molecule dihydroorotate dehydrogenase inhibitor, suppresses systemic lupus erythematosus in MRL-(Fas)lpr mice. *Am J Pathol* 2010 Jun; 176(6):2840-7. Epub 2010 Apr 22.
- **Ryu M**, Kulkarni OP, Radomska E, Miosge N, Gross O, Anders HJ. Bacterial CpG-DNA accelerates Alport glomerulosclerosis by inducing an M1 macrophage phenotype and tumor necrosis factor- α -mediated podocyte loss. *Kidney Int.* 2011 Jan;79(2):189-98. Epub 2010 Oct 20.

- Sayyed SG, **Ryu M**, Kulkarni OP, Schmid H, Lichtnekert J, Grüner S, Green L, Mattei P, Hartmann G, Anders HJ. An orally active chemokine receptor CCR2 antagonist prevents glomerulosclerosis and renal failure in type 2 diabetes. *Kidney Int*. 2011 Jul;80(1):68-78. doi: 10.1038/ki.2011.102. Epub 2011 Apr 20.
- Skuginna V, Lech M, Allam R, **Ryu M**, Clauss S, Susanti HE, Römmele C, Garlanda C, Mantovani A, Anders HJ. Toll-Like Receptor Signaling and SIGIRR in Renal Fibrosis upon Unilateral Ureteral Obstruction. *PLoS One*. 2011 Apr 22;6(4):e19204.
- Darisipudi MN, Kulkarni OP, Sayyed SG, **Ryu M**, Migliorini A, Sagrinati C, Parente E, Vater A, Eulberg D, Klussmann S, Romagnani P, Anders HJ. Dual blockade of the homeostatic chemokine CXCL12 and the pro-inflammatory chemokine CCL2 has additive protective effects on diabetic kidney disease. *Am J Pathol*. 2011 Jul;179(1):116-24. Epub 2011 Apr 30.
- Lech M, Weidenbusch M, Kulkarni OP, **Ryu M**, Darisipudi MN, Susanti HE, Mittrüecker HW, Mak TW, Anders HJ. Interferon-regulatory factor-4 deficiency abrogates lupus-like nephritis despite enhancing systemic cytokine production by antigen-presenting cells. *J Am Soc Nephrol*. 2011 Aug;22(8):1443-52. Epub 2011 Jul 8.
- Anders HJ and **Ryu M**. Renal microenvironments and macrophage phenotypes determine progression or resolution of renal inflammation and of fibrosis. Review. *Kidney Int*. 2011 Nov;80(9):915-25. Epub 2011 Aug 3.
- Lech M, Kantner C, Kulkarni OP, **Ryu M**, Vlasova E, Heesemann J, Anz D, Endres S, Kobayashi KS, Flavell RA, Martin J, Anders HJ. Interleukin-1 receptor-associated kinase-M suppresses systemic lupus erythematosus. *Ann Rheum Dis*. 2011 Dec;70(12):2207-17. Epub 2011 Aug 29.
- **Ryu M**, Mulay SR, Miosge N, Gross O, Anders HJ. Tumor necrosis factor- α drives Alport glomerulosclerosis by promoting the loss of podocytes. *J Pathol*. 2012 Jan;226(1):120-31. doi: 10.1002/path.2979. Epub 2011 Sep 26.
- Kulkarni OP, **Ryu M**, Kantner C, Sárdy M, Naylor D, Lambert D, Brown R, Anders HJ. Recombinant Chaperonin 10 suppresses cutaneous lupus and lupus nephritis in MRL-(Fas)lpr mice. *Nephrol Dial Transplant*. 2012 Apr;27(4):1358-67. Epub 2011 Oct 10.
- Lichtnekert J, Kulkarni OP, Mulay SR, Rupanagudi KV, Allam R, **Ryu M**, Vielhauer V, Muruve D, Tschopp J, Lindenmeyer M, Cohen CD, Anders HJ. Anti-GBM glomerulonephritis involves IL-1 but is independent of NLRP3/ASC inflammasome-mediated activation of caspase-1. *PLoS One*. 2011;6(10):e26778. Epub 2011 Oct 27.
- Mulay SR, Thomasova D, **Ryu M**, Anders HJ. Murine double minute-2 links inflammation and tubular healing in acute kidney injury of mice. *Kidney Int*. 2012 Jun;81(12):1199-211. doi: 10.1038/ki.2011.482. Epub 2012 Feb 1.
- **Ryu M**, Migliorini A, Miosge N, Gross O, Shankland S, Brinkkoetter PT, Hagmann H, Romagnani P, Liapis H, Anders HJ. Plasma leakage through glomerular basement membrane ruptures triggers the proliferation of parietal epithelial cells and crescent formation in non-inflammatory glomerular injury. *J Pathol*. 2012 May 3. doi: 10.1002/path.4046. [Epub ahead of print].
- Allan R, Scherbaum C, Darisipudi MN, Mulay SR, Hägele H, Lichtnekert J, Hagemann JH, Rupanagudi KV, **Ryu M**, Schwarzenberger C, Hohenstein B, Hugo C, Uhl B, Reichel CA, Krombach F, Monestier M, Liapis H, Moreth K, Schaefer L, Anders HJ. Histones from dying renal cells aggravate kidney injury

via TLR2 and TLR4. *J Am Soc Nephrol.* 2012 Aug;23(8):1375-88. Epub 2012 Jun 7.

CONGRESS ABSTRACTS

- **November. 2011:** Renal week 2011, American Society of Nephrology, Philadelphia, USA. Free communication invited. Etanercept Delays the Progression of Alport Glomerulosclerosis by Preventing Tumor Necrosis Factor-Driven Loss of Podocytes
- **September. 2011:** Kongress für Nephrologie 2011, Berlin. Poster presentation. Tumor necrosis factor- α -drives Alport glomerulosclerosis by promoting podocytes loss
- **July. 2011:** Fellows Night des Nephrologie-Forum. Munich, Germany. Oral Presentation. Tumor necrosis factor- α -drives Alport glomerulosclerosis by promoting podocytes loss
- **June. 2011:** European Renal Association (ERA-EDTA) 2011, Prague, Czech Republic. Free communication invited: Tumor necrosis factor- α -drives Alport glomerulosclerosis by promoting podocytes loss.
- **May. 2011:** Deutsche Gesellschaft für Innere Medizin (DGIM), Wiesbaden. Germany. Poster presentation 1: Tumor necrosis factor- α -drives Alport glomerulosclerosis by promoting podocytes loss. Poster presentation 2: An orally active chemokine receptor CCR2 antagonist prevents glomerulosclerosis and renal failure in type 2 diabetes.
- **March. 2011:** 23rd Annual Meeting of the European Renal cell study group, Lake Garda, Italy. Oral Presentation: Tumor necrosis factor- α -drives Alport glomerulosclerosis by promoting podocytes loss.
- **Nov. 2010:** Renal week 2010, American Society of Nephrology, Denver, USA. Free communication invited. Bacterial CpG-DNA accelerates Alport glomerulosclerosis by inducing an M1 macrophage phenotype and tumor necrosis factor- α -mediated podocyte loss.
- **July. 2010:** Fellows Night des Nephrologie-Forum. Munich, Germany. Oral Presentation. An orally active chemokine receptor CCR2 antagonist prevents glomerulosclerosis and renal failure in type 2 diabetes.
- **June. 2010:** European Renal Association (ERA-EDTA) 2010, Munich, Germany. Oral Presentation: Bacterial CpG-DNA accelerates Alport glomerulosclerosis by inducing an M1 macrophage phenotype and tumor necrosis factor- α -mediated podocyte loss.
Poster: An orally active chemokine receptor CCR2 antagonist prevents glomerulosclerosis and renal failure in type 2 diabetes.
- **March. 2010:** 22nd Annual Meeting of the European Renal cell study group, Wien, Austria. Oral Presentation: Bacterial CpG-DNA accelerates Alport glomerulosclerosis by inducing an M1 macrophage phenotype and tumor necrosis factor- α -mediated podocyte loss.

RESEARCH EXPERIENCES

Department of Internal Medicine/Infectious Diseases and Pulmonary Medicine, Charité-Universitätsmedizin Berlin. Berlin, Germany

Masters thesis (Diplomarbeit). “Influence of *Streptococcus pneumoniae* (S.p) on the function of the glucocorticoid receptor pathway in pulmonary epithelial cells”. August 2006 – April 2007.

Department of Cellular Microbiology, Max-Planck Institute for Infection Biology. Berlin, Germany

Study Project. “Development of the vector system to study the formation of neutrophil extracellular traps (NETs)”. July 2005 – November 2005.

AWARDS

- Academic scholarship, Technical University of Berlin (September 2004 – December 2004)
- Participation of scientists in joint projects under the agreement of scientific cooperation granted by DFG (September 2004)
- Academic scholarship of the German Academic Exchange Service (DAAD), Technical University of Berlin (October 2006 – August 2007)
- Best abstract presented by young authors, European Renal Association (ERA-EDTA) 2010 and 2011
- Teaching/Research Assistantship, LMU, 2010

Declaration: The above stated particulars are true to the best of my knowledge.

(Ms. Mi Ryu)